University of Pannonia

Doctoral School of Chemical Engineering and Material Sciences

Submitted for the degree of

Doctor of Philosophy

of the University of Pannonia, Hungary

Author: Rohit Khargotra

Supervisor: Dr. Singh Tej

Co-Supervisor: Dr. András Kovács

Dissertation Title: Experimental examination and development of innovative Eco-friendly insulation materials for highly-efficient solar thermal collectors

DOI:10.18136/PE.2024.880

Veszprém

2024

ENHANCING SOLAR THERMAL COLLECTOR PERFORMANCE: EXPERIMENTAL AND DESIGN OPTIMIZATION EMBEDDED WITH TURBULATOR AND SUSTAINABLE INSULATING MATERIALS

Thesis for obtaining a PhD degree in the Doctoral School of Chemical Engineering andMaterial Sciences of the University of Pannonia

in the branch of Material Sciences

and TechnologiesWritten by

Rohit Khargotra

Supervisor: Dr. Tej Singh
Co-supervisor: Dr. András Kovács

propose acceptance (yes / no)

……..……...……
Dr. Tej Singh
Supervisor

propose acceptance (yes / no)

……..……...……
Dr. András Kovács
Co-supervisor

As reviewer, I propose acceptance of the thesis:

Name of Reviewer: Dr. yes / no

……..……...……

1st reviewer

Name of Reviewer: Dr. yes / no

……..……...……

2nd reviewer

The PhD-candidate has achieved..... % at the public discussion.
Veszprém,

……..……...……

Chairman of the Committee

The grade of the PhD Diploma …..... (….....%)
Veszprém,

…….……...……

Chair of the UDHC

Submitted with 105 pages and 107 references

The Dissertation contains 35 Figures, and 19 Tables

Supervision

Dr. Tej Singh	Supervisor	PhD supervisor, Doctoral School of Chemical Engineering and Material Sciences, University of Pannonia. Associate Professor at Savaria Institute of Technology, Faculty of Informatics, ELTE Eötvös Loránd University, Budapest 1117, Hungary
Dr. András Kovács	Co-supervisor	PhD supervisor, Doctoral School of Chemical Engineering and Material Sciences, Universityof Pannonia.

ACKNOWLEDGEMENT

"In a day, when you don't come across any problems – you can be sure that you are travelling in a wrong path".

Swami Vivekanand

It is with a sense of gratitude that I wish to place on record my indebtedness to my supervising guide ***Dr. Tej Singh, Associate Professor, Savaria Institute of Technology, Faculty of Informatics, ELTE Eötvös Loránd University, Budapest 1117, Hungary,*** *whose guidance and constant encouragement was indispensable for the progress and completion of this thesis. I remember the timely care he had given me throughout my research period. He is my source of inspiration and my guide for teaching me to publish my results. It would have not been possible for me to bring out this thesis without their help and constant encouragement. His continuous support and guidance will always motivate me in my life.*

Additionally, I would like to extend my deepest gratitude to my co-supervisor, ***Dr. András Kovács****,* ***Department of Material Science and Chemical Engineering, University of Pannonia, Hungary****, for his invaluable advice, constructive critiques, and unwavering backing. His relentless pursuit of excellence and generous knowledge-sharing have significantly enriched this work and contributed to its success.*

My sincere thanks to my mother ***Smt. Rani Khargotra*** *and my father* ***Sh. Kamal Kumar Khargotra*** *for blessings hands over my head always. Special thanks to my elder brother* ***Vishal Khargotra*** *and my elder sister* ***Priya Khargotra*** *for supporting spiritually always.*

Rohit Khargotra

CONTENTS

Abstract

Solar water heating system (SWHS) is a cost-effective technology with high household adoption rates worldwide. The performance of SWHS significantly deteriorates due to several factors, including design parameters as well as radiative and convective heat losses from the system, which considerably impair the system's efficiency. Novel designs and unique heat transfer techniques are increasingly being explored to improve the efficiency of SWHS. In this framework, the following research focuses on designing and optimizing an SWHS integrated with perforated delta obstacles. The influence of Reynolds number (400, 800, 1200), angle of attack (15°, 30°, 45°), and pitch ratio (0.5, 1, 1.5, 2.0) on the friction factor, Nusselt number, and thermo-hydraulic performance was investigated and optimized. The combination of Reynolds number = 1200, angle of attack = 45°, and pitch ratio = 1 yielded the most significant Nusselt number (90.55). In contrast, the combination of Reynolds number = 1200, angle of attack = 15°, and pitch ratio = 0.5 yielded the lowest friction factor (0.38). The largest thermo-hydraulic efficiency (2.75) was obtained using Reynolds number = 400, angle of attack = 45°, and pitch ratio = 1. Since no single SWHS design alternative can meet all desired performance criteria, selecting the best among SWHS design alternatives is not easy. Therefore, a hybrid multi-criteria decision-making approach called AHP (analytic hierarchy process)-ARAS (additive ratio assessment) was implemented, suggesting the SWHS design alternative having the angle of attack = 45°, Reynolds number = 1200, and pitch ratio = 1 satisfies the preset performance criteria. Finally, sensitivity analysis and validation with other decision-making approaches were performed to verify the proposed decision-making framework's effectiveness, proving the results' robustness.

The influence of different parameter combinations such as Reynolds number (200, 600, 1000, 1400, 1800), pitch ratio (0.5, 1, 1.5), blockage ratio (0.15, 0.20, 0.25), and angle of attack (45°) on Nusselt number, friction factor and thermo-hydraulic performance of SWHS were analyzed.

For the combination of Reynolds number = 1800 and pitch ratio = 0.5, the Nusselt number remained highest for 0.25 of blockage ratio, whereas the friction factor remained lowest for a blockage ratio of 0.15. The maximum thermo-hydraulic efficiency was achieved using Reynolds number = 200, pitch ratio = 0.5, and blockage ratio = 0.20. The obtained results were intensely dependent on parameter combinations without any pronounced trend. Therefore, criteria importance through inter-criteria correlation (CRITIC) and complex proportional assessment (COPRAS) approach was implemented to find optimal design alternative. The results of the hybrid CRITIC-COPRAS approach showed that the combination of Reynolds number = 1800, pitch ratio = 0.5, blockage ratio = 0.20, and angle of attack = 45° is the best alternative for maximum thermal enhancement in SWHS. The sensitivity analysis proved the robustness of the results that the first-ranked alternative is the most dominant in all scenarios.

In the next stage we are analysed the influence of materials like rock wool for insulation in solar thermal collector in order to minimize heat loss. However, the use of such inorganic materials raises substantial concerns for both the industry and the environment. Therefore, it is crucial to decrease the reliance on these inorganic materials and instead adopt readily available biodegradable materials that pose no environmental risks to the system. The current research presents the usage of agricultural waste as insulating materials for S-FPC fabrication. The novelty of this current research work is the effective utilization of agriculture waste (rice husk, stubble fibre, coco-peat, and nitrile rubber) as an insulating material for the fabrication of S-FPC. Experiments were performed with insulating thicknesses of 50 mm and 70 mm. The optimum temperature was recorded to be 50–53 °C with an average thermal efficiency of 64–66 % by using rice husk as the insulating material at 70 mm thick.

List of Abbreviations

f	Friction factor
P_{dh}	Pitch ratio of delta hindrance
Re	Reynolds number
Nu	Nusselt number
f_p	Friction factor of plain tube
y	Twist ratio
η_{dh}	Thermo hydraulic Efficiency
k_w	Water thermal conductivity
SWHS	Solar water heating system
Nu_{dh}	Nusselt number of delta hindrance
Nu_p	Nusselt number of plain tubes
α_{dh}	Angle of attack for delta hindrance
f_{dh}	Friction factor of hindrance promoters
$\triangle T$	Temperature difference
m_w	Mass flow rate of water
ρ_w	Water density
A_{ht}	Area of heated tube
h_w	Heat transfer coefficient
MCDM	Multi-criteria decision-making
AHP	Analytic hierarchy process
ARAS	Additive ratio assessment
I_s	Intensity of solar radiation
T_{fo}	Outlet temperature
T_{fi}	Inlet temperature
Q_u	Useful heat gain
$\dot{m}$	mass flow rate, Kg/s
SC	Solar collector
S-FPC	Solar flat plate collector
SWHS	Solar water heating system

FPC	Flat plate collector
HE	Heat exchanger
PCM	Phase change materials
η_{avg}	Average thermal efficiency
I_g	Global solar radiation, (W/m^2)

List of Figures

List of Tables

CHAPTER 1
INTRODUCTION

1. Introduction

Thermodynamics is that branch of science that deals with the thermal energy conversion into useful work. The conversion of energy from one phase to another is the most significant area of research in thermodynamics [1]. The demand of energy is increasing rapidly in all the sectors such as agriculture, residential, commercial and industrial applications etc; that leads to the scarcity of natural resources, as well as enhance the destruction and humiliation of the natural environment in the present situation [2-5]. Therefore, the examination of energy conversion procedure has changed out to be a challenging process in the recent years. The current study is focussed on the utilization of solar radiation form the efficiency evaluation of solar thermal collector.

1.1 ENERGY

Energy has the capability for the production of physical outcomes. Energy take place in different form i.e., open and closed system that are shown in Fig. 1. The total is further classified into two main types: macroscopic and microscopic [6-9]. The macroscopic study is based on the external flow energy, potential and kinetic energy. The microscopic approach is based on the internal energy that are mainly focus on the moment of the molecular structure and is classified as sensible heat, latent heat, chemical and nuclear energy. The energy that are based on the phase change are refer to as latent change where as the rise in temperature of fluid is defined as sensible heat [10-14]. The sensible heat takes place in various form such as molecular rotation and translation, electron translation, molecular vibration and nuclear spin. The difference of energy in initial and final stage defined as energy change in system.

The energy inside the system can be converted into the useful work according to the need. The energy balanced between the dynamic and static form is referred to as conversion of energy principle or first law of thermodynamics [15-18]. It states that the energy can be transformed from one form to another form during interaction, the total amount of energy remains constant but cannot be destroyed or created.

The energy balance Equation is stated as:

$$E_{in} - E_{out} = \frac{dE_{system}}{dt} = 0 \ (Steady\ state\ condition) \qquad (1)$$

Where as $E_{in} - E_{out}$ represent the net energy transfer and $\frac{dE_{system}}{dt}$ shows the change in internal energy, kinetic energy and potential energy of the system.

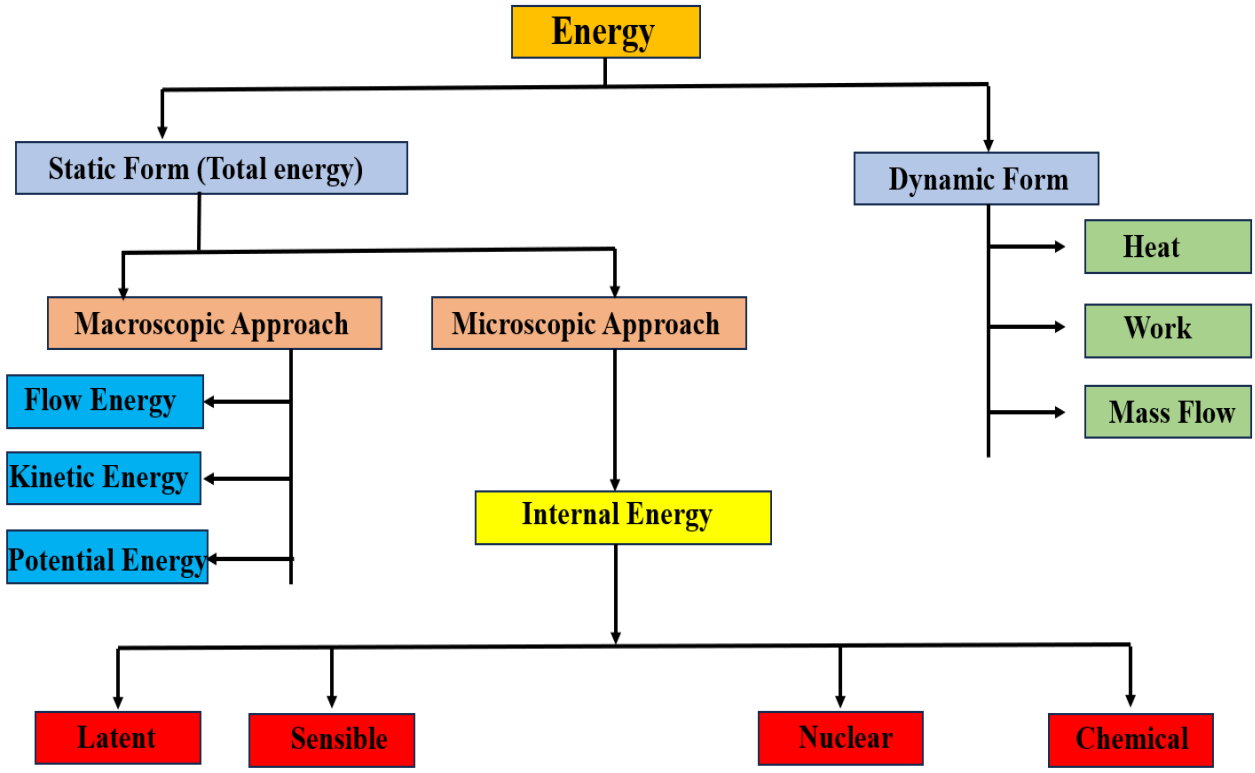

Fig.1. Representation of energy flow chart.

1.2 ENTROPY

As thermal energy is transferred from a high-temperature body to a low-temperature body, it deteriorates. Entropy and exergy were defined as a result of efforts to measure the quality or "work potential" of energy using the second law of thermodynamics. Entropy theory offers comprehensive understanding of the direction of spontaneous variation [19-23]. The idea of "entropy" served as the basis for the initial introduction of the difference between reversible and irreversible processes in thermodynamics.

Entropy analysis are measured the maximum amount of randomness or disorder inside the system. Due to dispersion of energy, the heat energy transfer inside the system and increase the entropy of the system. In other words, we can say that the entropy of the system increases due to thermal process. According to the Clausius equations, if Q is the amount of heat flows through the reservoirs at temperature, the entropy rise is defined as S= Q/T. It means that higher the entropy higher the disorder. It is better understood that even a small amount of reduction in entropy generation that may leads to the better performance of the system [24-27].

Higher the entropy, higher the disorder which means that, lower the availability of the system's energy to do the thermal process. The entropy generation indirectly specifies the irreversibility, which is present in the system during the process [28]. It is clearly, observed that even a small reduction in entropy generation may lead to a better performance of the system. Hence, the entropy balance for each system should be carried out to quantify the entropy generation.

Hence the energy balanced equation is defined as:

$$(S_{in} - S_{out}) + S_{gen} = \frac{dS_{sys}}{dt} = 0 \text{ (Steady state)} \quad (2)$$

$S_{in} - S_{out}$ represent the entropy change between the system and the surrounding. S_{gen} represent the entropy generated by the system.

1.3 EXERGY

In thermodynamics, energy inside the system has the ability to do work whereas the exergy of the system has the optimum energy that is extracted from the given energy [29]. The system's total energy, which stays constant during the operation, is split into two types: unavailable energy and accessible energy. Determining how much of the energy is worthless is crucial since the energy that is inaccessible cannot be transformed into useful labour [30]. Using the energy and entropy balance equations, the exergy balance equation is expressed as follows:

$$(X_{in} - X_{out}) + X_{des} = \frac{dX_{sys}}{dt}$$

According to the rule of energy conservation, the quantities of energy input and outflow are equal under thermally steady-state conditions; nevertheless, the amount of entropy outflow is more than the amount of entropy inflow according to the law of entropy growth, as shown in Figure 2. The quantity of exergy outflow is less than the amount of exergy intake because the entropy created by the system consumes exergy [31]. Exergy analysis evaluates the quality of heat in a waste stream by clearly identifying the points in the system where energy is degrading, which helps to advance the method or technology.

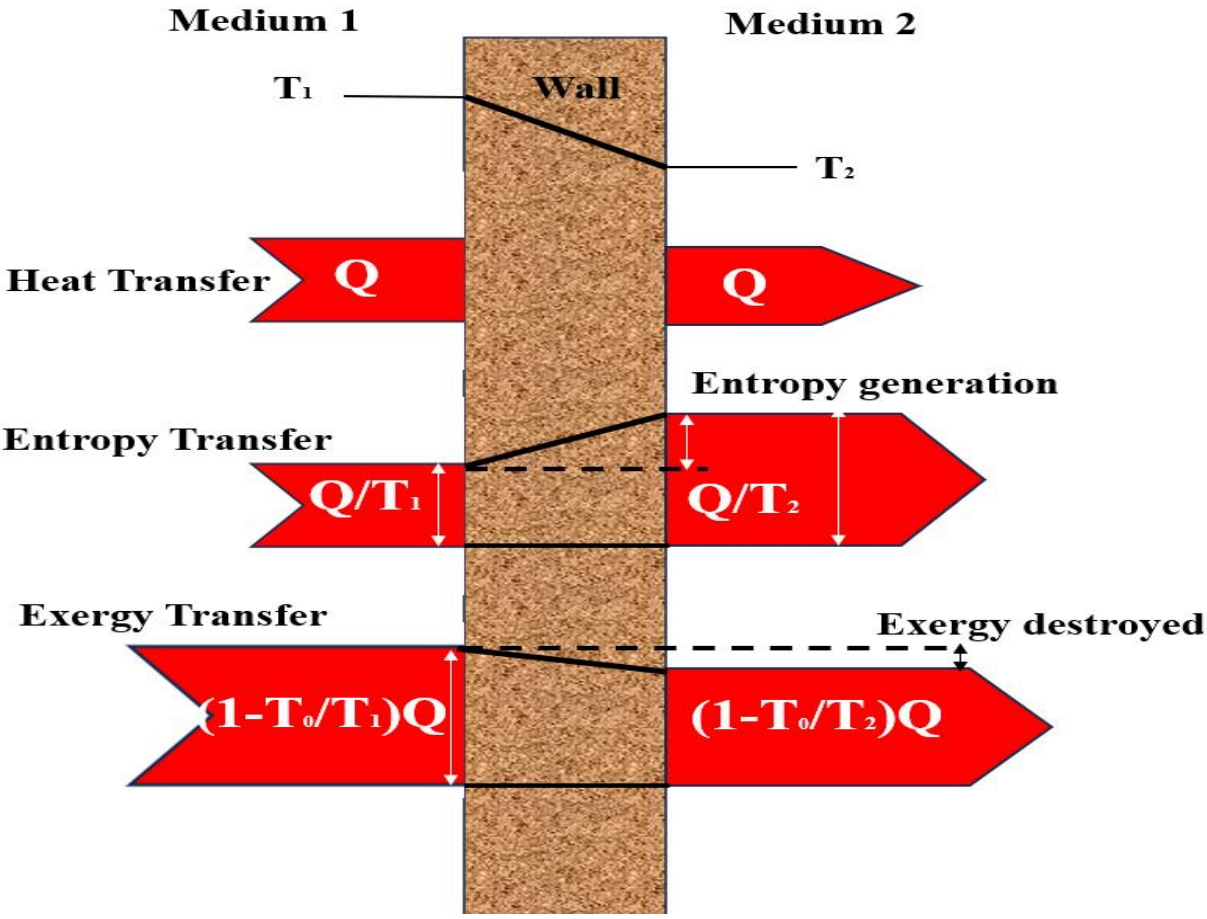

Fig. 2. Energy, Entropy, and Exergy Flow in and out of a System.

While a system's energy analysis just considers the measure of amount, a system's exergy analysis considers both the measure of quantity and quality. Therefore, examining a system's efficiency from an energetic perspective will enhance the system's functionality [32-34]. The ratio of the actual work done to the maximum amount of reversible work that might be done under the same circumstances is known as the exergy efficiency, second law efficiency, or second law of thermodynamics.

Exergy efficiency= Actual work done/ Exergy input.

Exergy efficiency= Maximum work-waste work/ Maximum work or 1-Waste work/Maximum work.

1.4 SOLAR THERMAL ENERGY

The sun is the most important feature in our solar system. The sun's release energy in the form of elaborate chemical process in the sun's core- a process of thermonuclear process. The energy is transmitted in all direction and a very little amount reached on the reach surface. In the present situation the need of renewable and clean energy is of great demand [35-49]. The solar energy fulfils all the need that are available from the fossil fuel. The solar energy in the form of light and heat can be used for various purpose such as domestic and horticultural purposes, industrial and commercial applications

Around 34% of solar energy is reflected into space by the Earth's atmosphere, clouds, and surface [50]. The Earth's surface only absorbs on average 47% of the remaining 66%, while water vapour, clouds, and the ozone layer each absorb 19%. The elements of the solar radiation that is available are listed in Table 1.

Table 1.1 Spectral Distribution of Solar Radiation

Type of Radiation	Wavelength Band (μ)	% of Total Radiation
Invisible Ultra-Violet (UV)	0.29 to 0.40	7
Visible Radiation	0.40 to 0.70	39
Near Infrared (IR)	0.70 to 3.50	52
Far Infrared (FR)	4.00 to 4.75	2

The sun's energy provides a reliable and renewable source of power. Photovoltaic cells and solar thermal collectors are two methods that solar energy may be converted into usable energy with no negative environmental effect. Solar photovoltaic (PV) panels transform solar energy into usable forms of energy by using a PV cell made of a semiconductor material [51].

Contrarily, Concentrating Solar Power (CSP) concentrates solar energy into a heat receiver, where it is transformed into mechanical energy and, ultimately, solar thermal power [52-55]. Since photovoltaic cells directly convert solar energy into electricity, they are more advantageous than thermal collectors.

1.4.1 SOURCES OF ENERGY

The conventional and non-conventional energy sources are divided into two groups and are depicted in Figure 3. Nuclear energy, fossil fuel energy, and hydraulic energy are examples of traditional energy sources. Contrarily, non-conventional energy sources are continually created via the utilisation of natural energy sources and are only employed for certain reasons [56].

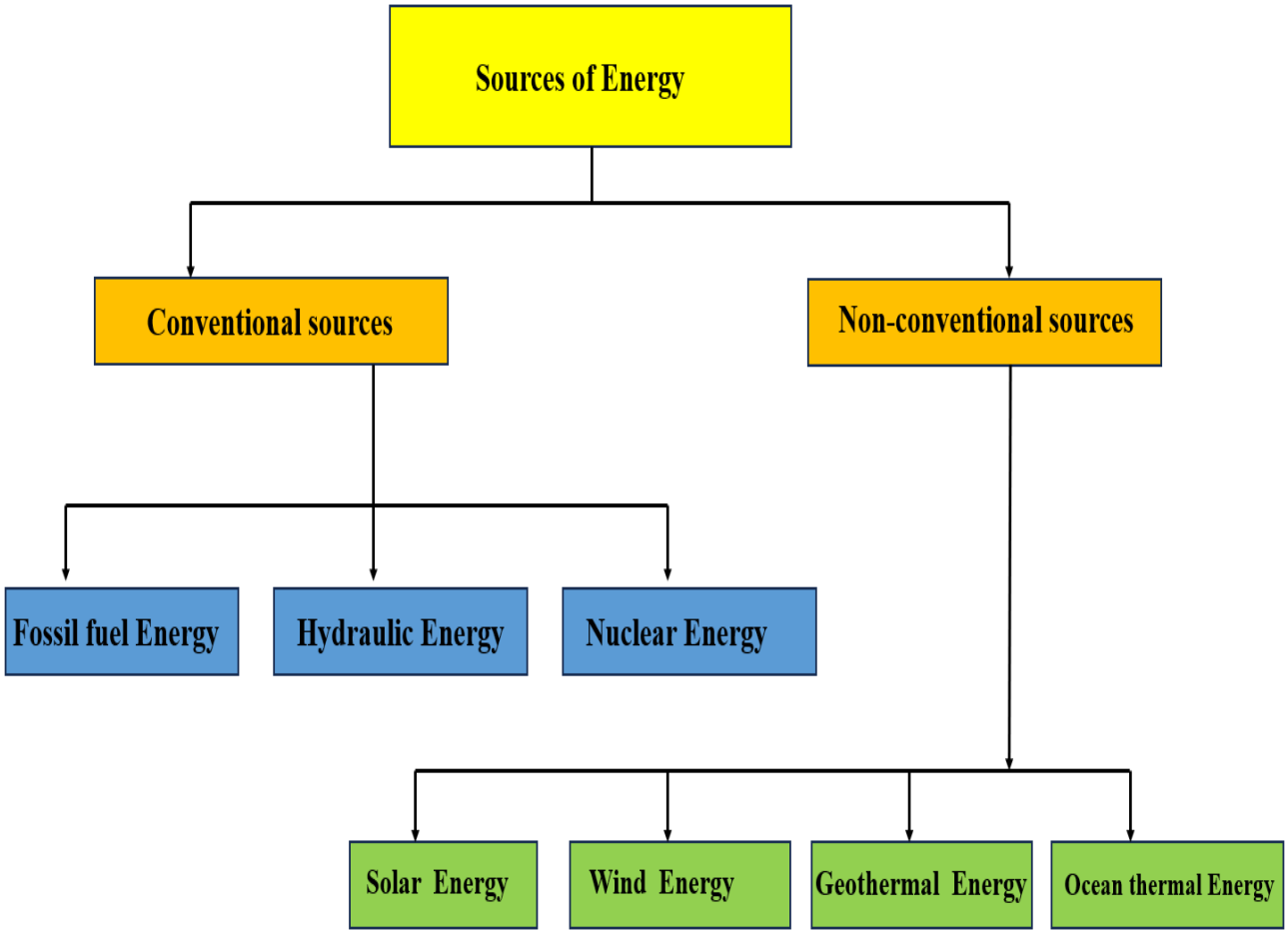

Fig. 3. Sources of Energy.

1.5. SOLAR WATER HEATER

SWH is mainly the common application of solar energy for various application of commercial and domestic purpose around the world. SWH utilised the solar radiation and convert it into the heat energy [57]. The heat energy further absorbed by the working fluid inside the absorber pipe and utilizing it in different purpose. The SWH can be utilized in various climatic application in the world.

The main component of SWH is given below:

- Glass plate (cover)
- Collector Plate/absorber plate
- Water pipes
- Storage tank

The following is SWH's operating theory: The absorber plate within the solar collector absorbs the sun radiation as it strikes it and transfers the thermal energy to the water flowing through the glass or metal tubes. As water is heated, its density falls as its temperature rises. So, through various tubes, hot water climbs to the top of the storage tank, warming the cold water in the tank as it drops to the tubes. The collectors that are most often used are:

- Evacuated tube collectors
- Flat plate collectors

1.6. EVACUATED TUBE SOLAR COLLECTOR

Figure 1.5 [58] depicts an evacuated tube solar collector (ETSC) that uses heat pipes and permits liquid to travel through them directly. ETSCs have a temperature range of roughly 120˚C. Multiple evacuated glass tubes each holding an absorber plate fused to a heat pipe, as illustrated in Figure 1.6, make up evacuated heat pipe tubes.

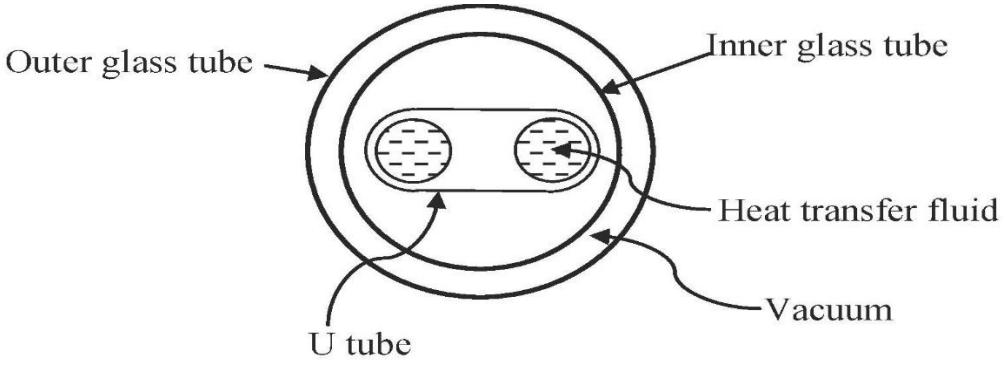

Fig. 4. Cross Sectional view of Evacuated Tube Collector

A common header pipe connects parallel rows of clear glass tubes found in an ETSC [59]. The fluid for the home hot water system receives heat from the hot end of the heat pipes. Convection and conduction heat loss are significantly reduced by the vacuum that surrounds the exterior of the tube. Therefore, especially in colder temperatures, more efficiency was realised than with flat plate collectors. Based on the absorber tube that is utilised in the collector, there are many types of evacuated solar collectors. The commonly used are:

- Glass-Glass evacuated tube collector
- Glass-Metal evacuated tube collector

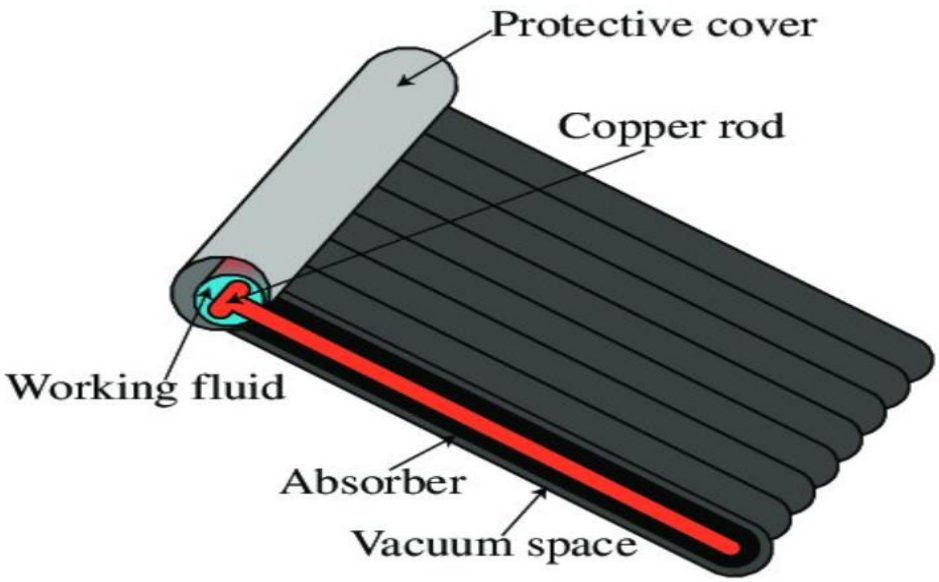

Fig. 5. Evacuated Tube Collectors

1.7 FLAT PLATE SOLAR COLLECTOR

A flat plate solar collector (F-PSC) is a special type of heat exchanger that turns the solar radiation that emitted from the suns into heat energy. The F-PSC collect the solar energy and utilize that energy to warm the water and utilize the various application such as washing, bathing and heating and even also utilize for various outdoor heating application such as Swimming pools and hot tubes [60].

Due to its straightforward design, cheap cost, and comparatively easy installation compared to other types of hot water heating systems, solar flat plate collectors tend to be more cost effective for the majority of domestic and small business hot water applications [61]. Additionally, solar flat plate collectors are more than capable of supplying the requisite volume and temperature of hot water.

A solar flat plate collector normally consists of a large heat-absorbing plate that has been painted or chemically etched black to absorb as much solar radiation as possible for optimal efficiency. Large sheets of copper or aluminium are frequently used because they are both strong heat conductors [62]. Several parallel copper pipes or tubes, known as risers, that run lengthwise across this blackened heat-absorbing surface hold the heat-transfer fluid, usually water.

In order to achieve the greatest possible surface contact and heat transmission, these copper pipes are directly glued, soldered, or brazed to the absorber plate. The temperature of the absorbent surface rises as a result of solar heating. The fluid moving inside the copper pipes is heated as the plate grows hotter, and this heat is subsequently absorbed by the fluid and utilised by the home. In order to protect the enclosed absorber plate and provide an insulating air space, the pipes and absorber plate are encased in an insulated metal or wooden box with a sheet of glazing material, either glass or plastic, on the front. The majority of the incoming

radiation strikes the darkened absorber since this glazing material does not significantly absorb the sun's heat energy.

This heat is kept from escaping back into the atmosphere by the air gap that exists between the plate and the glazing material. Warming up the absorber plate causes it to lose heat to its surroundings while also transferring heat to the fluid inside the collector. The bottom and sides of a flat plate collector are insulated with high temperature rigid foam or aluminium foil insulation, as illustrated, to reduce this heat loss.

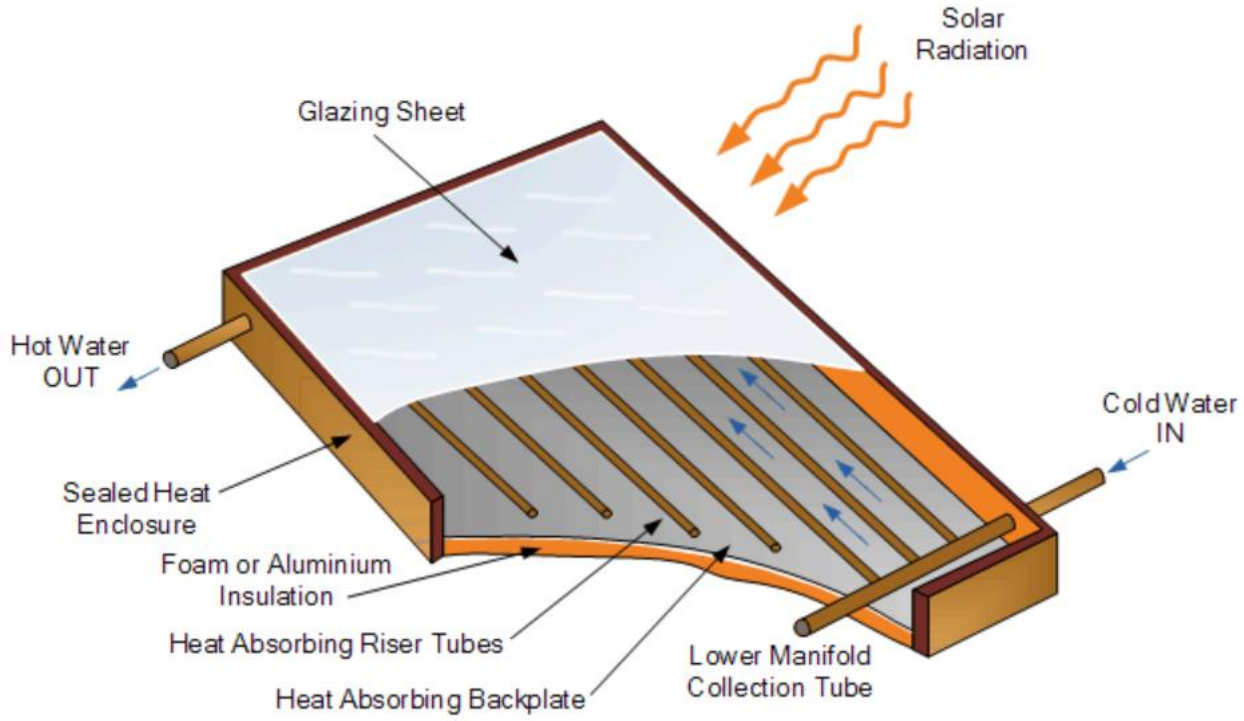

Fig. 6. Typical Flat Plate Collector

From a variety of angles, flat plate collectors can use direct or indirect sunlight to heat the fluid within. They also work in diffused light, which is common on overcast days since, in contrast to photovoltaic cells, the ambient heat is what is being absorbed rather than the light [63]. The time of year, how clear the sky is, and how slowly the water travels through the collection pipes will all have a significant impact on how hot the circulating water becomes.

1.7.1 Direct and Indirect Solar Thermal Systems

For usage in the house, water can be heated in a variety of ways. Flat plate solar collectors are used in solar water heating systems, which can be classified as direct or indirect systems depending on how the heat is transferred throughout the system [64]. You will require both a solar collector to gather the heat and transmit it to the water as well as a hot water tank to store this hot water for usage as needed in order to properly heat your water and utilise it both during the day and the night.

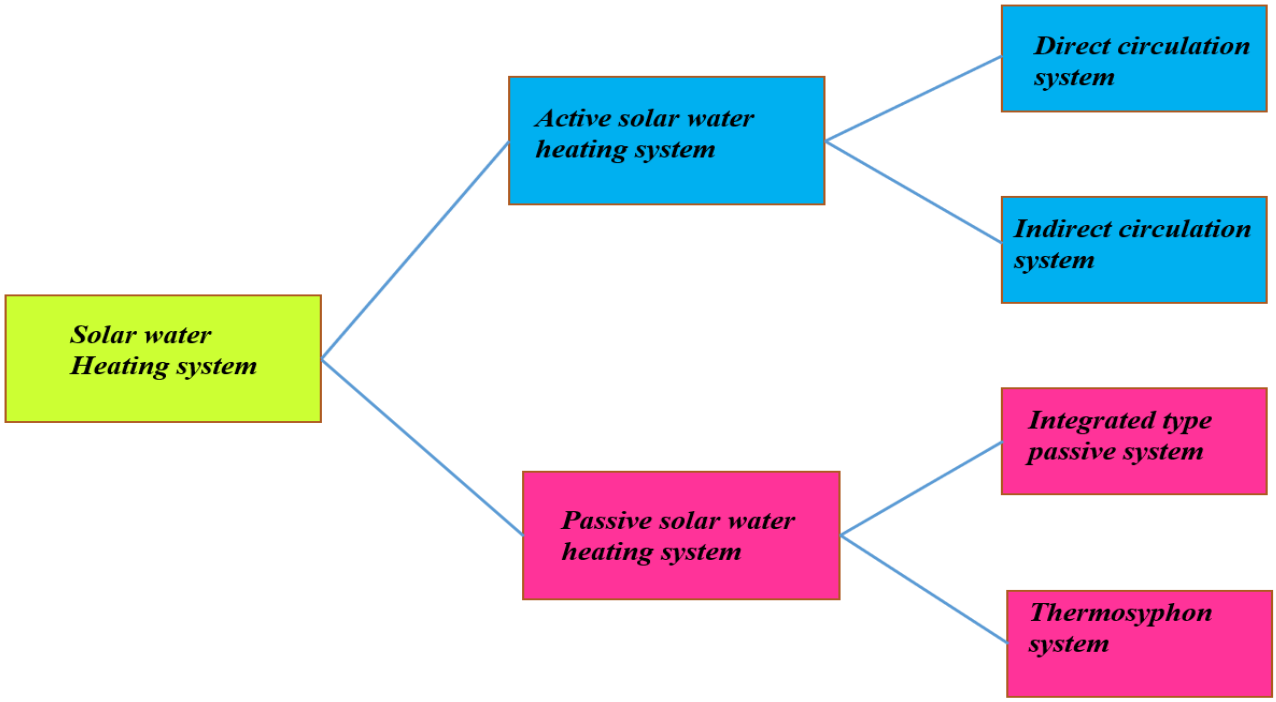

Fig. 7. Classification of solar water heating system

1.7.2. Direct Solar Thermal System

A pump is used to move water throughout a direct solar water heating system, sometimes referred to as an active open-loop system. Pumped straight from the house to an immersion tank or central water storage, the colder water is heated by passing through the solar collector [65]. The hot water exits the flat plate collector and flows continuously back towards the tank. The water is then piped back into the house where it may be used as hot water.

The system may be made greener by using a low-voltage 12-volt pump that can be supplied by a tiny solar cell or electronic controller. In warmer areas with fewer cold days, direct systems are typically employed, or they are emptied in the winter to prevent the water in the pipes from freezing. Since the same water that flows through the flat plate collector is used in the residence, chemicals cannot be added to the water to provide protection.

A passive direct hot water system transfers heat generated to the storage tank without the need of pumps or other control systems. Instead, passive systems are what are referred to as "open-loop systems" that employ gravity's inherent power to assist move water throughout the system. This kind of system combines a horizontally placed storage tank of some form just above the solar flat plate collector with a solar flat plate collector [66].

Sun-heated water rises naturally through the solar collector pipes through convection and fills the storage tank above. The colder water is driven out when the heated water enters the storage tank above, and as cold water is denser than hot water, it falls to the bottom of the collectors with the help of gravity. When the sun is shining, this cycle of hot water rising and colder water dropping is known as a "thermosyphon flow" and it repeats itself continually.

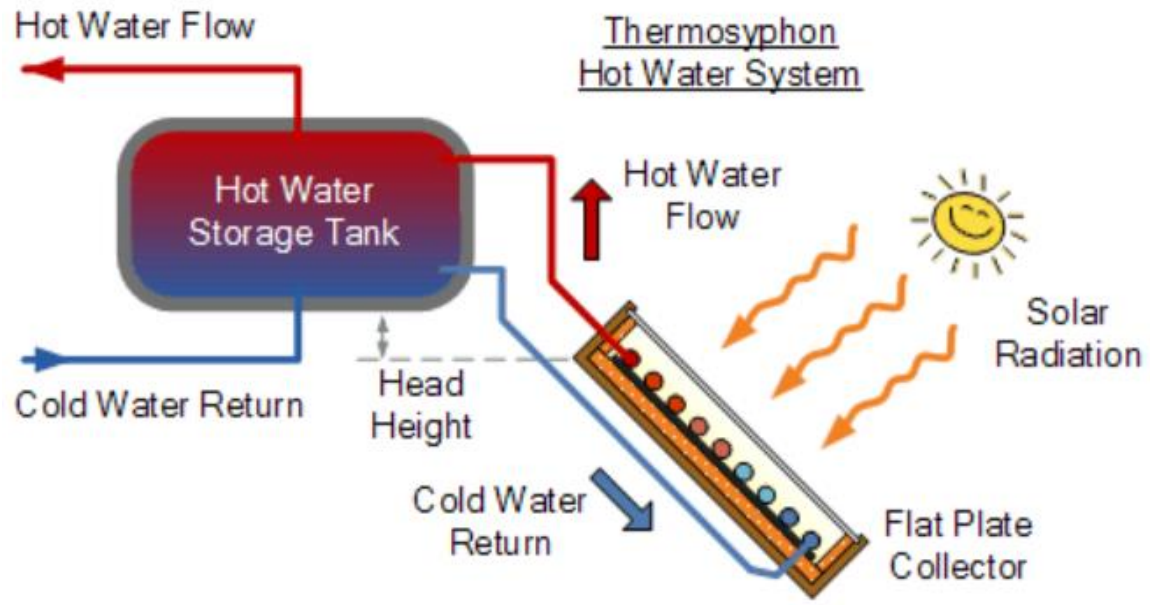

Fig. 8. Thermosyphon Hot Water System

The thermosyphon system is the most popular sun heated hot water system on the market, and it is the flat plate collector and storage tank configuration that is used in the majority of commercially available passive direct solar hot water systems. Care must be taken while building such a system, though, since the combined weight of the solar collector, storage tank, and water itself can be too much for the supporting roof's architecture. When larger structures than homes, enterprises, or offices employ passive solar hot water systems, there are sometimes many storage tanks used to hold the heated water [67].

The so-called remote thermosyphon system functions similarly to the previous passive direct thermosyphon system, with the exception that the storage tank is hidden inside a roof void or space, dispersing the weight over a larger area and shielding it from the elements. To ensure proper thermosyphoning, the water storage tank's base must be positioned at least one to two feet (300 to 500mm) above the tops of the flat plate collectors. The system's "head height" is another name for this distance.

1.7.3. Indirect Solar Thermal System

In contrast to the preceding thermosyphon system, an indirect hot water system, often referred to as a closed-loop system, employs a heat exchanger independent of the solar flat plate collector to heat the water in the storage tank.

Indirect hot water systems are active systems that need pumps to move the heat transfer liquid from the collector to the heat exchanger in the tank and around the closed-loop system. Instead of only water that is heated and stored off from the primary household hot water supply, the system has an antifreeze solution, often a 50% Glycol/water ratio [68].

The water in the water storage tank receives heat from the antifreeze solution in the collector through the heat exchanger. Either a flat plate exchanger outside the storage tank or a copper coil inside the bottom portion of the storage tank can serve as the heat exchanger.

One of the main benefits of this closed loop indirect heating system is that the antifreeze solution enables year-round operation in regions where the temperature drops below the freezing point. It also guards against the system's collectors being corroded by untreated tap water that contains gases and various dissolved salts.

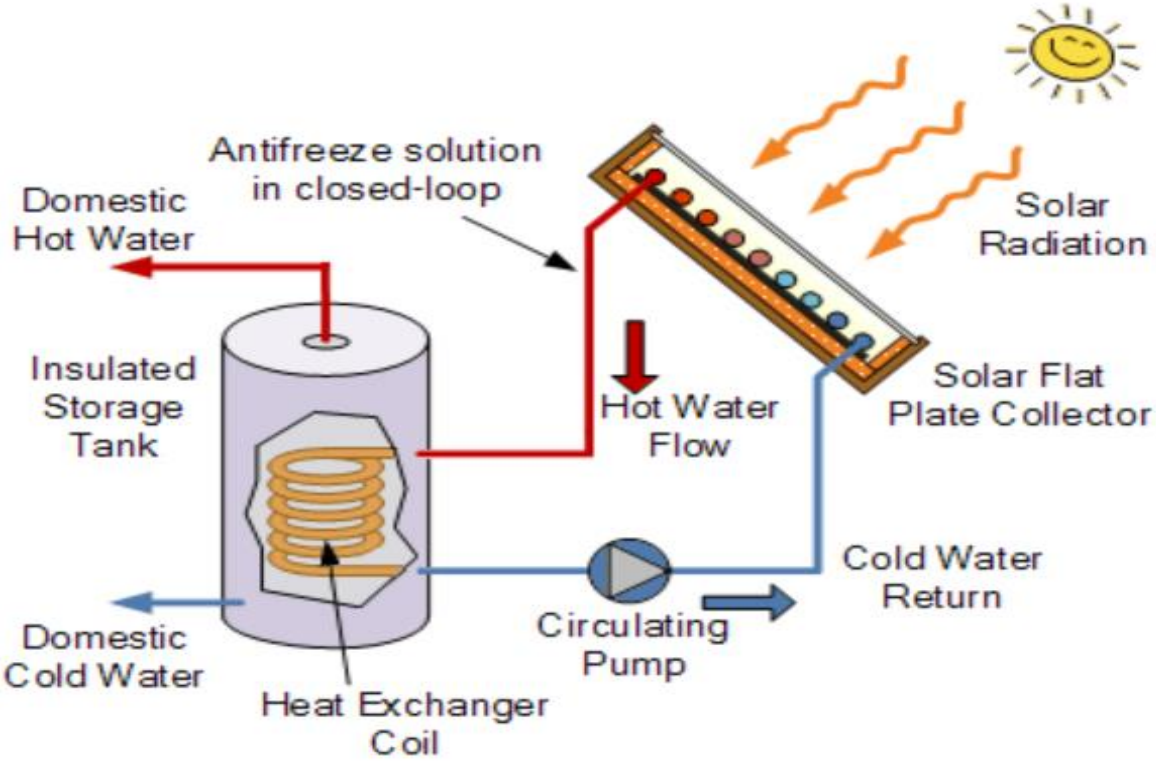

Fig. 9. Indirect Solar Thermal System

As most homes use gas or oil-fired boilers along with a hot water storage tank with built-in heat exchanger coil, the main benefit of a forced circulation indirect hot water system is that an existing domestic water heating system can be easily converted to solar heating of the water just by adding a flat plate collector and a single pump [69].

The hot water storage tank may be positioned anywhere in the house since it does not need to be higher than the collectors as in the prior passive or thermosyphon system, which increases the likelihood that the system will be more efficient.

The closed-loop system's reliance on energy for the circulating pump, which may be costly or unstable, is one drawback. Some designs make the system more effective and

environmentally friendly by adding a modest low voltage pump and solar panel next to the collector. Forced circulation indirect solar water heating is the standard for bigger systems and in cooler areas when hot-water tanks are built within buildings below the roof [70].

There are also some classifications of SWHS bases on concentrating and non-concentrating types of solar collector are shown in fig. 10.

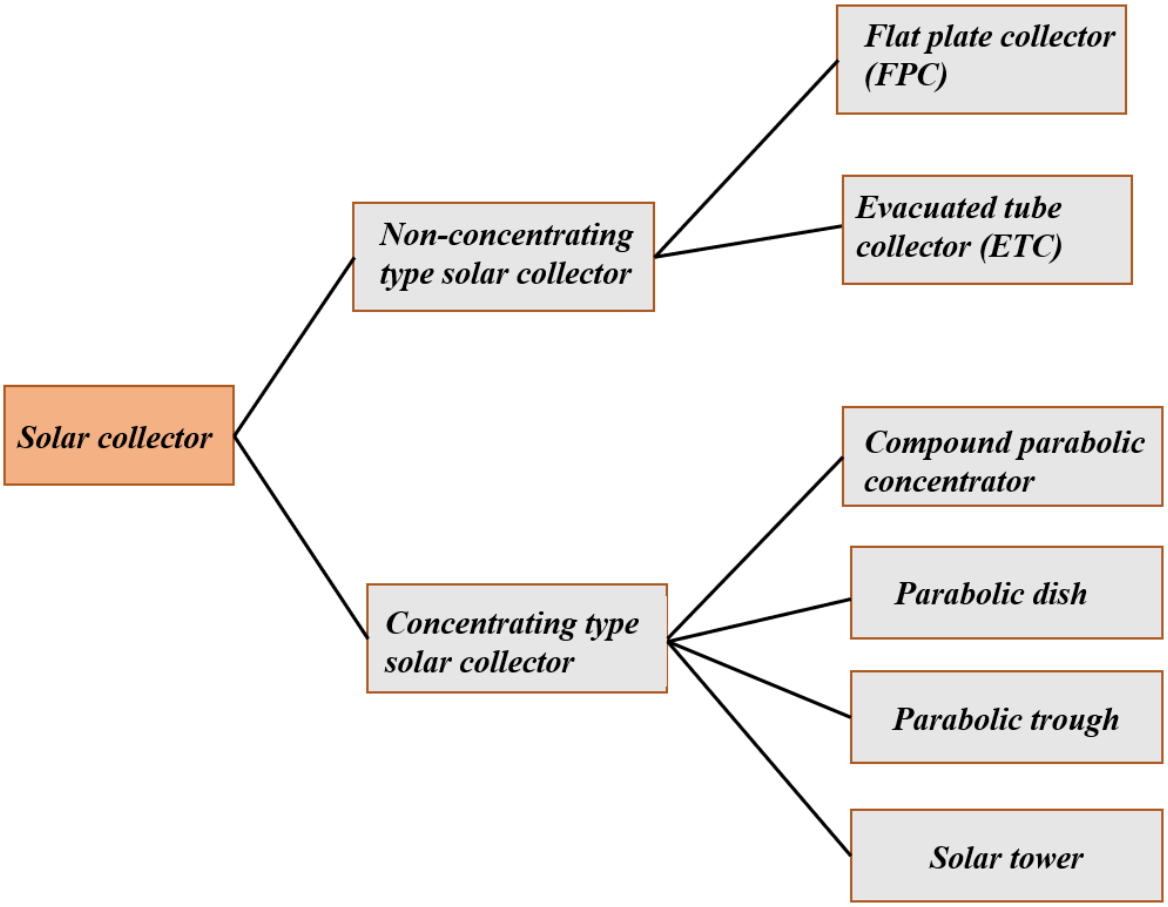

Fig. 10. Classification of solar collector based on concentrating and non-concentrating types

1.8. Preliminaries in Heat Transfer Analysis

Conduction, Convection, and Radiation are the three distinct nodes that make up the heat transmission process.

Conduction: It is the process through which heat is transferred from more energetic particles to their less energy neighbours as a result of particle interactions. Solids, liquids, and gases all

conduct. This phenomena in solids are brought on by the interaction of free electron energy transfer and molecular vibrations in a lattice.

Convection: It is a type of energy transmission mechanism that combines the effects of fluid motion and conduction between a solid surface and a nearby flowing liquid or gas. The fluid moves more quickly the more convectional heat transfer there is. Only the convection method can transfer heat from a solid surface to the nearby fluid.

Radiation: It is the energy that is released by matter as electromagnetic waves (or photons) as a result of modifications to atoms' or molecules' electronic structures. The transport of heat energy does not need the presence of an intermediary medium.

1.9. MOTIVATION AND OBJECTIVE

The main driver of the nation's economic growth and wealth creation is energy, and the availability of resources strongly correlates with economic activity. Because of the considerable developments in contemporary technology, the world's energy consumption is steadily rising. The quest for energy sources is sparked by this. The most accessible and limitless source of energy is solar energy. The conversion of solar energy into heat energy, which is incredibly helpful for thermal applications, is one of the productive methods to use solar energy. Due to its scientific feasibility and the economic allure of using solar energy, SWH has grown to be a well-liked form of solar energy.

Heat is produced when solar light hits the surface of the collector. Solar energy losses originate from irreversible heat transfer between the sun and the collection, between the collector and the surrounding air, and inside the collector itself. Thus, research into energy conversion techniques has greatly increased in importance in recent years. The design parameters of solar water heating systems are therefore expected to be improved by scientific organisations by reevaluating and regenerating energy conversion technologies that are both efficient and affordable. The present non-conventional energy methodologies based on the

first rule of thermodynamics are insufficient to quantify these losses since energy assessment is just a measure of quantity.

However, employing the second law of thermodynamics to change the solar system's design criteria and operational procedures provides a solid foundation for an amazing resolution. Therefore, in order to expand the use of solar energy for home, agricultural, industrial, and commercial purposes, it is required to explore the thermohydraulic performance based on both quality and quantity of energy.

There are many researchers that have investigated the thermal performance of the SWHS by providing the obstacle inside the absorber tube. The introduce of these obstacle technologies enhance the thermal performance of the system with good design and proper installation of these obstacle. The motivation of this study is to provide the thermal performance of the system by using the delta-shape obstacle inside the observer tube. After the experimental examination it was conclude that the heat losses are also one of the major concerns for lower the thermal performance of the system. Therefore, additionally a experimental study is also conducted by using the ecofriendly thermal insulating materials (rice husk, coco-peat, stubble fibre and nitrile rubber) for absorbing the heat from solar radiation on the sunshine hours and release this heat during the off-sunshine hours.

The objective of this study is as follows:

1. The experimental examination of solar water heating system with delta-obstacle for enhance the thermal performance of the system.

2. The utilization of ecofriendly thermal insulating materials (rice husk, coco-peat, stubble fibre and nitrile rubber) for efficiently work of the system during the off-sunshine hours.

3. To optimize the design parameters of a solar water heating system (SWHS) using various Multi-Criteria Decision Making (MCDM) approaches.

CHAPTER 2

LITERATURE REVIEW

2. Introduction

The literature underscores the persistent challenge in augmenting the overall efficiency of Solar Water Heating Systems (SWHS), often hindered by factors such as design parameters and heat losses. Active methods, reliant on external energy sources, pose drawbacks such as increased operating costs due to high-pressure drops in pump systems. In contrast, passive techniques, altering system design or material properties, offer promising avenues for efficiency enhancement. Notably, previous research has explored various passive techniques, including the integration of obstacles within absorber tubes. Among these, delta-shaped obstacles have demonstrated superior performance owing to their increased surface area and generation of vortices. Moreover, perforated delta-shaped obstacles exhibit even higher thermal efficiency gains. Recognizing the complex interplay between design and flow parameters in SWHS, the adoption of Multi-Criteria Decision-Making (MCDM) techniques becomes imperative for optimal system design. While MCDM analyses have predominantly focused on solar air heating applications, their application in solar water heating warrants further exploration. In response, this study proposes an integrated Analytic Hierarchy Process-Analytic Network Process (AHP-ANP) strategy to facilitate SWHS design selection, considering criteria such as Nusselt number, friction factor, and thermo-hydraulic efficiency. By synthesizing earlier SWHS designs and employing the proposed MCDM methodology, this research aims to identify the most promising design alternative offering optimal performance across all evaluation criteria.

2.1 Solar water heater

Pathak et al. (2023) works on the integrated PCMs with nano-enhanced fillers in solar water heater. In their study the author analysed the importance of the nano-enhanced PCMs for the sake of heat storage working medium. The author analysed that the PCMs is consider the best solution for the storage of heat emitted from the solar radiation into useful work. The study also highlights the key issue related to SWH. In addition, they also provide some recommendation associated with PCMs and nano-fillers. The author concludes that PCMs play an important role for thermal enhancement of SWHS.

Li et al. (2023) studied the experimental and simulation work on heat dissipation characteristic of evacuated tube SWH. The ice operation on all glass evacuated tube- SWH encountered the problem of ice damage. The nighttime heat dissipation also reduces the risk of frost damage in the winter times. The enthalpy equation is also introduced in the system for examine the heat dissipation rate. The vacuum tube's bottom is where the icing initially appears, and both the thickness and length of the icing there may reach 1145 mm and 15 mm, respectively. ETSWH is at a significant danger of wintertime frost damage in extremely cold places and frigid regions like Harbin and Beijing. The freezing issue can be effectively resolved, which has important ramifications for the promotion and use of all-glass evacuated tube collectors. It can be done by maintaining the initial working fluid temperature in the heater above 50 C, making sure there is a minimum insulation thickness of 50 mm, and lowering the emissivity of the heater's absorptive coating to below 0.07.

Chopra et al. (2023) studied the thermal and chemical reliability of paraffin wax for the thermal enhancement of SWH. In this work the hot water tank is designed by installing the paraffin wax so that the thermal storage of hot water will take place. It has been examined that by installing the paraffin wax in the tank it can improve the thermal output of the system. The

useful output energy of the system is improved by 36.81 %, 26.97 %, and 22.72 % for Run_40˚C, run_45˚C, and Run_50˚C respectively.

Wang et al. (2023) works on the thermal performance of integrated SWH with paraffin wax and fin height. Phase change materials (PCMs) have been the subject of several theoretical and practical research about the storage of thermal energy. In this work, a square solar water heater uses paraffin with certain qualities as the PCM. The flow of paraffin, whose melting point (MP) is 55 °C, the cause of heat transfer (HT) is temporary and natural convection. This study examined the impact fin geometry, including fin height (H) (3, 4, and 5 cm) and fin number (NoF) (double and threefold), on the heat exchanger's (HE) efficiency was looked into. For different parameters, the contours of temperature (T) and liquid percentage were created. The findings demonstrate that melting 3860 seconds is the time (MT) for scenario A (without fins). Calculations reveal a 71% reduction in MT for scenario B (with 3 fins). At H=3, 4, and 5 cm, the MT decrease is 48, 61, and 74%, respectively.

Yari et al. (2023) experimental investigation of a solar water heater's storage system including a cutting-edge absorber tank with a spherical double wall and a phase-change material was conducted. Water is continuously circulated between the collector and the storage tank throughout the thermal charging process in commercial active solar water heating systems. The water is heated within the collector before being kept in an insulated tank. In the development of solar thermal storage systems, the collector and tank designs are equally important. In this study, the collector and tank are designed as spherical, stationary, symmetrical structures that can monitor the sun's movement no matter where it is in the sky. Additionally, the solar thermal storage tank, which has a double-walled spherical shape, was designed using a novel technique. The inner chamber of this tank is used to retain the hot water from the collector, and the outer chamber contains Phase Change Material (PCM). By

functioning as both thermal insulation and a container for thermal energy, the PCM fulfils a dual function. Importantly, in addition to being an excellent insulator, it can also absorb solar energy from the tank's exterior surface.

The tank is enclosed in a greenhouse-like environment with a clear glass top to reduce heat losses. The system reaches its greatest storage temperature of 80.3°C and its peak thermal efficiency of 74% during the thermal charging phase, which takes place when the flow rate is 1.75 litres per minute. The system can provide enough warm water under these circumstances to cover the demands of 8.43 people on average. At a flow rate of 1.25 litres per minute, the most significant thermal stratification is seen, and when the flow rate is raised, this impact weakens.

Pambudi et al. (2023) experimentally examine the energy efficiency of v-corrugated zinc collector in SWH. Solar water heaters (SWH) offer an economical way to produce hot water for a variety of uses. Therefore, the focus of this study is on the investigation of a modified V-shaped corrugated zinc collector that is combined with an insulating layer constructed of aluminium foil foam, with a 5 mm thick plywood foundation located at the bottom. The studies were carried out in Indonesia's Central Java area, which has a hot temperature. With both passive and open systems, the study especially looked at the effects of varied flow rates, including 120, 180, and 240 litres per hour (Lph). Data was gathered from 8:00 a.m. to 3:00 p.m. at 10-minute intervals.

The study's findings showed that a flow rate of 240 Lph produced the maximum energy efficiency, which reached 50%. Meanwhile, the levels of energy efficiency were 40% and 34%, respectively, at flow rates of 180 Lph and 120 Lph. Furthermore, a peak efficiency of 61% for the collector was noted. These results demonstrated that SWH systems with V-shaped corrugated zinc collectors performed better when greater flow rates were used. As a result, it

is advised to choose V-corrugated collectors since they are affordable and have a 50% energy efficiency rating.

Esmaeili et al. (2023) works on the influence of hybrid nanofluids and turbulators on the thermal improvement of SWH. An efficient method for raising the thermal efficiency of parabolic solar collectors (PTCs) is to simultaneously use turbulators and nanofluids as the operating fluid. In the current study, the effects of adding a turbulator and hybrid nanoparticles on the rates of heat transfer and entropy generation within a parabolic trough collector are explored using a three-dimensional numerical simulation. The study covers two different kinds of turbulators, one of which is innovative. The effects of variables like the Bejan number, thermal entropy, viscous entropy, and friction coefficient are carefully considered.

Heat transmission is increased by 35.7% when conical helical gear rings are used as discs inside the absorber tube as opposed to situations without turbulators. In addition, the development of total entropy is significantly reduced in these cases by 32.8%. Notably, every instance has a Bejan number greater than 0.9, which shows that thermal entropy creation is common.

Ravanbakhsh et al. (2023) studied the 3E thermo-modelling and optimization of turbulator in SWH. In this paper, the author investigates the thermodynamic and financial modelling of a photovoltaic solar system coupled with a single-effect absorption chiller cycle. We take a multi-perspective approach, combining thermodynamics, computational fluid dynamics, and optical analysis. The main goal is to use solar energy to power the absorption chiller cycle, which cools residential structures. Our solar centralization system combines fluid movement to store energy, solar panels to produce power, and energy utilisation within the absorption cycle.

The author closely monitor system pressure decreases and outlet temperatures during our numerical simulations. Our thermodynamic study digs into important performance indicators,

such as the efficiency of the second law of thermodynamics, cooling load, and cooling flow temperatures, as well as the performance coefficient of the absorption chiller cycle.

We compare our results to those acquired by optical analysis and numerical solutions to guarantee their validity. This comparison shows a minimum maximum divergence of 7.6% from the findings of the reference study. For instance, according to computer calculations, the highest heat flux imparted to the water flow reaches 11884 (W/m2) in June, with the peak temperature at T_{out}, CPVT = 368.8 (K). In light of the system's thermodynamic modelling, we determine that the ideal flow rate for CPVT corresponds to m CPVT = 0.15 (kg/s). The Q_{Eva} = 8.509 (kW) cooling demand is met by this specific flow rate while keeping acceptable production coefficients and efficiency levels. Additionally, the overall startup costs are 0.0424 ($/hr) and the energy efficiency is 0.2714 ($/hr), respectively.

Khargotra et al. (2023) studied the design optimization of working parameter of delta-obstacle in SWH. A solar water heating system (SWHS) is an economical technology that has become widely used in homes throughout the globe. However, a number of issues, such as design specifications and heat losses from the system brought on by radiation and convection, can considerably impair SWHS performance and thus lower the system's overall efficiency. Innovative designs and cutting-edge heat transfer methodologies are constantly being investigated to address these problems and improve SWHS efficiency. In this context, the design and optimisation of a SWHS that uses perforated delta barriers is the main focus of our research. Three important parameters including Reynolds number (400, 800, and 1200), angle of attack (set at 15, 30, and 45), and pitch ratio (varying from 0.5 to 2.0)—were studied in order to better understand and optimise the effects they have on crucial variables such as the friction factor, Nusselt number, and thermo-hydraulic performance.

According to results, the Reynolds number of 1200, the angle of attack of 45 degrees, and the pitch ratio of 1 produced the Nusselt number with the greatest value (90.55). The lowest friction factor (0.38) was produced by the combination of Reynolds number = 1200, angle of attack = 15, and pitch ratio = 0.5. It also noted that the Reynolds number of 400, angle of attack of 45, and pitch ratio of 1 resulted in the highest thermo-hydraulic efficiency (2.75).

Negeed et al. (2023) works on the numerical simulation of FPSC fitted with turbulator using nano-fluids for enhancing the thermal performance of the system. Due to its environmental friendliness and consequent reduction in pollutants, the use of solar systems has attracted significant attention from a variety of businesses. For capturing mild heat from the sun, flat plate solar collectors (FPSC) stand out among solar technologies and have several uses in the engineering sector. In this investigation, it was investigating the effects of a novel turbulator with different geometric features and a two-phase Cu-GO/water hybrid nanofluid on the thermal-hydraulic performance, exergy efficiency, and energy efficiency of an FPSC, particularly under turbulent flow conditions. Using the QUICK method, the governing equations are discretized. The volume fraction () fluctuates between 1% and 4%, whereas the Reynolds number (Re) ranges from 17,000 to 47,000. The system is characterised by turbulent flow, which is modelled using the mixed two-phase approach and the RNG k-turbulence model. Additionally, it is also taken into account different turbulator geometries (y = 0.5, 1, 1.5, and 2) located inside the FPSC's absorber tube. The research shows that, compared to a design without a turbulator, adding one to the absorber tube greatly improves the thermal-hydraulic performance. Additionally, it sees that the curvature angle () has a significant impact on the amplification of the pressure drop (p) as well as the rate of heat transfer (HT), with an increase in producing noticeable results.

Poongavanam et al. (2023) studied the performance of the SWH with three approaches i.e., nanofluids, absorber roughness, and surface coating. For the solar water heater (SWH), a surface-modified (resurfacing) absorber plate was produced using the steel shot-blasting procedure. This was the first of three distinct approaches used in this research. Furthermore, synthetic activated carbon nanomaterials (ACNMs) derived from naturally occurring sources were used as coating materials and nanofluids (NFDs) on absorber plates. Additionally, utilising a two-step process, ACNMs and water-based nanofluids (DIW) were created and used as heat transfer media (HTM). Additionally, experimental measurements of the thermal characteristics of DIW-ACNM, including ratios of thermal conductivity (TC), specific heat, viscosity, and density, were made. Zeta potential analysis and SEM analysis were also used to guarantee the colloidal stability of NFDs. The HTM's temperature throughout the SWH was measured at 0, 0.1, 0.25, and 0.4 vol% of ACNMs loading, respectively, to be 7.5, 9.8, 10.6, and 12.04 C. Despite an increase in pressure drop and pumping power of 23.5 and 22.1%, respectively, the thermal efficiency of modified SWH was raised up to 52.7% with a volume fraction of 0.4%. Overall, the SWH performance was greatly enhanced by using ACNM as an NFD, coating material, and shot-blasting on the absorber plate, with a performance augmentation factor of 1.14.

Variyenli et al. (2023) experimentally examine the performance of helically-coiled turbulator for the thermal enhancement of system. Solar water collectors are frequently used to generate hot water for usage in a variety of applications. In order to determine its overall performance, a solar water collector with a helically coiled absorber has been developed, constructed, and tested under various situations. By creating a perpendicular angle between the absorber and the incident solar rays, a tube-type absorber can improve the thermal efficiency of the collection. Additionally, compared to typical solar water collectors, adopting a helically-

coiled construction allows for an increase in absorber surface in a comparatively small volume. A solar radiation model has been used to simulate the planned helically-coiled solar collector in the first stage of this research. Next, three distinct inclination angles and varying water flow rates have been used to experimentally evaluate the constructed helically-coiled solar collector. The mean thermal efficiencies of horizontal, vertical, and angular helically-coiled collectors were found to be in the ranges of 29.48-48.23%, 27.17-47.03%, and 32.50-52.71%, respectively, according to the experimental data. Additionally, sustainability index values of 1.0041-1.0091, 1.0039-1.0087, and 1.0043-1.0102, respectively, were attained for horizontal, vertical, and angular helically-coiled collectors. Furthermore, it was determined that there was a maximum 14% difference between the numerical and experimental results.

Ghanbari et al. (2023) A parabolic trough collector (PTC) is a useful tool for capturing solar heat. Recent years have seen a tremendous increase in academics' interest in improving these devices' efficiency. The goal of the current work was to use a magnetic hybrid nanofluid and a new geometric form of compound turbulator to boost the thermal efficiency in the PTC. In this work, a two-step procedure is used to create the magnetic hybrid nanofluid of MWCNT-Fe3O4-Cu/Water. Then, in the current investigation, a working fluid with its thermophysical characteristics is employed. The examined PTC's absorber tube is fitted with three distinct geometrically designed compound turbulators (Cases A, B, and C). The vertical or horizontal positioning of the geometric forms in Cases A and B is different. By adding the compound turbulator, the fluid particles in the direction perpendicular to the movement channel are also mixed and travel randomly, in contrast to laminar flow where the fluid particles move in layers. The findings of the thermal-hydraulic performance assessment criteria analysis show that the compound turbulator used in the PTC absorber tube always plays a positive role in this study.

The absorber tube with a combination of a compound turbulator and circular coil is connected to the absorber tube with the highest energy efficiency and productivity.

Abdalla and Shahsavar (2023) studied the influence of a rotary propeller type turbulator on the energy and exergy efficiencies of a concentrating photovoltaic/thermal hybrid collector has been mathematically investigated. Photovoltaic/thermal hybrid collectors (PTHCs) are created by fusing solar collectors that can capture heat with photovoltaic panels that can convert solar energy into electricity. These systems perform better than individual photovoltaic panels and solar collectors because solar energy is concurrently transformed into electricity and heat in them. This is why researchers have constantly focused on enhancing these systems' performance. The goal of the current numerical research is to examine how the energy and exergy characteristics of the collector are affected by the use of a rotary propeller type turbulator in a concentrating PTHC (CPTHC). The outcomes are contrasted with information from instances with and without stationary turbulators. Additionally, it was discovered that the useable electrical power, first law electrical efficiency, second law electrical efficiency, and second law overall efficiency of the CPTHC all exhibit an ascending-descending trend as increases, with their greatest values occurring at = 5000 rpm. The case of Re = 20000 and = 10000 rpm had the best total energy efficiency, which was equal to 130.78%, whereas the case of Re = 20000 and = 5000 rpm had the highest exergy efficiency, which was equal to 17.24%.

Bhattacharyya et al. (2017) used twisted tape at various entrance angles to create the solar water heater to improve heat transmission. At various entry angles, the twisted tape is detached from the tube wall. The entry angle and pitch are taken into account while configuring. The entry angle range is considered to be between 180 and 160 and 140 with a range of 100 to 20,000 for the Reynolds number. The CFD analysis is also utilised to verify the superior outcomes. The Nusselt number increases more when using the greater entry angle

(180 degrees) than when using the lower entrance angle, according to the results. The testing findings indicate that the entry angle of 180 degrees and twist ratio of 18.0 produced the greatest rate of heat transmission.

Kulkarni and Deshmukh (2015) designing and conducting an experimental study on the effectiveness of a solar water heater. He describes the water heater's design parameters in this essay. The performance of solar water is also influenced by a number of other elements, including sun irradiation, wind speed, ambient temperature, and solar thermal losses.

Nikam et al. (2016) experimental study examines the V-shaped aluminium turbulator put in a tube for improving heat transmission. The primary goal of this research project is to improve the friction and heat transfer coefficients for V-shaped turbulators. The experiment is run for the plain tube first, and then the absorber tube is equipped with a turbulator. The test section's length is split into three segments of 120 mm, 160 mm, and 200 mm. Utilising aluminium turbulators in the shape of a V, the average heat transmission rate was found to be 198%, 213%, and 241%. The experiment is conducted under various operating conditions depending on the tube diameter, and the Reynolds number ranges from 3000 to 10000.

Yuan (2018) conducted an experiment to study the flow via a circular tube with a ball turbulator. Flow turbulation is one of the most used techniques for increasing heat. This research examines the impact of the ball introduced into the tube as well as the impact on heat transfer characteristics. The Reynolds scale ranges from 5000 to 35,000. The turbulator ball was constructed with varying spacer lengths and diameter ratios. The spacer length varies from 40 mm to 62.5 mm, and the diameter ratio ranges from 0.5 to 1. In comparison to a larger friction ratio, the smaller diameter ratio produced the lower friction ratio.

Ngoka (2008) does experimental research on the straightforward pipe solar water heater. He employed this kind of water heater to provide hot water for residential usage. Solar water heaters in the form of pipes are employed. Following experiments, it was discovered that the efficiency ranges between 85% and 90%.

Balaji et al. (2017) conducted an experimental investigation into the energy, exergy, and environmental analyses of forced convection in solar water heaters. He conducts an experimental investigation into the impact of a heat enhancer in a pipe in this study and contrasts the outcomes with a plain pipe. It has been discovered that the environment's impact is crucial for improving heat transmission. First, the energy, exergy, and economic cost of a solar flat plate collector are examined in this study. According to the exergy study, the rod type heat enhancer has a greater exergy efficiency than a flat plate collector made of a simple tube. The highest energy efficiency for rod-type heat enhancers was determined to be 8.3%, 10.9%, and 11.3%, respectively, when compared to plain-type solar collector.

Khorasani et al. (2018) studied the impact of helical twist turbulators on solar water heater thermal increase. In this paper, he conducts an experimental investigation of the impact of the spire wire turbulator's geometrical characteristics on the water heater. The only sort of turbulator that can be simply put into the tube wall is a spiral wire turbulator. It is necessary to measure both the entrance and output temperatures in order to compute the convective heat transfer coefficient. The findings demonstrate the impact of wire diameter and pitch on heat exchanger thermal enhancement. The Nusselt number can be raised by 70–73% as a result of wire diameter and pitch effects on turbulators.

Balaji et al. (2017) used a velocity enhancer to test the thermal efficiency of a solar water heater. In this study, he uses a passive approach to remove the barrier while conducting an experimental investigation of the thermal performance of a water heater utilising a velocity

enhancer. Increasing the convective heat transfer coefficient while minimising pressure drop and maximising thermal enhancement factor is the major goal of this effort. The engagement factor was destroyed by the velocity enhancer's continued interaction with the thermal boundary layer. It is discovered that the velocity enhancer has a bigger impact on the enhancer configuration than the pumping power, which is at its minimum. When the findings are compared, it is discovered that the velocity enhancer is 10-15% more effective.

Sadhish Kumar and Balusamy (2014) studied the thermal performance of solar water heating systems. He focuses on various testing techniques for improving solar water heaters. It has been discovered that direct solar water heater conversion is 70% more efficient than previous methods. He makes it apparent in this piece that whereas forced circulation is the subject of the majority of study, natural convection systems have received far less attention.

2.2 Salient points from the literature review

The water heating system was improved by the obstruction promoter that was introduced into the absorber tube because it provided a considerably more efficient rate of heat transmission. It is clear from the literature that there aren't as many studies on the usage of corrugations at intake locations to improve stratification in solar water heaters. There is further room for improving stratification in solar water heaters by refining latent heat storage. An organised investigation is required to create an effective SWHS design. Current research also examines how a hindrance promoter affects a solar water heater. The large storage density and isothermal functioning of the turbulator are its key benefits.

It was also examined from the experiment that the design parameters of the working obstacle are not depend on the working parameters that we fix during the experiment. The outcome result will change if we are going to change the objective set of design parameters.

Therefore, it is very important to optimize our working parameters by applying the multi-criteria decision approach. In current research work the author applying the different MCDM approach such as CRITIC-COPRAS and AHP-MEW technique to find out the optimum set of design parameters.

Additionally, it was also examined from the experiment that the heat losses in one of the major concerns in SWHS. Therefore, in this research work an experiment is carried out to examine the influence of the eco-friendly thermal insulation materials to examine their importance and impact on enhancing the heat transfer rate.

2.3 Research gap

After carefully studied the number of research work, we discovered that many researchers employed heat enhancer devices to increase the effectiveness of the collector. In this study, the author experimentally examines the influence of the delta-obstacle by providing the MCDM approach to optimize the design parameters. Besides these, the author also examined that the loss of heat is also the major concern in regard to thermal performance of the system. The author used different type of eco-friendly thermal insulation materials such as Rice husk, coco-peat, stubble fibre and nitrile rubber for making the system ideal.

CHAPTER 3
MATERIALS AND METHODOLOGY

This chapter inside the details description of the fabrication and the design of SWHS with natural circulation system and also describe the mathematical equations that are needed to solve the complex problems. The delta obstacle is used as hindrance promoter for increasing the heating effect. The details description of the SWHS is described below:

3.1 Introduction

A major area of concentration has been on the study of using delta obstacle to improve the thermal performance of solar water heaters. The creation of boundary layers is delicately disrupted by these winglets, enhancing the overall thermal efficiency of solar water heaters. As a result, in compared to other options, they are thought to be the most efficient devices for improving thermal performance. The examination of the experimental technique involving the insertion of delta obstacle into the absorber tube is briefly described in this chapter. It is crucial to carefully study the procedure's specifics through an extensive literature research to ensure the effective execution of the experimental setup. Every element of the experiment is carefully set up with an emphasis on measurement accuracy. Additionally, choosing measuring tools with the least amount of uncertainty has received a lot of attention. In order to avoid any potential setup errors, consideration is also given to the solar water heater's physical design. The computation of measurement uncertainty is also covered in detail in this chapter, and gives a thorough analysis of all the different parts of the experimental setup.

Due to a number of factors, including design specifications and heat losses from radiation and convection, solar water heating systems (SWHS) incur a considerable drop in performance. Researchers are progressively looking at novel designs and distinct heat transfer techniques to increase SWHS efficiency. The current work is concerned with the design and optimisation of

a SWHS that includes perforated and non-perforated delta obstacle. We examined and fine-tuned the effects of several factors on elements like friction factor, Nusselt number, and thermo-hydraulic performance, including Reynolds number, angle of attack, pitch ratio, blockage ration and spacer length. Figure 3.1 (a) and (b) shows the schematic, and real view of the SWHS.

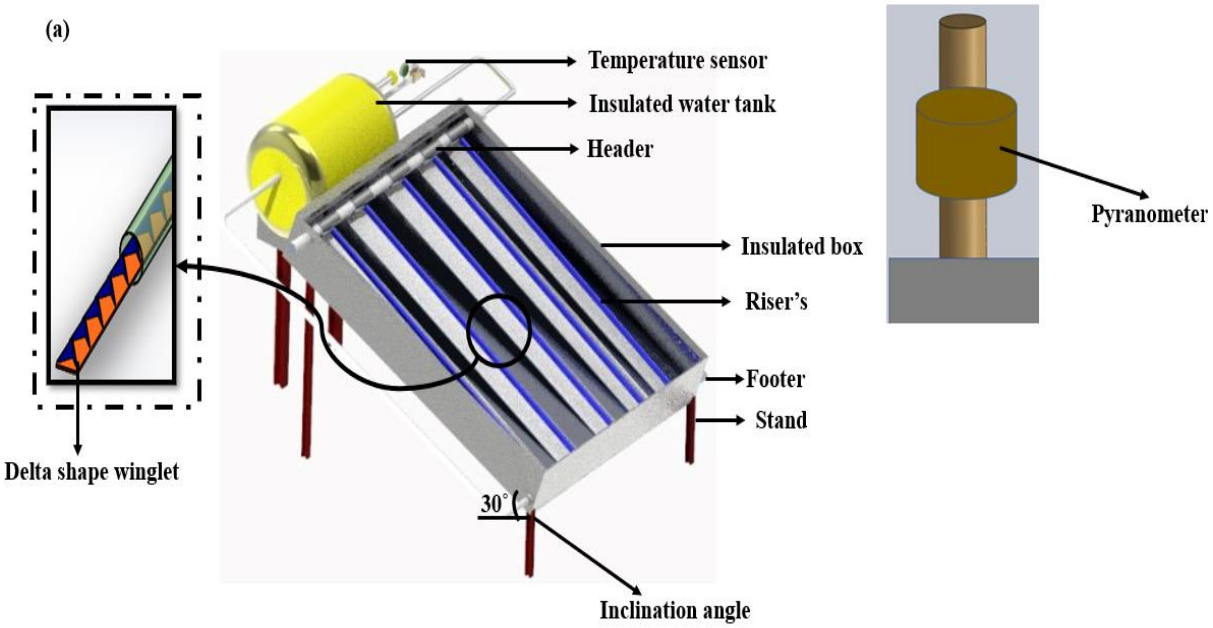

Fig. 3.1 (a) Schematic, and (b) Real view of the SWHS.

Table 3.1. Specification of SWHS.

Specifications	Standards
Type	Flat plate water heater
Testing area	$1m^2$
Glass Thickness	4 mm
Material of glass	Toughened
Inner diameter of tubes	50 mm
Outer diameter of tubes	54 mm
Material of the tube	Copper
Delta-shaped obstacles material	Copper
Lower side insulation	(Rockwool) 50 mm
Reflective insulation	Aluminum foil
Side part insulation	(XP Sheet) 15 mm
Absorbing plate	Aluminum (0.5 mm)

From 10:30 am until 4:30 p. pm, the working fluid was allowed to run through the tubes for six hours. An instrument called a pyranometer is used to evaluate the intensity of sun radiation. A flow metre is used to control and measure the water flow rate. The sun energy is transmitted to the absorber pipe via a single piece of transparent glass with a thickness of 4 mm, helping to raise the temperature of the running fluid. To reduce heat loss from the collector, the collection and absorber tubes are both insulated. The storage tank is entirely emptied each day at the conclusion of data gathering and then filled back up with new water. The SWHS's specifications are displayed in table 3.1.

3. 2 Geometric parameters with hindrance promoter

By employing the hindrance promoter put into the SWHS tubes, the performance of the SWHS was intended to be improved. Inserted obstacles with a delta form generate swirls inside the tube. The delta-winglet breaches the laminar boundary layer along the wall when water enters the tube, enhancing eddy formation and the water's thermal conductivity. Figure 3.3 depicts the

primary stream and the production of the secondary stream as a result of the insertion of a SWHS barrier in the form of a delta. Figure 3.2 (a) and (b) shows the schematic and actual view of delta-shaped obstacles.

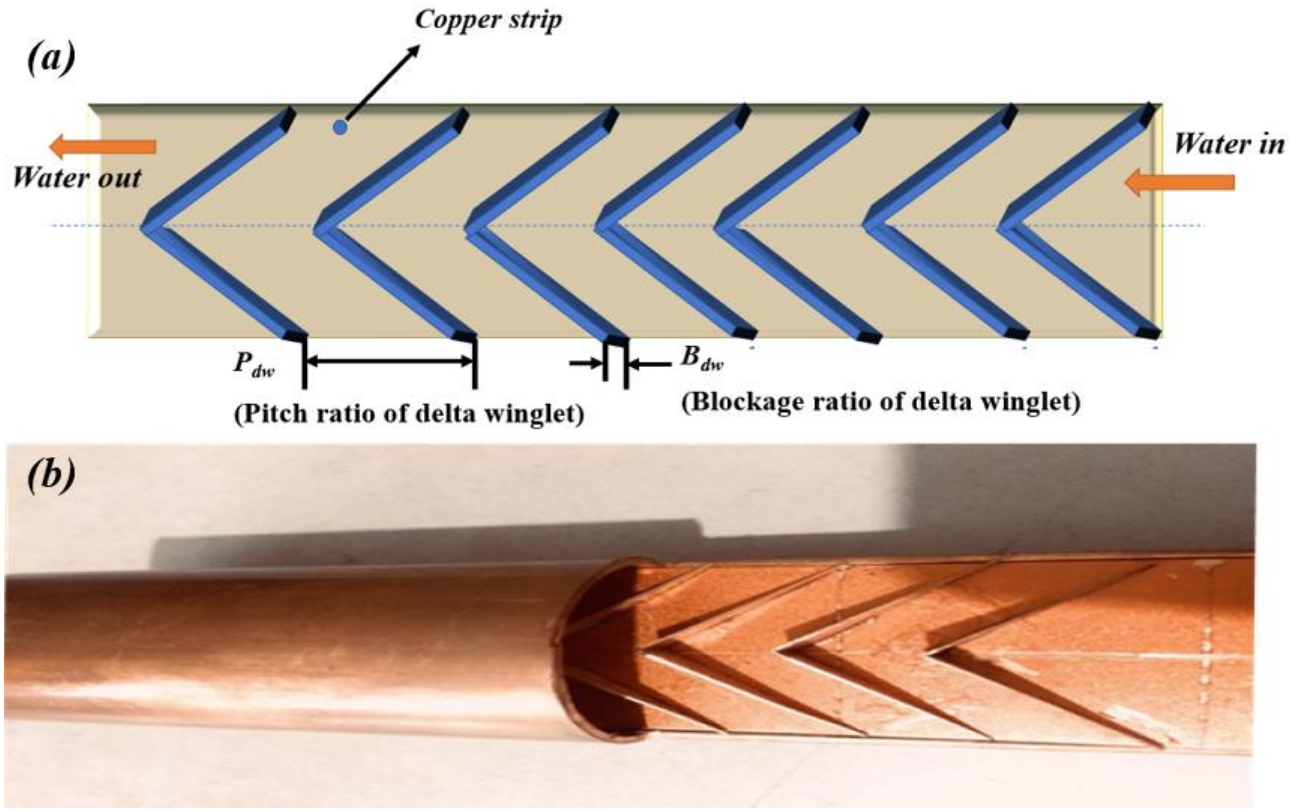

Fig. 3.2. (a) Schematic, and (b) Actual view of delta-shaped obstacles.

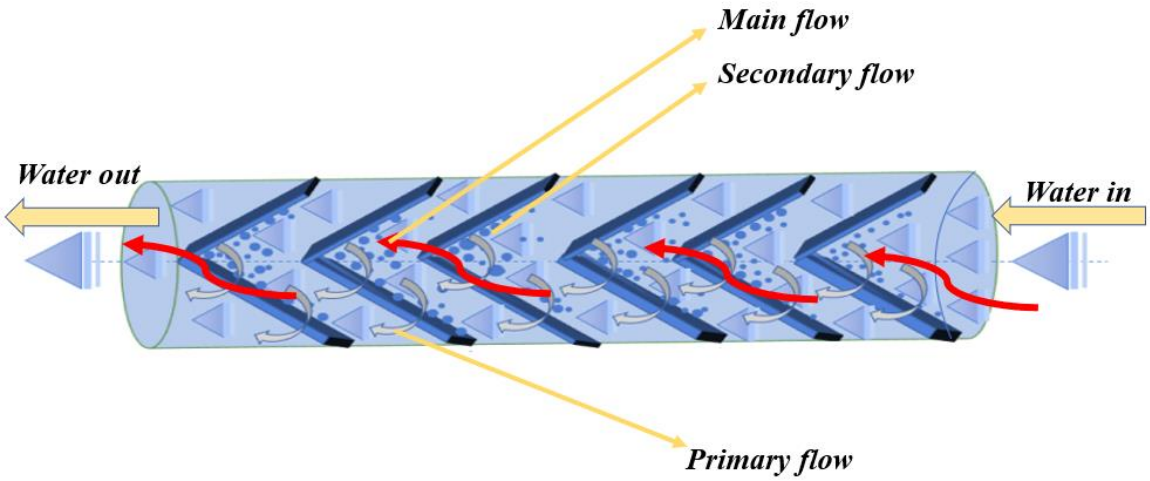

Fig. 3.3. Primary and secondary flow in the tube of SWHS.

Choosing the optimum SWHS design from the available options is difficult since no single SWHS design can satisfy all of the needed performance requirements. To solve this problem, the CRITIC-COPRAS approach for non-perforated delta obstacle and AHP (analytic hierarchy process)-ARAS (additive ratio assessment), a hybrid multi-criteria decision-making technique for perforated delta obstacle was used. The efficiency and dependability of the outcomes from the suggested decision-making framework were then confirmed by sensitivity analysis and validation with other decision-making techniques.

The pitch ratio—which is defined as the ratio of the precise distance between each winglet and the tube's diameter—is one of the geometric characteristics of the delta winglet installed on both sides of the copper strip that is taken into account for the current inquiry. and blockage ratio, which is the proportion of the tube's diameter to the height of the winglet. To determine how friction factor and heat transfer affected the thermal performance of the SWHS, a range of operational and geometrical factors, including Reynolds number (Re; 200, 600, 1000, 1400, 1800), P_{dw} (0.5, 1, 1.5), B_{dw} (0.15, 0.20, 0.25), and fixed angle of attack (α_{dw}=45°), were taken into account.

Table 3.2 Design alternatives for non-perforated obstacle.

	Experimental parameters				Experimental parameters		
Alternatives	*Re*	B_{dw}	P_{dw}	Alternatives	*Re*	B_{dw}	P_{dw}
Alternative-1	200	0.15	0.5	Alternative-14	1400	0.2	1
Alternative-2	600	0.15	0.5	Alternative-15	1800	0.2	1
Alternative-3	1000	0.15	0.5	Alternative-16	200	0.2	1.5
Alternative-4	1400	0.15	0.5	Alternative-17	600	0.2	1.5
Alternative-5	1800	0.15	0.5	Alternative-18	1000	0.2	1.5
Alternative-6	200	0.2	0.5	Alternative-19	1400	0.2	1.5
Alternative-7	600	0.2	0.5	Alternative-20	1800	0.2	1.5
Alternative-8	1000	0.2	0.5	Alternative-21	200	0.25	0.5
Alternative-9	1400	0.2	0.5	Alternative-22	600	0.25	0.5
Alternative-10	1800	0.2	0.5	Alternative-23	1000	0.25	0.5
Alternative-11	200	0.2	1	Alternative-24	1400	0.25	0.5
Alternative-12	600	0.2	1	Alternative-25	1800	0.25	0.5
Alternative-13	1000	0.2	1				

Table 3.3 The selected design alternatives for perforated obstacle.

Alternatives	Re	Angle (α_w)	Pr
Alternative-1	400	15	0.5
Alternative-2	800	15	0.5
Alternative-3	1200	15	0.5
Alternative-4	400	30	0.5
Alternative-5	800	30	0.5
Alternative-6	1200	30	0.5
Alternative-7	400	45	1.5
Alternative-8	800	45	1.5
Alternative-9	1200	45	1.5
Alternative-10	400	45	1
Alternative-11	800	45	1
Alternative-12	1200	45	1
Alternative-13	400	45	2
Alternative-14	800	45	2
Alternative-15	1200	45	2

3.3 Validation of the test setup and uncertainty analysis

Testing was done to validate the experimental setup and determine how accurately it matched the published heat transfer and friction factor formulae. The results of the experimental setting are contrasted with the correlations reported in the literature. Without the presence of any obstructions, the friction factor (f_p) and Nusselt number (Nu_p) of plain tubes were calculated and compared to the original Dittus-Boelter [85] and modified Blassius equation [86].

Dittus-Bolter equation:

$$Nu_p = 0.023\,\mathrm{Re}^{0.8}\,\mathrm{Pr}^{0.4} \tag{3.1}$$

Modified Blasius equation:

$$f_p = 0.316\,\mathrm{Re}^{-0.25} \tag{3.2}$$

Figure 3.4 shows the comparison of the expected and actual values of Nup and fp as a function of Re. The findings from the experiment and those from the conventional equations are within 2-4% of one another, validating the precision of the experimental apparatus. No matter how much care is taken, mistakes can still happen during experiments. As a result, it is crucial to identify any potential errors, which is why Kline and McClintock's method [87] was used to validate the data.

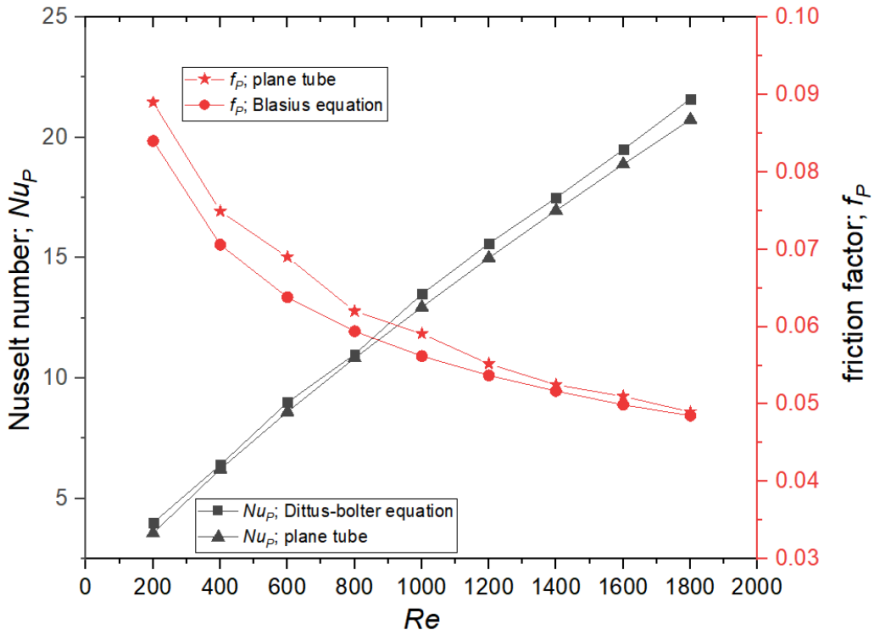

Fig. 3.4. Comparison of experimental and predicted value of Nu_p andf_p.

3.4 Identification of performance criteria and governing equations

Three performance defining parameters, including Nusselt number of tubes with delta-shaped obstacles (Nu_{dw}), friction factor of tube with delta-shaped obstacles (f_{dw}), and thermo-hydraulic efficiency (η_{dw}), have been analysed for the performance of the delta-shaped obstacles in the SWHS. The Nu_{dw} is employed to determine the rate of heat transfer between the flow fluid and the solid body, and the f_{dw} stands in for the pressure loss experienced by the fluid inside the pipe as a result of contact with the fluid. The hindrance promoter is used by the scientist to compare the performance of the SWHS to that of the plain tube SWHS. The ideal properties of a SWHS are often greater Nu_{dw} and η_{dw} values with a lower f_{dw} value.

Table 3 and 4 show the instrumental and experimental error respectively. The equations used in the calculation of selected criteria values are given below.

The *Re* is calculated by the following equation.

$$\mathrm{Re} = \frac{\rho_w u D_p}{\mu} \tag{3.3}$$

Where ρ_w is water density, u is speed of flow and D_p is pipe diameter.

The f_w value is calculated using the pipe length (L_p), the pipe inner diameter (D_i), and the pressure drop (Δp) using the following equation:

$$f_w = \frac{\Delta P}{\left(\frac{L_p}{D_i}\right)\left(\frac{\rho_w u^2}{2}\right)} \tag{3.4}$$

The heat gain (Q_w) is determined using the inlet (T_{in}) and outlet (T_{out}) temperatures from the flow of water as follows:

$$Q_w = m_w C_p (T_{out} - T_{in}) \tag{3.5}$$

The heat transfer coefficient is calculated by using the equation below:

$$h_w = \frac{Q_w}{A_{ht}(T_w - T_f)} \tag{3.6}$$

A_{ht} is the surface area of the heated tube, T_w is the wall temperature of tube and T_f is the fluid bulk temperature.

The Nusselt number is calculated as:

$$Nu_{dw} = \frac{h_w D_i}{k_w} \tag{3.7}$$

The thermo-hydraulic efficiency is determined using the following equation:

$$\eta_{dw} = \frac{Nu_{dw}}{Nu_p} \Bigg/ \left(\frac{f_{dw}}{f_p}\right)^{0.33} \tag{3.8}$$

Table. 3.4 Uncertainty intervals of various measurements.

PARAMETER	EQUIPMENT/ INSTRUMENT	ACCURACY
Solar Intensity	Pyranometer	±0.5 W/m^2
Length	Linear scale	$\pm 1mm$
Temperature measurement	Digital type	±1˚C
Pressure measurement	Pressure gauge	±0.1 (Pa)
Pipe Diameter	Varnier caliper	±0.05 mm

Table. 3.5 Experimental error.

Sr.No.	**PARAMETER**	**Symbols**	**Unit**	**Experimental error (%)**
1	Area of flow pipe	A_{fp}	m^2	0.002%
2	Area of heated tube	A_{ht}	m^2	0.12%
3	Determination of density	ρ_w	Kg/m^3	0.15%
4	Mass flow rate	m_w	kg/s	0.25%
5	Useful heat gain	Q_w	W	2.2%
6	Heat transfer coefficient	h_w	W/m^2k	2.2%
7	Nusselt number	Nu_w	Dimensionless	2.2%
8	Reynolds Number	Re	Dimensionless	0.27%
9	Friction factor	f_w	Dimensionless	1.22%
10	Thermal hydraulic performance parameter	η_{dw}	Dimensionless	3.43%

Additionally, it is also examined that the heat losses are one of the major concerns in the solar collector. There are various ways in which the heat losses will take place due to conduction,

convection and radiation. The researcher used the toughened glass in order to minimize the heat losses and helps in adverse climatic conditions. In order to ensure the lower heat losses from the collector, it is very important to have the better thermal insulation from the side and bottom of the system. Insulation materials are designed to absorb solar radiation, capturing and retaining heat from the sun. This enhances the energy efficiency of buildings and reduces the reliance on heating and cooling systems [88]. These materials are typically installed in walls, roofs, and floors of buildings, and can be made from a range of materials, including fibreglass, cellulose, foam board, and reflective coatings [89]. One common type of insulating material that are used for solar radiation absorption is spray foam insulation, which is made from a mixture of liquid chemicals that expand and harden into a solid foam. Spray foam insulation provides an air-tight seal and high insulation value, making it an effective way to reduce heat loss and gain through walls and roofs. Other types of insulation materials, such as reflective coatings, are designed to reflect solar radiation away from buildings, reducing the amount of heat that is absorbed by the building envelope. By incorporating insulation materials that can absorb or reflect solar radiation, buildings can be made more energy-efficient and environmentally friendly. Traditionally, insulating materials like rock wool, ceramic wool, glass wool, polyurethane foam, etc. are utilized to reduce these heat losses [90]. Even though there is much high-performing thermal insulation on the market, these materials nevertheless face a number of difficulties, including costs, mechanical and thermal qualities, and health issues. Thermal insulation is an essential component of many buildings, helping to reduce energy consumption and improve indoor comfort. However, some insulation materials can pose health hazards if they are not handled or installed properly. One such material is asbestos, which was commonly used as insulation until the 1970s when its health risks were discovered. Asbestos fibers can become airborne when insulation is disturbed or damaged, and when inhaled, can lead to serious respiratory diseases, including lung cancer and mesothelioma.

Other insulation materials, such as fibreglass, can also cause respiratory irritation if inhaled in large quantities. To minimize the risk of health hazards, it is important to use insulation materials that are non-toxic and safe for human exposure, and to follow proper handling and installation procedures. These typical thermal insulations produce harmful compounds throughout the design, manufacture, and implementation process in the form of mineral fiber and synthetic binder dust or other air pollution or hazardous waste creation. Figure 3.5 shows the detailed representation of S-FPC.

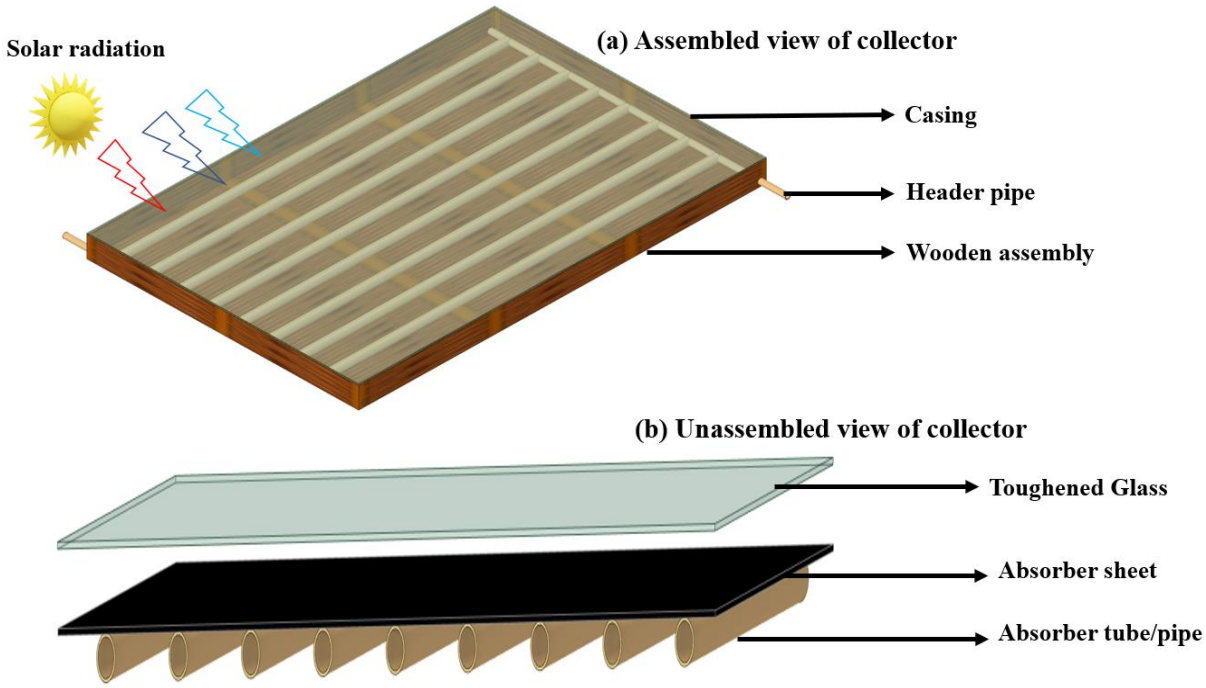

Fig. 3.5 Detailed representation of S-FPC.

In this experimental work, a study is also conducted to examine the importance of the eco-friendly insulating materials for solar thermal collector. The different type of insulating biodegradable materials that are used in this research work are rice waste, coco peat, stubble waste and nitrile rubber as a naturally occurring biodegradable and eco-friendly easily available waste materials.

These dried insulating materials are then prepared for the experimental examination. In this experimental examination nitrile rubber play a very crucial role for the preparation of the thermal insulating materials. Nitrile rubber exhibits high thermal resistance, making it suitable for insulation applications where heat retention or insulation against extreme temperatures is required. Now the Nitrile rubber is prepared according to the collector size. The three different nitrile sheets are prepared with three different Insulating materials coco peat, rice waste and stubble waste. These insulating materials are fix on the upper surface of the nitrile sheet and after that put again the nitrile sheet on the upper surface of it. Then there a sandwich type of three insulating sheet is prepared for the experimental examination. The actual view of this sheet is shown below. Figure 3.6 (b) illustrate the preparation of a sandwich insulating sheet using nitrile rubber with various types of insulating materials.

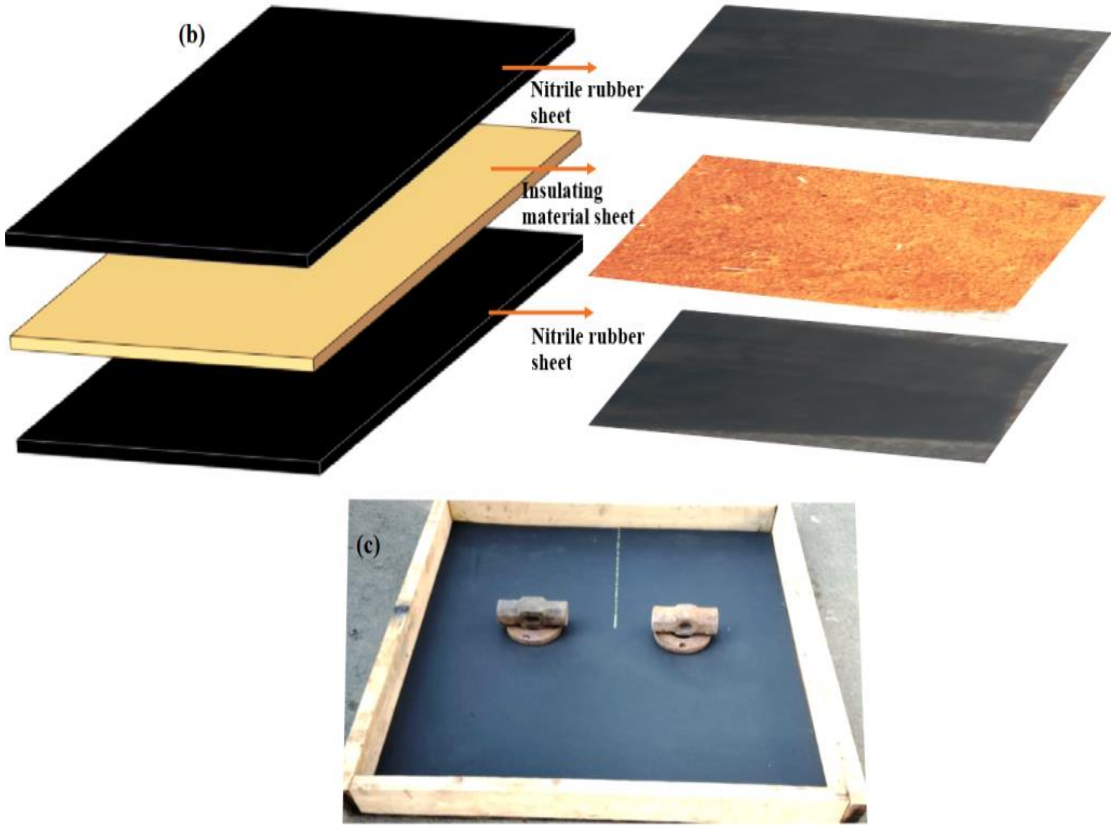

Fig. 3.6. (a) Open dried insulating materials; (b) illustrate the preparation of a sandwich insulating sheet, and (c) Prepared sandwich insulating sheet.

The prepared sandwich sheet is then fixed inside the collector. In the experiment, a weight of 80 kg was applied to the prepared sandwich nitrile rubber sheet of coco peat; rice husk and stubble waste are shown in Figure 3.6 (c). This weight was kept in place for 48 hours. Subsequently, the weight was removed, and the mixture was dried under direct sunlight for a period of 5 days. These insulation sheets were then installed in the casing of the S-FPC to prevent heat loss from the bottom of the system.

3.5 Performance assessment of an S-FPC

Insulation produced from coco-peat, stubble fibre and rice husk were used in the SWHS, and its performance was evaluated under controlled settings to ensure it met ISO standards. Prior to the evaluation, a visual inspection of the SC was performed to identify any signs of cracks. The riser and header pipes were subsequently filled with water to ensure there was no leakage

of water. Throughout the tests, a constant flow rate of 0.02 l/s of cold water at the inlet were maintained. The pyranometer is used to measure the I_s. This particular device is capable of accurately measuring solar radiation levels up to 2000 W/m^2. The various measuring instrument used in this experimental work are Linear scale, thermocouple, pressure gauge and vernier clipper etc. Figure 3.7 show the schematic representation of S-FPC using thermal insulating materials.

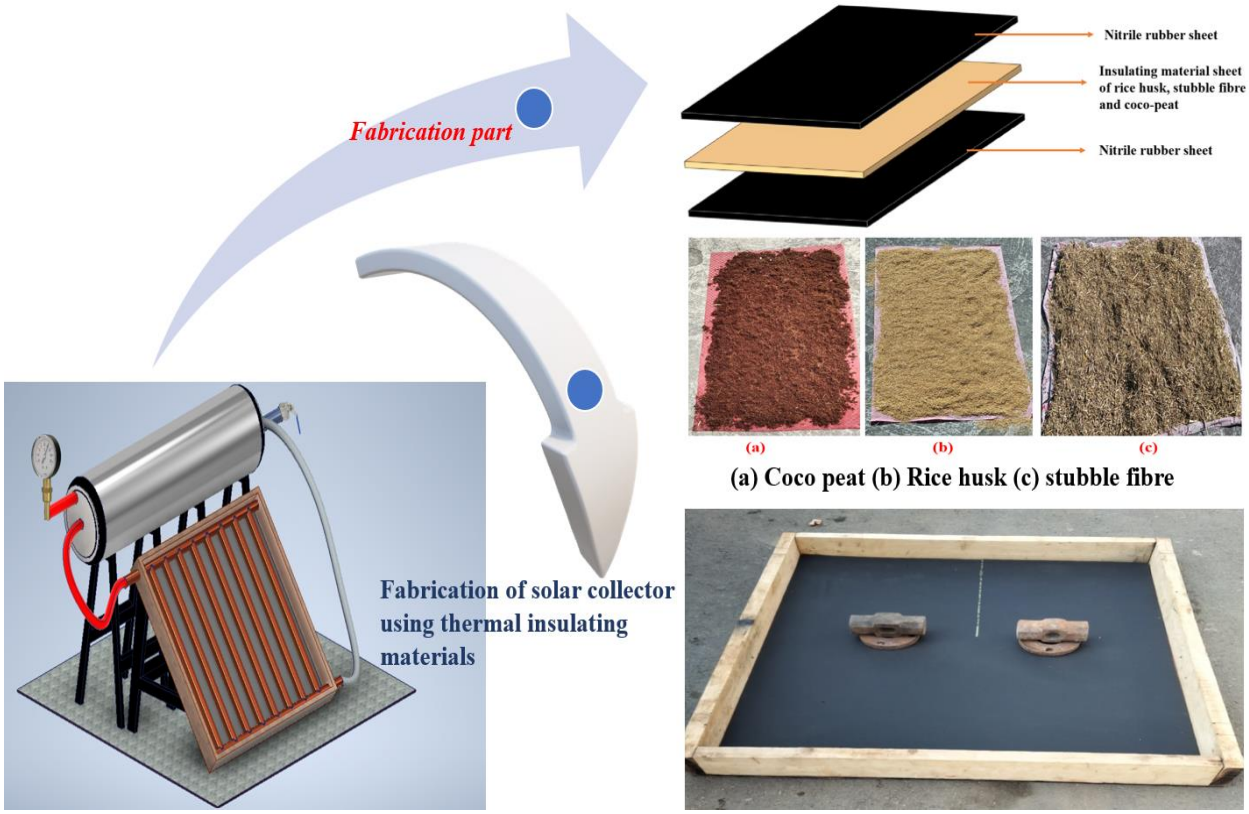

Fig. 3.7 Schematic representation of S-FPC using thermal insulating materials.

The S-FPC (solar flat plate collector) water heating system's effectiveness was assessed in diverse weather conditions by employing specifically designed insulation materials. To gauge the system's performance, various factors were measured, including the water's mass flow rate, the temperatures of the fluid at the inlet/outlet, the collector area, and the I_s. The efficiency of S-FPC (denoted as η) is calculated using the subsequent formula.

$$\eta = \frac{Q_u}{I} = \frac{\dot{m}C_p(T_{fo}-T_{fi})}{A_c I_s} \quad (3.9)$$

In the equation provided by [30], the solar collector efficiency (η), expressed as a percentage, is determined by several variables. These variables include the useful heat output (Qu) in watts (W), the mass flow rate (ṁ) in kilograms per second (kg/s), the specific heat capacity of water (CP) in joules per kilogram per degree Celsius (J/kg˚C), the gross collector area (A_c) in square meters (m^2), the incident global solar radiation (I_s) in watts per square meter (W/m^2), and the fluid outlet temperature (T_{fo}) and inlet temperature (T_{fi}) in degrees Celsius (˚C).

CHAPTER 4
RESULTS AND DISCUSSIONS

4. Introduction

This chapter discuss the experimental details of SWH by using the delta obstacle. On based on these experimental results we are applied the different MCDM approach with perforated and non-perforated delta obstacle. The CRICTIC-COPRAS optimization technique is applied to non-perforated delta obstacle and AHP-ARAS optimization technique is applied to perforated delta obstacle. Beside these the author also examined the importance of the heat losses control by using the different types of eco-friendly insulating materials in solar thermal collector. The importance of the different eco-friendly insulating materials such as rice husk, coco-peat and stubble fibre are experimental studied in details. The details result of the MCDM approach for perforated and non-perforated delta obstacle and experiments results for eco-friendly insulating materials are discussed in details in this chapter. The result part is divided into three main classes:

1. CRITIC-COPRAS MCDM optimization approach applies on non-perforated delta obstacles.

2. AHP-ARAS MCDM optimization approach applies on perforated delta obstacles.

3. Experimental examination of eco-friendly insulating materials to analyse their impact on heat transfer characteristics.

4.1 Case I: CRITIC-COPRAS MCDM optimization approach applies on non-perforated delta obstacles.

Proposed Methodology

Figure 4.1 depicts the overall algorithm of the suggested MCDM model employed in this study. The suggested model is divided into three phases (Table 4.1), which are:

Phase 1: Alternatives, criterion, and performance matrix

Phase 2: CRITIC method

Phase 3: COPRAS method

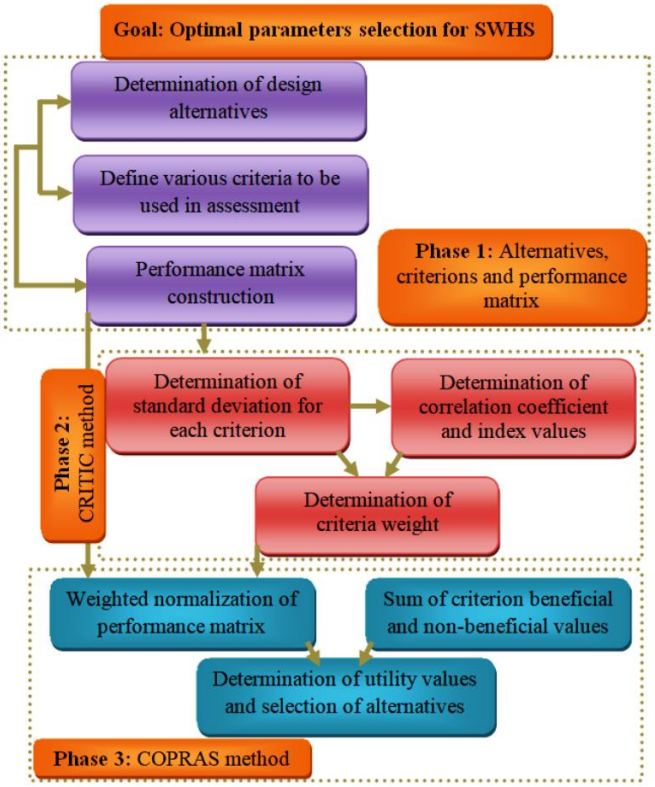

Fig. 4.1 Structural design of the proposed methodology.

Table 4.1 Various parts of proposed MCDM model.

Criterion			
C_1	C_2	…	C_λ
Weight			
ω_1	ω_2	…	ω_λ

Alternatives					Ranking
	Performance matrix				
A_1	p_{11}	p_{12}	$\cdots$	$p_{1\lambda}$	Ω_1
A_2	p_{21}	p_{22}	$\cdots$	$p_{2\lambda}$	Ω_2
$\cdots$	$\cdots$	$\cdots$	$\cdots$	$\cdots$	$\cdots$
$A_\hbar$	$p_{\hbar 1}$	$p_{\hbar 2}$	$\cdots$	$p_{\hbar\lambda}$	$\Omega_\hbar$

Phase 1: Alternatives, criterion, and performance matrix

For any decision-making problem a performance matrix must be first formulated for the selected design alternatives and performance criteria. For $\hbar$ alternatives and λ criteria, a performance matrix can be structured as follows:

$$p_{\hbar\times\lambda} = \begin{array}{c} \\ A_1 \\ A_2 \\ \vdots \\ A_i \\ \vdots \\ A_\hbar \end{array} \begin{array}{c} \begin{array}{cccccc} C_1 & C_2 & \cdots & C_j & \cdots & C_\lambda \end{array} \\ \begin{vmatrix} p_{11} & p_{12} & \cdots & p_{1j} & \cdots & p_{1\lambda} \\ p_{21} & p_{22} & \cdots & p_{2j} & \cdots & p_{2\lambda} \\ \vdots & \vdots & \cdots & \vdots & \cdots & \vdots \\ p_{i1} & p_{i2} & \cdots & p_{ij} & \cdots & p_{i\lambda} \\ \vdots & \vdots & \cdots & \vdots & \cdots & \vdots \\ p_{\hbar 1} & p_{\hbar 2} & \cdots & p_{\hbar j} & \cdots & p_{\hbar\lambda} \end{vmatrix} \end{array} \tag{4.1}$$

$A_i \left(A_i, i = 1, 2, \cdots, \hbar\right)$ is the i^{th} alternative, $C_i \left(C_j, j = 1, 2, \cdots, \lambda\right)$ is the j^{th} criterion, while p_{ij} denotes the i^{th} alternative value with respect to the j^{th} criterion.

Phase 2: CRITIC method

The CRITIC method, developed by Diakoulaki et al. [91], is generally utilized to determine the attributes weight in a decision-making problem. Generally, the procedure of CRITIC method includes the following steps: -

Step I: Data normalization, where the structured performance matrix was normalized using the following equation.

$$\nabla_{ij} = \frac{p_{ij} - \min(p_j)}{\max(p_j) - \min(p_j)}, \text{ if } j \text{ is favourable criterion and}$$

$$\nabla_{ij} = \frac{\max(p_j) - p_{ij}}{\max(p_j) - \min(p_j)}, \text{ if } j \text{ is non-favourable criterion} \quad (4.2)$$

Step II: Correlation coefficient (χ_{jk}), a correlation value is determined between two criterion using following equation:

$$\chi_{jk} = \frac{\sum_{i=1}^{\hbar}\left(\nabla_{ij} - \overline{\nabla_j}\right)\left(\nabla_{ik} - \overline{\nabla_k}\right)}{\sqrt{\sum_{i=1}^{\hbar}\left(\nabla_{ij} - \overline{\nabla_j}\right)^2 \sum_{i=1}^{\hbar}\left(\nabla_{ik} - \overline{\nabla_k}\right)^2}} \quad (4.3)$$

where $\overline{\nabla_j}$ and $\overline{\nabla_k}$ are the mean of compared j^{th} and k^{th} criterion, computed as follows:

$$\overline{\nabla_j} = \frac{1}{\lambda}\sum_{j=1}^{\lambda}\nabla_{ij}; \quad i = 1, \cdots, \hbar \quad (4.4)$$

Step III: Calculation of standard deviation (ρ_j), where ρ_j is determined using following equation.

$$\rho_j = \sqrt{\frac{1}{\lambda - 1}\sum_{j=1}^{\lambda}\left(\nabla_{ij} - \overline{\nabla_j}\right)^2}; \quad i = 1, \cdots, \hbar \quad (4.5)$$

Step IV: calculation of criterion performance index value (ε_j), according to the following equation:

$$\varepsilon_j = \rho_j \sum_{j=1}^{\lambda}\left(1 - \chi_{jk}\right); \quad j = 1, \cdots, \lambda \quad (4.6)$$

Step V: In the last step the criterion weights are calculated using the following equation:

$$\omega_j = \frac{\varepsilon_j}{\sum_{j=1}^{\lambda}\varepsilon_j}; \quad j = 1, \cdots, \lambda \quad (4.7)$$

Phase III: COPRAS method

In COPRAS the ranking is described though relative significance of alternatives with different criterion which was proposed by Zavadskas et al. [92]. The various steps associated with COPRAS method are described as follow:

Step I: Normalization of the performance matrix is performed by using following equation.

$$\aleph_{ij} = \frac{p_{ij}}{\sum_{i=1}^{\hbar}\left(p_{ij}\right)} \quad i = 1, 2, \cdots, \hbar \text{ and } j = 1, 2, \cdots, \lambda \tag{4.8}$$

Step II: Weighted normalized performance matrix (ϖ_{ij}) formulated using following equation.

$$\varpi_{ij} = \aleph_{ij} \times \omega_j \quad i = 1, 2, \cdots, \hbar \text{ and } j = 1, 2, \cdots, \lambda \tag{4.9}$$

Step III: The sum of weighted normalized performance matrix is computed according to the implication of the criterion as:

$$\left.\begin{aligned} \phi_{+i} &= \sum_{j=1}^{\lambda} \alpha_{+ij} \\ \phi_{-i} &= \sum_{j=1}^{\lambda-\lambda} \alpha_{-ij} \end{aligned}\right\} \tag{4.10}$$

Where λ and $\lambda - \lambda$ are the criteria to be maximized and minimized.

Step IV: The relative importance of the design alternatives (Ω_i) determined in this step using following equation.

$$\Omega_i = \phi_{+i} + \frac{\sum_{i=1}^{\hbar}\phi_{-i}}{\phi_{-i}\sum_{i=1}^{\hbar}\frac{1}{\phi_{-i}}} \tag{4.11}$$

Step V: The absolute priority of the alternatives is finding in terms of utility values using following equation.

$$\Phi_i(\%) = \frac{\Omega_i}{\Omega_{\max}} \times 100 \qquad \text{for i} = 1, 2, \ldots, \hbar \tag{4.12}$$

Where Ω_{max} is the upmost relative importance value. The absolute priority of the alternatives remains in between 0-100% and the design alternative with highest absolute priority is the most suited design.

4.1.1 Experiment results

4.1.1.2 Effect of parameters on performance criteria

The experimental results of the investigated SWHS alternatives in terms of selected criteria are presented in Table 4.2 and depicted in Figs. 4.2-4.4. Where C-1, C-2 and C-3 represent nusselt number, friction factor and thermo-hydraulic efficiency respectively and 'A' represent alternative.

Table 4.2 Experimental data of the alternatives.

Alternatives	C-1	C-2	C-3	Alternatives	C-1	C-2	C-3
A-1	18.60	0.718	2.47	A-14	68.80	0.641	1.77
A-2	37.20	0.618	2.07	A-15	79.80	0.635	1.63
A-3	50.20	0.561	1.82	A-16	16.07	0.720	2.25
A-4	62.50	0.543	1.69	A-17	35.10	0.610	1.98
A-5	72.30	0.534	1.57	A-18	48.10	0.560	1.77
A -6	20.10	0.928	2.91	A-19	60.09	0.541	1.63
A -7	43.30	0.816	2.55	A-20	69.80	0.535	1.52
A -8	61.00	0.763	2.36	A-21	21.80	0.923	2.75
A -9	76.60	0.746	2.20	A-22	43.60	0.811	2.25
A-10	90.90	0.734	2.12	A-23	63.50	0.758	2.08
A-11	17.31	0.820	2.41	A-24	79.50	0.741	1.93
A-12	39.61	0.710	2.12	A-25	93.50	0.731	1.83
A-13	55.73	0.660	1.89				

From the experimental results, it can be inferred that the flow and geometric parameter combinations of *Re*, P_{dw} and B_{dw} have a significant effect on the evaluated performance characteristics of SWHS. For the alternative set of A-1 to A-5 (Table 4.2, Fig. 4.2), the *Re* varies from 200-1800 while the B_{dw} and P_{dw} values are fixed at 0.15 and 0.5, respectively. The

outcome shows that the value of the Nu_{dw} increases from 18.60 for alternative A-1 to 72.30 for alternative A-5. This enhancement in Nu_{dw} is credited to properly mixing the fluids at this particular range of B_{dw} and P_{dw}. As the B_{dw} changed from 0.15 to 0.2 (alternatives A-6 to A-10), an enhancement of ~8-26% in Nu_{dw} was recorded and remained between from 20.10 to 90.90. For increased B_{dw} from 0.15 to 0.2, the flow rate of fluid increases. With this increased flow, the fluid particle gets maximum congregation and carries heat along the pipe's boundary that's helps to yield optimum heat.

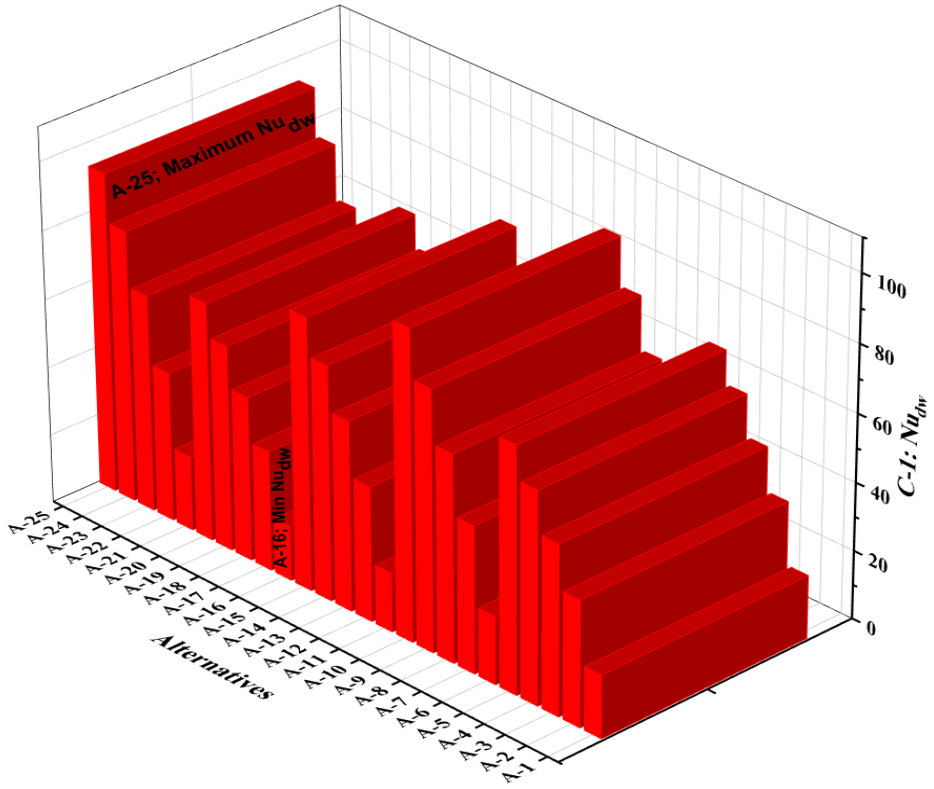

Fig. 4.2. Variation of Nu_{dw} (C-1) with alternatives.

Furthermore, the P_{dw} changed from 0.5 to 1 for alternatives A-11 to A-15; a gradual decrease of ~12-14% in Nu_{dw} was recorded, further reducing by ~7-12% as the P_{dw} changed from 1 to 1.5 for alternatives A-16 to A-20. This low heat transfer with increased pitch ratio was described to the increased distance between the two consecutive winglets. With increased distance, fluid does not create swirl generation, resulting in a low heat transfer rate. The highest range heat transfer rate was recorded for the alternatives A-21 to A-25, having *Re* of 200-1800, B_{dw} of 0.25 and P_{dw} of 0.5. The fluid-particle mixes properly inside the pipe and absorb heat

from the surface of the tube. The fluid gets favourable time to flow from one end to another and create the vortex generation along the face of the winglet and gain maximum heat. The minimum and maximum Nu_{dw} values of 16.07 and 93.50 were recorded for A-16 and A-25, respectively. The results of f_{dw} are presented in Fig. 4.3. The figure revealed that the f_{dw} was found to decrease with increased *Re* values. For alternatives A-1 to A-5 (*Re* = 200-1800, B_{dw}=0.15, P_{dw}=0.5) the f_{dw} was decreased from 0.718 for A-1 to 0.534 for A-5. This may be understandably attributed to the retardation of the flowing fluid is not enough to create friction at this particular range of alternative.

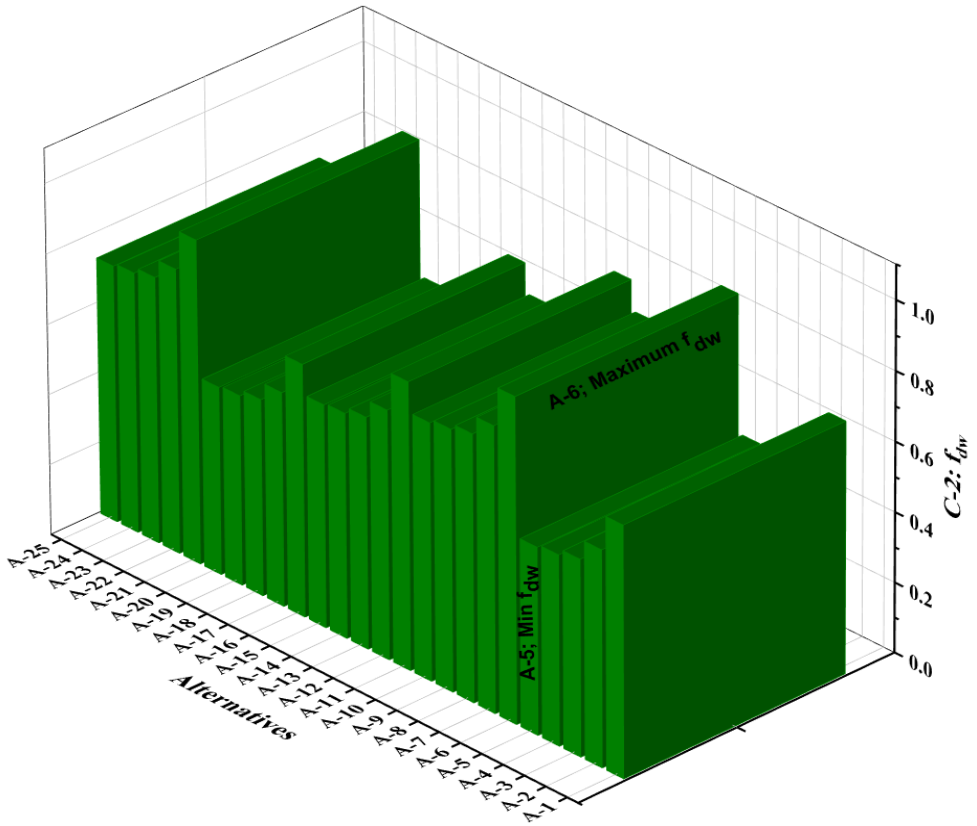

Fig. 4.3. Variation of f_{dw} (C-2) with alternatives.

As the B_{dw} increased to 0.20 for the exact condition of *Re* and P_{dw}, a gradual increase in f_{dw} was noted in alternatives A-6 to A-10 and remained between 0.734 and 0.928. As the B_{dw} is increased the fluid gets large surface area of the winglet to create the friction along the path. The lowest and highest f_{dw} values of 0.534 and 0.928 were recorded for A-5 and A-6, respectively. With a further increase in B_{dw} to 0.25 (alternatives A-21 to A-25), a slight decrease

in f_{dw} was recorded for the same conditions of *Re* and P_{dw}. This might be ascribed to the height of the winglet is large witch restrict the flow rate of fluid and resulted in lower friction rate. Compared to alternatives A-6 to A-10, the value of f_{dw} was found to decrease as the P_{dw} changed from 0.5 to 1 for alternatives A-11 to A-15. With a further increase in P_{dw} to 1.5 (alternatives A-16 to A-20), the f_{dw} decreased further to 0.535-0.720. As the P_{dw} is increased the fluid hindrance rate between two consecutive winglets is less which interns create a low friction rate. Also, the η_{dw} which evaluates the overall performance improvement of the SWHS was computed using Eq. 3.8 and depicted in Fig. 4.4.

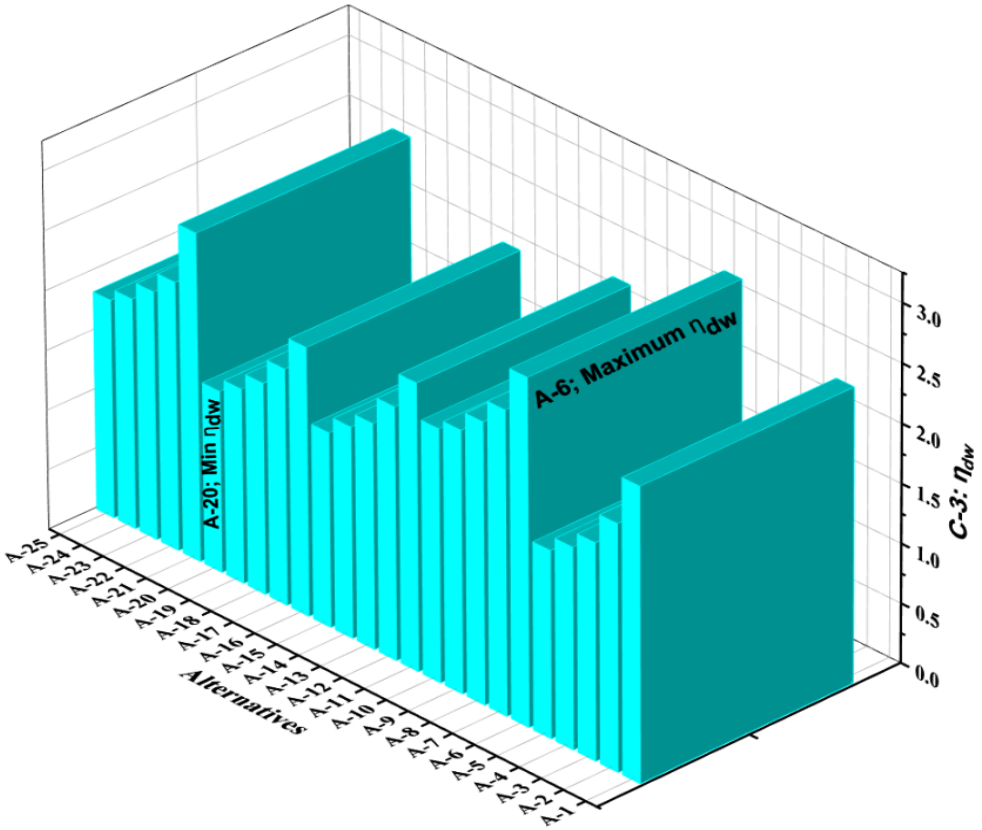

Fig. 4.4 Variation of η_{dw} (C-3) with alternatives.

It can be evident from Table 4.2 and Fig. 4.4 that with an increase in *Re* from 200 to 1800, at a constant B_{dw} of 0.15, P_{dw} of 0.5 (i.e., alternatives A-1 to A-5), the η_{dw} decreases. However, as the B_{dw} increased to 0.20, a steep increase of 18-35% in η_{dw} was noted for alternatives A-6 to A-10 and remained between 2.12-2.91. With a further increment in B_{dw} to 0.25, the η_{dw} decreased for alternatives A-21 to A-25 and fluctuated between ~1.83-2.75. As the P_{dw}

increased from 0.5 to 1, η_{dw} decreased by 17-23% and fluctuated between ~1.63-2.41. With a further increase in P_{dw} to 1.5, a decrement in η_{dw} was recorded for alternatives A-16 to A-20. The smallest η_{dw} was registered for alternative A-20 with Re = 1800, B_{dw} = 0.2 and P_{dw} = 1.5. Whereas the maximum η_{dw} value of 2.91 was recorded for the alternative A-6 having Re of 200, B_{dw} of 0.20 and P_{dw} of 0.5. At this range of P_{dw}, the fluid gets maximum hindrance with the delta-shaped obstacles. The final performance of SWHS depends upon the combination of design and flow parameters such as; Re, P_{dw} and B_{dw}. The optimal combination of these parameters contributes to enhancing device performance in terms of working criteria of Nu_{dw}, f_{dw} and η_{dw}. For efficient working of SWHS, higher values are preferred for Nu_{dw} and η_{dw}, whereas a lower value is desirable for f_{dw}. As indicated in Table 4.2 and Figs.4.2-4.4, the results of the evaluated criteria are found to be intensely dependent on the combination of design parameters and without any pronounced trend. The Nu_{dw} of alternative A-25 was higher (93.5), but its η_{dw} remains on the lower side (1.83). The f_{dw} of alternative A-25 was lowest (0.534) among all investigated design alternatives, but it exhibits the second-lowest η_{dw} value (1.57). Conversely, the η_{dw} value remains highest (2.91) for alternative A-6, but it exhibits the highest f_{dw} (0.928) value with a smaller Nu_{dw} value of 20.10. The results uncover no particular design alternative that shows the best performance by considering all criteria simultaneously. Hence, it is difficult to suggest a design alternative for the SWHS to deliver the highest performance. Accordingly, to pick the best design candidate by considering all criteria together, the COPRAS approach coupled with the CRITIC method was implemented.

4.1.1.3 CRITIC method for criteria weight calculation

The solar water heater design selection problem consists of three criteria and twenty-five alternatives, as presented in the form of a performance matrix in Table 4.2 using Eq. 4.1. In hybrid COPRAS-CRITIC approach, the criterion weight has great significance. The criterion weights are computed by using CRITIC method. The method was initiated by normalizing the

performance matrix by using Eq. 4.2. Thereafter, the normalized matrix was used to calculate the correlation coefficient (χ_{jk}) and standard deviation (ρ_j) values using Eq. 4.3 and Eq. 4.5, respectively. After calculating the performance index value (ε_j) using Eq. 4.6 the criterion weight was determined using Eq. 4.7. The results obtained from CRITIC method are summarized in Table 4.3. The order of criterion weight was obtained as C-3 (0.3970) >C-2 (0.3137) >C-1 (0.2893).

Table 4.3 Results of CRITIC method.

	Criteria		
	C-1	C-2	C-3
ρ_j	0.3020	0.2944	0.2663
ε_j	0.6867	0.7447	0.9426
ω_j	0.2893	0.3137	0.3970

4.1.1.4 COPRAS approach for final ranking

After criterion weight calculation COPRAS approach was implemented to find the combination of design and flow parameters with optimal device performance. For ranking analysis, the performance matrix was first normalized by applying Eq. 4.8 and presented in Table 4.4.

Table 4.4 Normalized performance matrix.

Alternatives	C-1	C-2	C-3	Alternatives	C-1	C-2	C-3
A-1	0.0041	0.013	0.0190	A-14	0.0150	0.0116	0.0136
A-2	0.0081	0.0112	0.0159	A-15	0.0174	0.0115	0.0125
A-3	0.0110	0.0101	0.0140	A-16	0.0035	0.0130	0.0173
A-4	0.0136	0.0098	0.0130	A-17	0.0077	0.0110	0.0152
A-5	0.0158	0.0097	0.0121	A-18	0.0105	0.0101	0.0136
A -6	0.0044	0.0168	0.0224	A-19	0.0131	0.0098	0.0125
A -7	0.0095	0.0147	0.0196	A-20	0.0152	0.0097	0.0117
A -8	0.0133	0.0138	0.0182	A-21	0.0048	0.0167	0.0212
A -9	0.0167	0.0135	0.0169	A-22	0.0095	0.0147	0.0173
A-10	0.0198	0.0133	0.0163	A-23	0.0139	0.0137	0.0160
A-11	0.0038	0.0148	0.0186	A-24	0.0174	0.0134	0.0149
A-12	0.0086	0.0128	0.0163	A-25	0.0204	0.0132	0.0141
A-13	0.0122	0.0119	0.0145				

Next step was to obtain the weighted normalized performance matrix (ϖ_{ij}) by using Eq. 4.9. After that sum of weighted normalized performance matrix values was computed according the implication of the criterion using Eq. 4.10. The sum of weighted normalized (ϕ_{+i} and ϕ_{-i}) values were associated with the performance implication (larger-is-better and smaller-is-better) of the selected criteria. The relative importance of the alternatives (Ω_i) was computed using Eq. 4.11 while the absolute priority of the alternatives is determined in terms of utility values (Φ_i) using Eq. 4.12. The computed Ω_i , Φ_i values and ranking of the alternatives are tabulated in Table 4.5. It was evident that the utility value (Φ_i) for the design alternative A-10 has the highest performance (100%) which is closely followed by design alternative A-25 with a performance of 96.85%. Whereas for design alternative A-16, the utility value was 68.49% and found to remains lowest. Therefore, the hybrid COPRAS-CRITIC analysis showed that the design alternative A-10 with parameters *Re* =1800, B_{dw}= 0.2 and P_{dw}=0.5 is considered as the best design for solar water heating application.

Table 4.5 The ranking of the alternatives.

Alternatives	Ω_i	Φ_i	Ranking	Alternatives	Ω_i	Φ_i	Ranking
A-1	0.0349	73.32	23	A-14	0.0418	87.82	10
A-2	0.0377	79.20	17	A-15	0.0432	90.76	6
A-3	0.0402	84.45	13	A-16	0.0326	68.49	25
A-4	0.0423	88.87	9	A-17	0.0368	77.31	20
A-5	0.0437	91.81	5	A-18	0.0393	82.56	16
A -6	0.0359	75.42	21	A-19	0.0413	86.76	11
A -7	0.0395	82.98	15	A-20	0.0427	89.71	7
A -8	0.0426	89.50	8	A-21	0.0352	73.95	22
A -9	0.0450	94.54	3	A-22	0.0372	78.15	18
A-10	0.0476	100.00	1	A-23	0.0411	86.34	12
A-11	0.0328	68.91	24	A-24	0.0438	92.02	4
A-12	0.0369	77.52	19	A-25	0.0461	96.85	2
A-13	0.0396	83.19	14				

4.1.1.5 Sensitivity analysis

Furthermore, the sensitivity analysis of the proposed CRITIC-COPRAS approach was conducted by generating new weights, and their effect on the changes in the rankings of the alternatives was analysed. This sensitivity analysis has been performed by decreasing and increasing a criterion weight in three steps (±5%, ±10% and ±15%). The weight ratios of the other criteria were obtained concerning the proportionality that the total weight of all the criteria equal one. Figure 4.5 shows the alternative's ranking with a change in the weights of the selected criteria for sensitivity analysis.

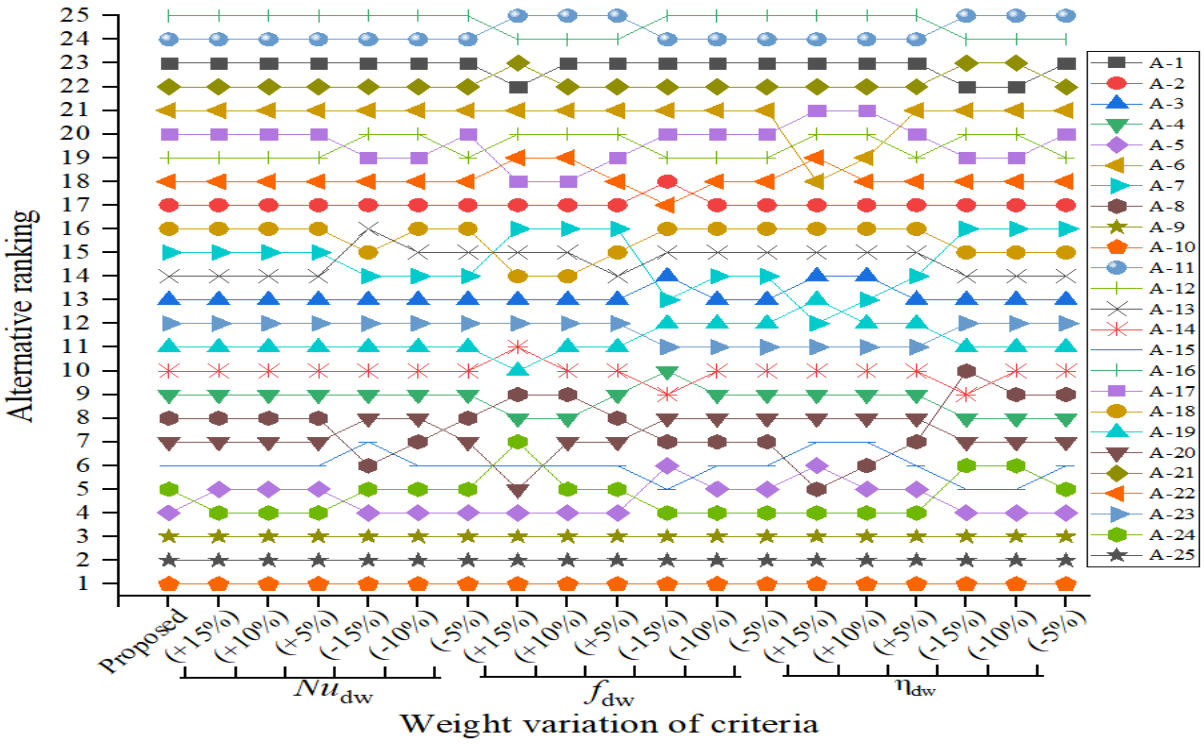

Fig. 4.5 Sensitivity analysis.

Analyzing the data presented in Fig. 4.5, it can be concluded that the alternative A-10 remains first-ranked, whereas the alternatives A-25 and A-9 remain the second-and third-ranked in the sensitivity analysis. After that, some sensitivity in the ranking was observed as the alternatives swap places. However, these changes do not significantly affect the final results of the proposed CRITIC-COPRAS approach, as the target was to find out the optimal alternative from a pool

of available alternatives. In all analyzed scenarios, alternative A-10 remains dominant. The sensitivity results were also confirmed by the Spearman correlation coefficient value, which was greater than 0.983 in all scenarios, indicating a high correlation. As a result, it can be concluded that the proposed ranking is valid and reliable.

4.2. Case II. AHP-ARAS MCDM optimization approach applies on perforated delta obstacles Overview of integrated AHP-ARAS method

An integrated AHP-ARAS approach has been developed in this work for ranking the best SWHS alternatives. The proposed method's algorithm is depicted in 4.6. The approach involves AHP to determine SWHS criteria weight and the ARAS method to determine the best SWHS alternative.

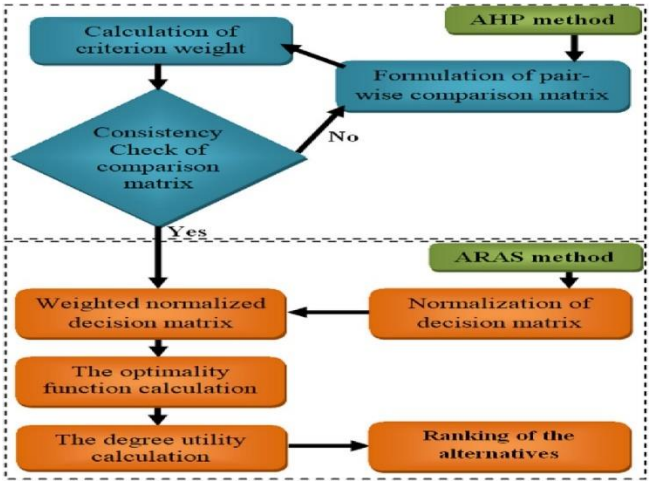

Fig. 4.6. Algorithm of proposed AHP-ARAS method.

Table 4.6 The selected design alternatives.

Alternatives	*Re*	α_{dh}	P_{dh}	Alternatives	Re	α_{dh}	P_{dh}
A_1	400	15	0.5	A_9	1200	45	1.5
A_2	800	15	0.5	A_{10}	400	45	1
A_3	1200	15	0.5	A_{11}	800	45	1
A_4	400	30	0.5	A_{12}	1200	45	1
A_5	800	30	0.5	A_{13}	400	45	2
A_6	1200	30	0.5	A_{14}	800	45	2
A_7	400	45	1.5	A_{15}	1200	45	2
A_8	800	45	1.5				

4.2.1 AHP method for weight calculation

AHP is a well-recognized MCDM tool widely applicable for prioritizing and selecting sub-criteria, criteria, and alternatives using a comparison matrix [93]. This method's main advantages include the ease of handling tangible and intangible criteria and a consistency check to validate the final judgments. The AHP approach is utilized in this study to determine the weight of specified criteria for SWHS selection. For this, a pair-wise comparison matrix is constructed using a standardized comparison scale of 9 points [93]. For N criterions $\left(C_j,\ j=1,\ 2,\cdots,\ N\right)$ the pair-wise comparison matrix $\left(\mathrm{P}_{NN}\right)$ is constructed as:

$$\mathrm{P}_{NN}=\begin{array}{c} \\ C_1 \\ C_2 \\ \vdots \\ C_N \end{array}\begin{array}{c} \begin{array}{cccc} C_1 & C_2 & C_3\cdots & C_N \end{array} \\ \begin{bmatrix} p_{11} & p_{12} & p_{13}\cdots & p_{1N} \\ p_{21} & p_{22} & p_{23}\cdots & p_{2N} \\ \vdots & \vdots & \vdots & \vdots \\ p_{N1} & p_{N2} & p_{N3}\cdots & p_{NN} \end{bmatrix} \end{array} \quad p_{ij}=1 \,if\, i=j,\ p_{ji}=\frac{1}{p_{ij}},\ p_{ij}\neq 0 \qquad (4.13)$$

Normalization of the geometric mean method is used to determine the weight (w_j) of each criteria as [94];

$$\omega_j=\frac{\left\{\prod_{j=1}^{N} p_{ij}\right\}^{\frac{1}{N}}}{\sum_{i=1}^{q}\left\{\prod_{j=1}^{N} p_{ij}\right\}^{\frac{1}{N}}} \quad i=1,2,\cdots,N \qquad (4.14)$$

It is reported in the literature that AHP superiority is firmly related to the consistency of the pair-wise comparison outcomes. The consistency ratio (CR) is computed as,

$$\mathrm{CR}=\frac{\text{Consistenc y index (CI)}}{\text{Random Iindex (RI)}} \qquad (4.15)$$

Here RI value is decided according to the order of the constructed pair-wise comparison matrix [93]. The CI value is determined using following equation,

$$\mathrm{CI}=\frac{\lambda_{\max}-N}{\mathrm{N}-1} \qquad (4.16)$$

Here N is the number of criteria and λ_{max} is the maximum eigenvalue.

Suppose the calculated CR value is equal to or less than the recognized limit of 0.1. In that case, it shows that the evaluation within the matrix is appropriate or that the comparison judgments expressed in that matrix have a suitable level of consistency. If the CR value is more than 0.1, the pair-wise comparison matrix is recreated to increase consistency.

4.2.2 ARAS method

Zavadskas et al. [92] present the ARAS (additive ratio assessment) technique, which has proven to be a more effective tool for prioritizing and ranking diverse alternatives in various engineering and management areas. The ARAS technique has been used to efficiently manage complex and ambiguous decision-making situations by estimating the utility degree for each alternative and considering the selected criteria' optimal value. After utilizing AHP to evaluate the weights for each selected criterion, ARAS analysis calculates the utility degree values for each selected option. The ARAS approach has a total of five steps in its mathematical version:

Step I: Creation of a decision matrix

Here the selected alternatives and criteria are expressed in the form of a decision matrix. Generally, a decision matrix (U) for any MCDM problem with M alternatives $\left(A_i \middle| i = 0,1,2,\cdots, M\right)$ to be evaluated by N criteria $\left(C_j \middle| j = 1, 2,\cdots, N\right)$ is constructed as:

$$U = \begin{array}{c|cccccc} & C_1 & C_2 & \cdots & C_j & \cdots & C_N \\ A_0 & u_{01} & u_{02} & \cdots & u_{0j} & \cdots & u_{0N} \\ A_1 & u_{11} & u_{12} & \cdots & u_{1j} & \cdots & u_{1N} \\ \vdots & \vdots & \vdots & \ddots & \vdots & \ddots & \vdots \\ A_i & u_{i1} & u_{i2} & \cdots & u_{ij} & \cdots & u_{iN} \\ \vdots & \vdots & \vdots & \ddots & \vdots & \ddots & \vdots \\ A_M & u_{M1} & u_{M2} & \cdots & u_{Mj} & \cdots & u_{MN} \end{array} \tag{4.17}$$

An element u_{ij} of the decision matrix signifies the performance score of the i^{th} alternative, A_i with respect to the j^{th} criterion, C_j. Also, the u_{0j} in the decision matrix indicates the optimal value of j^{th} criterion and determined using following equations.

$u_{0j} = Max(u_{ij})$, if j ∈ beneficial criterion

$u_{0j} = Min(u_{ij})$, if j ∈ non-beneficial criterion

Unlike other MCDM methods, the ARAS technique provides a line of optimal values in the initial matrix for each criterion.

Step II: Decision matrix normalization

For comparative analysis following formulae are used for matrix normalization:

$$\Re_{ij} = \frac{u_{ij}}{\sum_{i=0}^{M} u_{ij}}, \text{ if j} \in \text{beneficial criterion} \tag{4.18}$$

$$\Re_{ij} = \frac{\frac{1}{u_{ij}}}{\sum_{i=0}^{M} \frac{1}{u_{ij}}}, \text{ if j} \in \text{non-beneficial criterion} \tag{4.19}$$

Step III: Weighted normalized decision matrix

In this step weighted normalized decision matrix was obtained using the following equation.

$$\varpi = \begin{vmatrix} \varpi_{01} & \varpi_{02} & \cdots & \varpi_{0j} & \cdots & \varpi_{0N} \\ \varpi_{11} & \varpi_{12} & \cdots & \varpi_{1j} & \cdots & \varpi_{1N} \\ \vdots & \vdots & \ddots & \vdots & \ddots & \vdots \\ \varpi_{i1} & \varpi_{i2} & \cdots & \varpi_{ij} & \cdots & \varpi_{iN} \\ \vdots & \vdots & \ddots & \vdots & \ddots & \vdots \\ \varpi_{M1} & \varpi_{M2} & \cdots & \varpi_{Mj} & \cdots & \varpi_{MN} \end{vmatrix} \tag{4.20}$$

Where, $\varpi_{ij} = \Re_{ij} \times \omega_j$

Step IV: Optimality function calculation

The optimality function (Ψ_i) of each alternative is determined using the weighted matrix as follows:

$$\Psi_i = \sum_{j=1}^{N} \varpi_{ij} \tag{4.21}$$

The value of the optimality function of the i[th] alternative is denoted by Ψ_i. The highest Ψ_i value is regarded as the best, while the lowest Ψ_i value is regarded as the worst.

Step V: Utility degree calculation

The process is finished in the final step by computing the utility degree (Ω_i) and determining the ranks. According to the following equation, Ω_i is derived by comparing the optimality function of the alternatives (Ψ_i) to the optimality degree of the best decision option (Ψ_0):

$$\Omega_i = \frac{\Psi_i}{\Psi_0} \tag{4.22}$$

The candidate with the highest Ω_i is suggested as the optimum alternative.

4.2.3 Experiment results

4.2.3.1 Angle of attack and pitch ratio impact on thermal performance

The angle of attack (α_{dh}) plays a vital role in the thermal enhancement of the system. The experiments are performed at three α_{dh}=15°, 35°, and 45°. The experimental outcomes show that different α_{dh} gives different heat transfer rates. It was concluded from the results that at α_{dh}=45°, the system displays an optimum heat transfer rate. The surface area of the delta obstacle has sufficient so that the flowing fluid comes in contact with this winglet and carries away the maximum heat. At α_{dh}=15°, the secondary fluid stream generation caused by the transversality of the obstacle in the fluid channel is less, which results in substantially less heat transfer enhancement. The analysis can be evident with the help of Fig. 4.7. The effect of the P_{dh} is also analyzed with the help of Fig. 4.8. The space between each winglet is sufficient for

fluids with greater P_{dh} to generate the maximum amount of swirl, which speeds up the rate of heat transfer. As P_{dh} decreases to 0.5, the flow reattachment does not happen, resulting in low heat transfer rate.

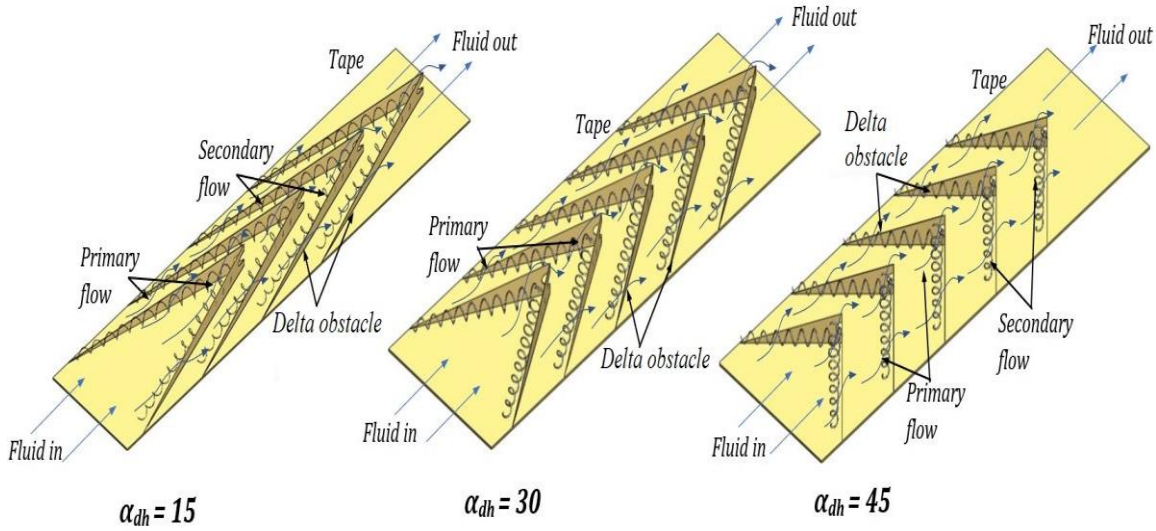

Fig. 4.7 Schematic representation of delta obstacle with different angles of attack.

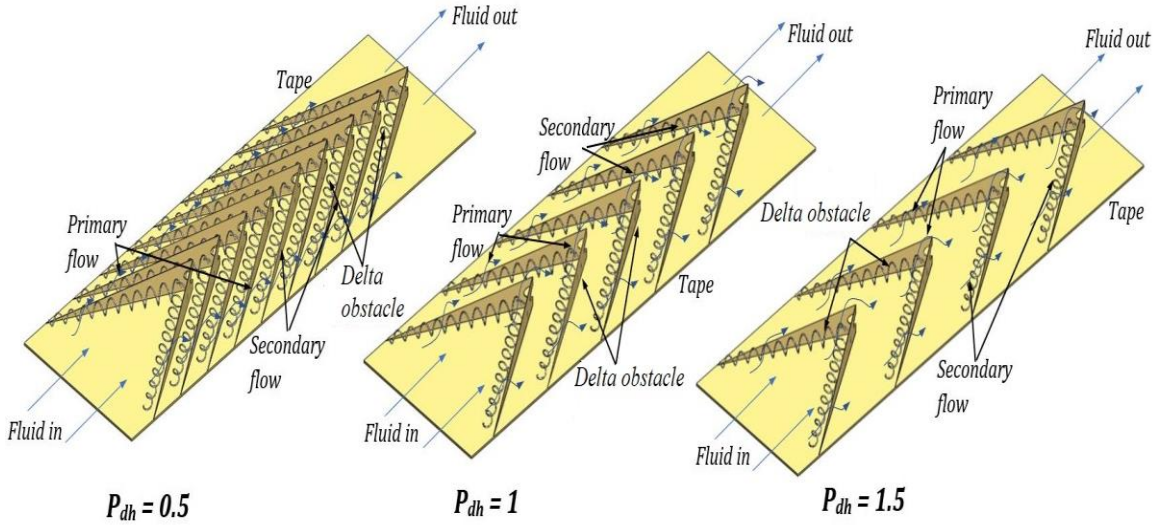

Fig. 4.8. Represent the schematic representation of delta obstacle with varying pitch ratios.

4.2.4 Influence of design parameters on the performance of selected criteria

The outcomes of the evaluated SWHS design alternatives are illustrated in Fig. 4.9 and Fig. 4.10. Figures 4.9 and 4.10 consists of fifteen SWHS design alternatives (A_1 to A_{15} as described in Table 4.6) and three properties (Nu_{dh}= C_1, f_{dh}= C_2, and η_{dh}= C_3) fixed as selection criteria. The results demonstrate that the various combinations of design parameters significantly affect the performance of the examined criteria. For design alternatives A_1 to A_3 (Fig. 4.9), the *Re*

varies from 400-1200 while the α_{dh} (15°) and P_{dh} (0.5) are fixed. With increased *Re* values, the Nu_{dh} increases to 26.28 for design alternative A_1 to 66.54 for design alternative A_3. This improvement in Nu_{dh} is credited to swirl generation by adequately mixing of the working fluid inside the absorber tube for this particular range of the α_{dh} and P_{dh}. As the α_{dh} changed from 15° to 30° and P_{dh} remained unchanged (0.5), the Nu_{dh} enhanced from 33.3 for design alternative A_4 to 79.54 for design alternative A_6. Further enhancement in Nu_{dh} is due to the change in α_{dh}. As the α_{dh} increases from 15° to 30°, the impact of obstacle is comparable to that of a transverse obstacle, which has a high rate of heat transfer due to the creation of a secondary vortex fluid stream. For design alternatives A_7 to A_9, α_{dh} changed from 30° to 45°, and P_{dh} changed from 0.5 to 1.5. A slight enhancement in Nu_{dh} was recorded as it increased from 34.30 for design alternative A_7 to 80.54 for design alternative A_9.

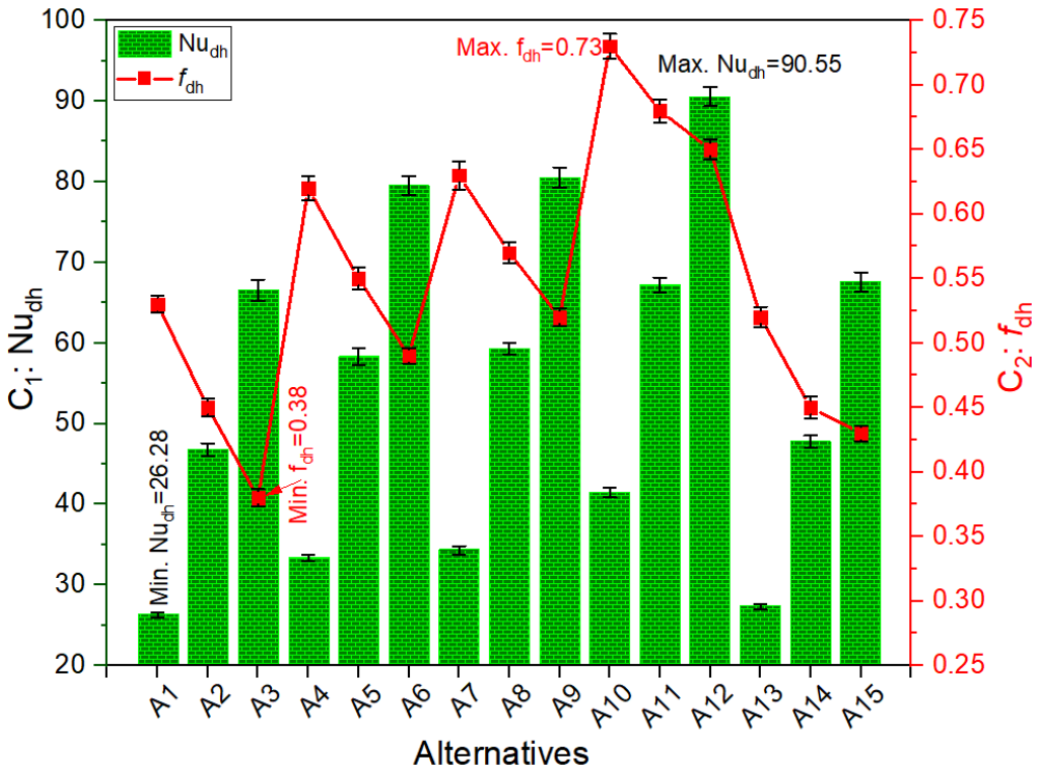

Fig. 4.9 Variation of Nu_{dh} (C_1) and f_{dh} (C_2) with alternatives.

For the alternative A_{10} to A_{12}, the *Re* varied from 400-1200, while α_{dh} is 45° and P_{dh} is 1. The results show that the C increases from 41.45 for alternative A10 to 90.55 for alternative A_{12}.

The alternative A_{12} offers the highest value of Nu_{dh}. At this particular α_{dh}=45° and P_{dh}=1, the water gets the maximum surface area of the winglet and the appropriate distance between the winglet that can help the fluid to gain the maximum heat from the wall surface of the absorber tube and also due to the proper mixing of the fluids. This could be result of a surge in turbulence that accelerated mixing, shattered the thermal boundary layer, and increased the Nu in the pipe. Near the leading edge of the perforation, the water flow creates a swirl from the delta obstacle surface and after that; the flow was reattached to the delta obstacle at the back of the perforation. Therefore, some sought of vortex are generated that helps to rise the local mixing of flow close to adjoining area. That will enhance the exchange of energy and therefore enhance the heat transfer rate [95, 96]. Compared to alternatives A_{10}-A_{12}, as P_{dh} changes from 1 to 2 and α_{dh} remains constant at 45°, a decline of 25-34% in Nu_{dh} for alternatives A_{13} to A_{15} was observed. This decrease in Nu_{dh} occurs because the distance between the winglets is too great for large values of P_{dh}. As a result, the fluid that is moving obtains the maximum amount of time for stagnation along the path. As a result, the fluid does not produce a full swirl, and the rate of heat transfer is also reduced. The f_{dh} results are presented in Fig. 4.9, revealing that the f_{dh} decreased with increased *Re* values. For instance, in design alternatives A_1 to A_3 (*Re* = 400-1200, α_{dh}= 15°, P_{dh} = 0.5), the f_{dh} was reduced from 0.53 for A_1 to 0.38 for A_3. For this range of parameters, the fluid retardation was insufficient to cause friction, resulting in a decrease in f_{dh}. The same is the case for the alternative set A_4 to A_9, and the f_{dh} is decreased from 0.62 for A4 to 0.52 for A9. It is concluded from the results that the minimum and maximum f_{dh} are found for the alternatives A_3 (0.38) and A_{10} (0.73), respectively. The enhancement in f_{dh} for alternative A_{10} is due to the larger surface of the winglet, i.e., α_{dh} (45°) and P_{dh} value of 1 between the winglet is not enough to stagnated the fluid inside the pipe and create maximum swirl along the path. This contributes to making the fluid flow more turbulent.

But as we have seen for the alternative set A_{13} to A_{15} (Re = 400-1200), α_{dh}= 15°, P_{dh}= 2, the f_{dh} was decreased from 0.52 to 0.43.

From the investigation of Nu_{dh} and f_{dh} behaviours, it is concluded that insertion of perforated delta barrier in the absorber tube of SWHS leads to enhanced heat transfer, but at the cost of increased friction factor. Therefore, it is important to choose a design that not only provides maximum heat transfer but also keeps the friction factor at the lowest possible level. In order to achieve this goal of simultaneous consideration of thermal as well as hydraulic performance a parameter known as thermohydraulic efficiency/performance (η_{dh}) has been utilized by the researchers [97, 98]. The η_{dh} for various SWHS design alternatives was calculated using Eq. 3.8 and corresponding results are depicted in Fig. 4.10.

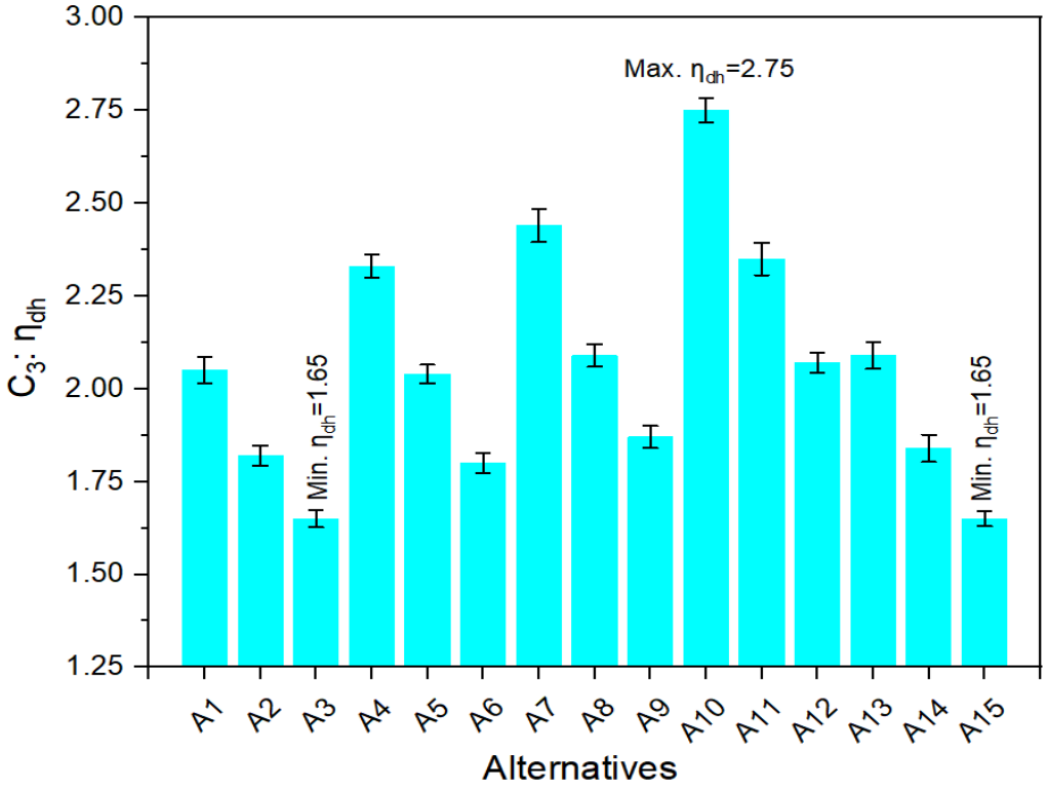

Fig. 4.10 Variation of η_{dh} (C_3) with alternatives.

For the design alternatives A_1 to A_3 (Fig. 4.10), the Re varies from 400-1200 while the α_{dh} (15°) and P_{dh} (0.5) are fixed. With increased Re values, the η_{dh} decreases from 2.05 for design alternative A_1 to 1.65 for design alternative A_3. With the further increase in the α_{dh} from 15°-30° and the value of the P_{dh} remaining constant at 0.5, it was noted that the η_{dh} increases for

alternatives A_4 to A_6 and remains between 2.33 to 1.80. The further increment in the P_{dh} from 0.5 to 1.5 and α_{dh} from 30° to 45° for alternatives A_7 to A_9, η_{dh} fluctuated between ~2.44-1.87. The η_{dh} performance remains lowest (1.65) for design alternatives A_3 (Re = 1200, α_{dh}= 15°, and P_{dh}=0.5) and A_{15} (Re= 1200, α_{dh}=45°, and P_{dh}=2). In contrast, the highest η_{dh} value (2.75) was registered for design alternative A_{10} (Re = 400, α_{dh}= 45° and P_{dh}= 1).

It is evident from Fig. 4.9 and Fig. 4.10 that the changes in design parameters (Re, P_{dh}, and α_{dh}) considerably influence the evaluated performance criteria (Nu_{dh}, f_{dh}, and η_{dh}). The findings for the examined criteria are incredibly reliant on the parameter's combination and without any distinct trend. The highest value of 90.55 for Nu_{dh} was recorded with design alternative A_{12} but exhibited the third highest f_{dh} value (0.65). For design alternative A_3, the f_{dh} value remains the smallest (0.38) but also displays the lowest η_{dh} value (1.65). The largest η_{dh} value of 2.75 was recorded for design alternative A_{10} but showed highest f_{dh} (0.73) value with a lower for Nu_{dh} (41.45). The results show that no single design alternative performs best when all criteria are considered together. As such, it becomes challenging for SWHS to recommend a design option that best serves each criterion. Accordingly, to select the best SWHS design alternative, the ARAS approach was proposed in conjunction with the AHP method.

4.2.5 Ranking of the design alternatives

4.2.5.1 AHP for criteria weight prioritization

The AHP method was carried out to calculate the weight of the various performance criteria. Table 4.7 shows the pair-wise comparison matrix and results of AHP. Considering the values presented in pair-wise comparison matrix (Table 4.7), the weights are calculated as 0.461, 0.231, and 0.308 for each criterion including Nu_{dh} (C_1), f_{dh} (C_2) and η_{dh} (C_3) respectively.

Table 4.7 Comparison matrix and weight results.

	Pair-wise comparison matrix			Results of AHP	
	C_1	C_2	C_3	Consistency parameters	Weight (ω_j)
C_1	1	2	3/2	λ_{max}=3.000001	0.461
C_2	1/2	1	3/4	RI=0.58	0.231
C_3	2/3	4/3	1	CR=0.0000008	0.308

For determined value of λ_{max} = 3.000001, the CI value for N=3 is calculated using Eq. 4.16 as;

$$CI = \frac{\lambda_{max} - N}{N-1} = \frac{3.000001-3}{3-1} = 0.0000005$$

For N=3, the RI value is 0.58, the CR is calculated using Eq. 4.15 as;

$$CR = \frac{CI}{RI} = \frac{0.0000005}{0.58} = 0.0000008$$

The criteria weights are acceptable as the computed CR value is nearly zero, indicating that the generated pair-wise comparison matrix has a high level of consistency.

4.2.6 Final ranking of the alternatives

After calculating the weight of the different performance criteria, the ranking of selected SWHS alternatives has been evaluated. The results of the fifteen SWHS design alternatives concerning the three selected performance criteria are tabulated in a decision matrix as presented in Table 4.8. The normalized (Table 4.9) and weighted normalized (Table 4.10) decision matrix are formulated using Eq. 4.18-4.20.

Table 4.8 Experimental results arranged in the form of a decision matrix.

Alternatives	C_1	C_2	C_3	Alternatives	C_1	C_2	C_3
A_0	90.55	0.38	2.75	A_8	59.30	0.57	2.09
A_1	26.28	0.53	2.05	A_9	80.54	0.52	1.87
A_2	46.77	0.45	1.82	A_{10}	41.45	0.73	2.75
A_3	66.54	0.38	1.65	A_{11}	67.20	0.68	2.35
A_4	33.30	0.62	2.33	A_{12}	90.55	0.65	2.07
A_5	58.30	0.55	2.04	A_{13}	27.28	0.52	2.09
A_6	79.54	0.49	1.80	A_{14}	47.77	0.45	1.84
A_7	34.30	0.63	2.44	A_{15}	67.54	0.43	1.65

Table 4.9 The normalized decision matrix.

Alternatives	C_1	C_2	C_3	Alternatives	C_1	C_2	C_3
A_0	0.0987	0.0850	0.0819	A_8	0.0647	0.0567	0.0622
A_1	0.0287	0.0609	0.0610	A_9	0.0878	0.0621	0.0557
A_2	0.0510	0.0718	0.0542	A_{10}	0.0452	0.0442	0.0819
A_3	0.0725	0.0850	0.0491	A_{11}	0.0733	0.0475	0.0700
A_4	0.0363	0.0521	0.0694	A_{12}	0.0987	0.0497	0.0616
A_5	0.0636	0.0587	0.0607	A_{13}	0.0297	0.0621	0.0622
A_6	0.0867	0.0659	0.0536	A_{14}	0.0521	0.0718	0.0548
A_7	0.0374	0.0513	0.0726	A_{15}	0.0736	0.0751	0.0491

Table 4.10 The weighted normalized decision matrix.

Alternatives	C_1	C_2	C_3	Alternatives	C_1	C_2	C_3
A_0	0.0455	0.0196	0.0252	A_8	0.0298	0.0131	0.0192
A_1	0.0132	0.0141	0.0188	A_9	0.0405	0.0143	0.0171
A_2	0.0235	0.0166	0.0167	A_{10}	0.0208	0.0102	0.0252
A_3	0.0334	0.0196	0.0151	A_{11}	0.0338	0.0110	0.0215
A_4	0.0167	0.0120	0.0214	A_{12}	0.0455	0.0115	0.0190
A_5	0.0293	0.0136	0.0187	A_{13}	0.0137	0.0143	0.0192
A_6	0.0400	0.0152	0.0165	A_{14}	0.0240	0.0166	0.0169
A_7	0.0172	0.0118	0.0224	A_{15}	0.0339	0.0174	0.0151

Using weighted normalized (Table 4.10) decision matrix, for each alternative the Ψ_i (optimality function) values are calculated using Eq. 4.21 as follows:

$$\Psi_0 = 0.0455 + 0.0196 + 0.0252 = 0.0903$$

$$\Psi_1 = 0.0132 + 0.0141 + 0.0188 = 0.0461$$

$$\Psi_2 = 0.0235 + 0.0166 + 0.0167 = 0.0568$$

$$\vdots$$

$$\Psi_{15} = 0.0339 + 0.0174 + 0.0151 = 0.0664$$

The computed Ψ_i values for each alternative are presented in Table 4.11. Finally, by considering the Ψ_0 as optimum value the utility degree (Ω_i) of each alternative is computed using Eq. 4.22 as follows:

$$\Omega_1 = \frac{0.0461}{0.0903} = 0.5105$$

$$\Omega_2 = \frac{0.0568}{0.0903} = 0.6290$$

$$\vdots$$

$$\Omega_{15} = \frac{0.0664}{0.0903} = 0.7353$$

Table 4.11 shows the Ω_i values and the related rank of each alternative. The Ω_i of the A_{12} is discovered to be greatest (0.8416), indicating that it is the best among all accessible choices, followed by A_9 (0.7962) and A_6 (0.7940). With a $\Omega_i = 0.5105$, Alternative A1 exhibits the least desirable performance. Under the assessment of three criteria, it is concluded that option A_{12} (Re = 1200, P_{dh} = 1.0, α_{dh} = 45°) is determined to be the best contender for improving SWHS performance.

Table 4.11 ARAS results for alternatives rank.

Alternatives	Ψ_i	Ω_i	
Optimum value	0.0903	1.0000	Rank
A_1	0.0461	0.5105	15
A_2	0.0568	0.6290	10
A_3	0.0681	0.7542	4
A_4	0.0501	0.5548	13
A_5	0.0616	0.6822	8
A_6	0.0717	0.7940	3
A_7	0.0514	0.5692	12
A_8	0.0621	0.6877	7
A_9	0.0719	0.7962	2
A_{10}	0.0562	0.6224	11

A_{11}	0.0663	0.7342	6
A_{12}	0.0760	0.8416	1
A_{13}	0.0472	0.5227	14
A_{14}	0.0575	0.6368	9
A_{15}	0.0664	0.7353	5

4.2.7 Sensitivity analysis

The results of any MCDM approach can be inaccurate or prone to change under various conditions, such as changing the weighting of criteria due to the evolving experts' viewpoints. Consequently, it becomes essential to perform a sensitivity analysis to assess the robustness of the MCDM results. For sensitivity analysis, additional criterion weights per the literature's recommendations were created, and their impact on the ranking of alternatives was examined [99]. In this study, the criteria weights were adjusted in three steps of ±10%, ±20%, and ±30%, and new alternatives rankings were assessed. When a criterion's weight was increased or decreased, the weights of the remaining two criteria were altered proportionally to achieve a cumulative weight of one. For instance, a +10% weight increment for C_2 (f_{dh}) indicates that the real weight of C_2 (0.231) is increased by 10% ($0.231\times\frac{10}{100}$=0.0231), while the weights of C_1 (Nu_{dh}) and C_3 (η_{dh}) are dropped by $\frac{0.0231}{2}$, resulting in a sum of all the criterion weights of 1.

The weights for various criteria with +10% increments in C_2 weight are as follows:

$$f_{dh} = 0.231 + (0.231\times\frac{10}{100}) = 0.254$$

$$Nu_{dh} = 0.461 - \frac{0.0231}{2} = 0.449$$

$$\eta_{dh} = 0.308 - \frac{0.0231}{2} = 0.296$$

The generated new weight by adopting ±10%, ±20%, and ±30% variation in different criteria is listed in Table 4.12. There are a total of eighteen weight exchange scenarios for three criteria.

As a result, eighteen sets of rankings of SWHS alternatives are provided in Fig. 4.11. In all scenarios, alternative A_{12} remains first-ranked, whereas alternative A_1 remains last-ranked.

Table 4.12 The new criteria weights.

	Weight levels for variation in C_1						
	+30%	+20%	+10%	Actual	-10%	-20%	-30%
Nu_{dh}	0.599	0.553	0.507	0.461	0.415	0.369	0.323
f_{dh}	0.162	0.185	0.208	0.231	0.254	0.277	0.300
η_{dh}	0.239	0.262	0.285	0.308	0.331	0.354	0.377
	Weight levels for variation in C_2						
Nu_{dh}	0.426	0.438	0.449	0.461	0.473	0.484	0.496
f_{dh}	0.300	0.277	0.254	0.231	0.208	0.185	0.162
η_{dh}	0.273	0.285	0.296	0.308	0.320	0.331	0.343
	Weight levels for variation in C_3						
Nu_{dh}	0.415	0.430	0.446	0.461	0.476	0.492	0.507
f_{dh}	0.185	0.200	0.216	0.231	0.246	0.262	0.277
η_{dh}	0.400	0.370	0.339	0.308	0.277	0.246	0.216

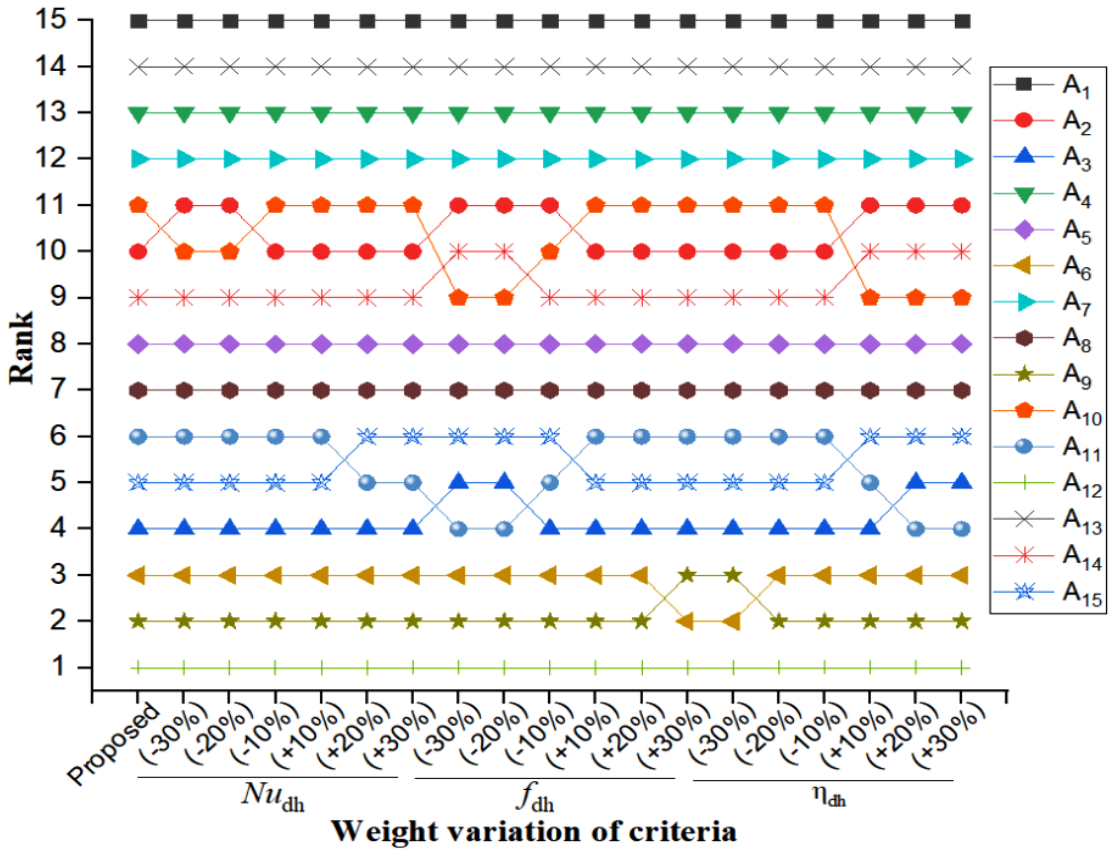

Fig. 4.11. Sensitivity analysis.

It is observed that the ranking of SWHS concerning the weightage of Nu_{dh} (C_1) is quite robust. A slight sensitivity was noticed as alternative A_2, and A_{10} swap their positions when the weightage of Nu_{dh} is decreased by -30% and -20%. Also, alternatives A_{11} and A_{15} switch their places for the increase in the weightage of Nu_{dh} by +30% and +20%. The ranking of the SWHS alternatives remains more susceptible to the weightage changes made for f_{dh} (C_2) and η_{dh} (C_3). Interestingly, alternatives A_{10} and A_{11} are most vulnerable to the shift in weightage of f_{dh} and η_{dh}. As the weightage of f_{dh} is decreased by 20% and 30%, the ranking of the alternatives A_{10} and A_{11} goes up by two places. Similarly, the order of alternatives A_{10} and A_{11} goes up by two places as the weightage of η_{dh} is increased by +20% and +30%. However, the swapping in sensitivity analysis has no significant effect on the ranking of the AHP-ARAS model, which is also confirmed by the Spearman correlation coefficient, determined using Eq. 4.23 [100].

$$\text{Spearman Correlation coefficient} = 1 - \frac{6\sum_{i=1}^{M} X_i^2}{M\left(M^2 - 1\right)} \tag{4.23}$$

Here, M is the number of alternatives and X_i is the difference between the nominal rank and rank obtained using change in a criterion weight.

For all scenarios, the obtained correlation coefficient value is larger than 0.98, suggesting the reliability of the ranking results.

4.2.8 Validation using other MCDM techniques

Before making a final decision, it is necessary to check whether the proposed MCDM model satisfies the literature. Therefore, the ranking results of the proposed ARAS technique were compared with those of other decision-making tools such as TOPSIS [101], VIKOR [102], and COPRAS [103] models, as demonstrated in Fig. 4.12. The ranks of the alternatives using the various MCDM approaches in (Fig. 4.12) show that A_{12} is the most dominating (first-ranked) alternative. At the same time, A_1 is the worst alternative, ranking last across all models. The results showed that ARAS, VIKOR, and COPRAS did not affect ranking. However, a

negligible effect on the ranking was recorded with the TOPSIS model, which was a fourth- and fifth-ranked alternative swap position. Further, Spearman's correlation coefficient was determined to analyse the statistical significance of the difference obtained between the ranking results of the proposed MCDM models and the other decision-making tools. The results show a significant statistical correlation greater than 0.999, which helps us conclude that the obtained ranking is reliable and valid.

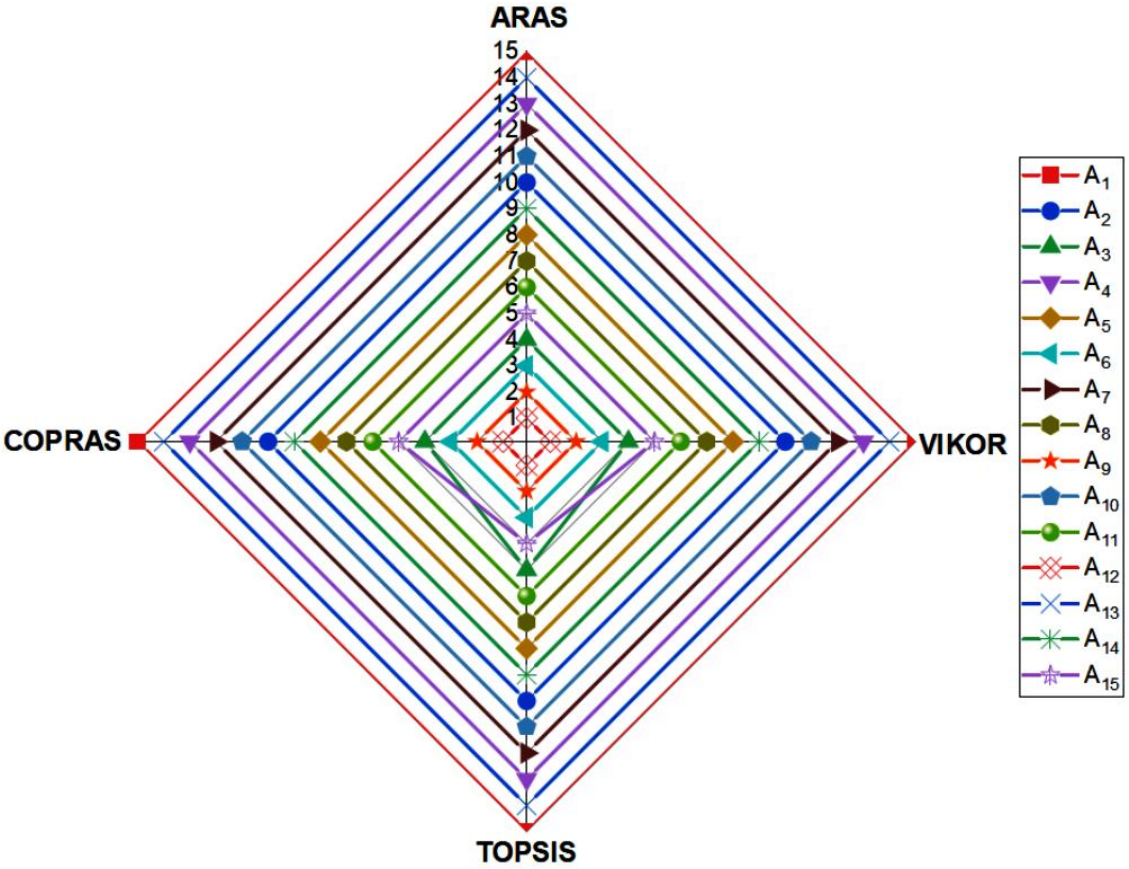

Fig. 4.12 The ranks of the alternatives in terms of different MCDM methods.

4.3. CASE III. Experimental examination of eco-friendly insulating materials to analyse their impact on heat transfer characteristics.

The conventional solar flat plate collector commonly uses rock wool or other insulating materials to lower thermal losses. These inorganic materials are one of the significant concerns to the industry and the environment. Thus, reducing these inorganic materials and utilizing the naturally occurring biodegradable materials available in abundance and without any

environmental hazards to the system is imperative. The current research presents agricultural waste as an insulating material for S-FPC fabrication. The novelty of this current research work is the utilization of rice husk, stubble fibre, coco-peat, and nitrile rubber as an insulating material for the fabrication of S-FPC. Experimentation is performed with insulating thicknesses of 50 mm and 70 mm. The optimum temperature is attaining 50-53˚C with an average thermal efficiency of 64-66% by using rice husk as the insulating material with a thickness of 70 mm. Traditionally, insulating materials like rock wool, ceramic wool, glass wool, polyurethane foam, etc. are utilized to reduce these heat losses [104]. Even though there is much high-performing thermal insulation on the market, these materials nevertheless face a number of difficulties, including costs, mechanical and thermal qualities, and health issues. Thermal insulation is an essential component of many buildings, helping to reduce energy consumption and improve indoor comfort. However, some insulation materials can pose health hazards if they are not handled or installed properly. One such material is asbestos, which was commonly used as insulation until the 1970s when its health risks were discovered. Asbestos fibers can become airborne when insulation is disturbed or damaged, and when inhaled, can lead to serious respiratory diseases, including lung cancer and mesothelioma. Other insulation materials, such as fibreglass, can also cause respiratory irritation if inhaled in large quantities. To minimize the risk of health hazards, it is important to use insulation materials that are non-toxic and safe for human exposure, and to follow proper handling and installation procedures. These typical thermal insulations produce harmful compounds throughout the design, manufacture, and implementation process in the form of mineral fiber and synthetic binder dust or other air pollution or hazardous waste creation. Figure 4.13 shows the detailed representation of S-FPC.

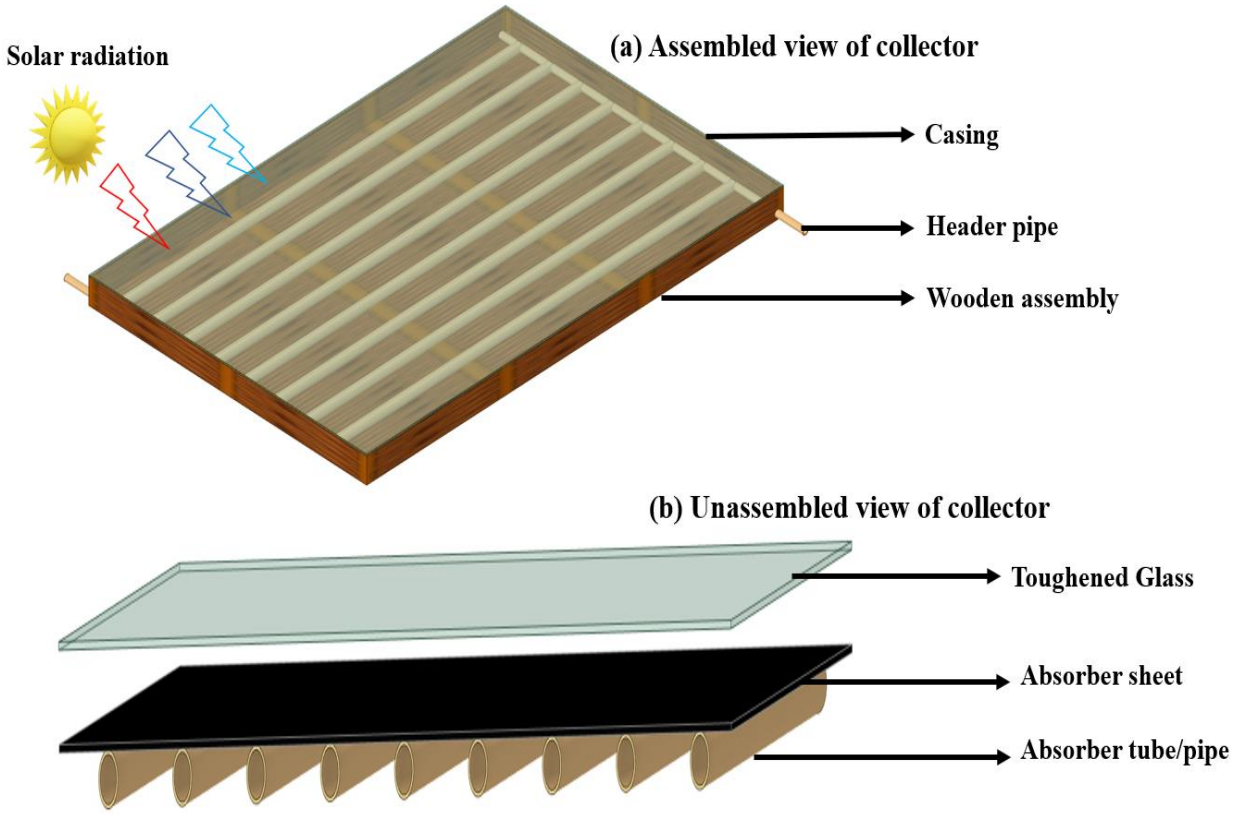

Fig. 4.13 Detailed representation of S-FPC.

4.3.1 Performance assessment of an S-FPC

Insulation produced from coco-peat, stubble fibre and rice husk were used in the SWHS, and its performance was evaluated under controlled settings to ensure it met ISO standards. Prior to the evaluation, a visual inspection of the SC was performed to identify any signs of cracks. The riser and header pipes were subsequently filled with water to ensure there was no leakage of water. Throughout the tests, a constant flow rate of 0.02 l/s of cold water at the inlet were maintained. The pyranometer is used to measure the I_s. This particular device is capable of accurately measuring solar radiation levels up to 2000 W/m^2. The various measuring instrument used in this experimental work are Linear scale, thermocouple, pressure gauge and vernier clipper etc. Figure 4.14 show the schematic representation of S-FPC using thermal insulating materials.

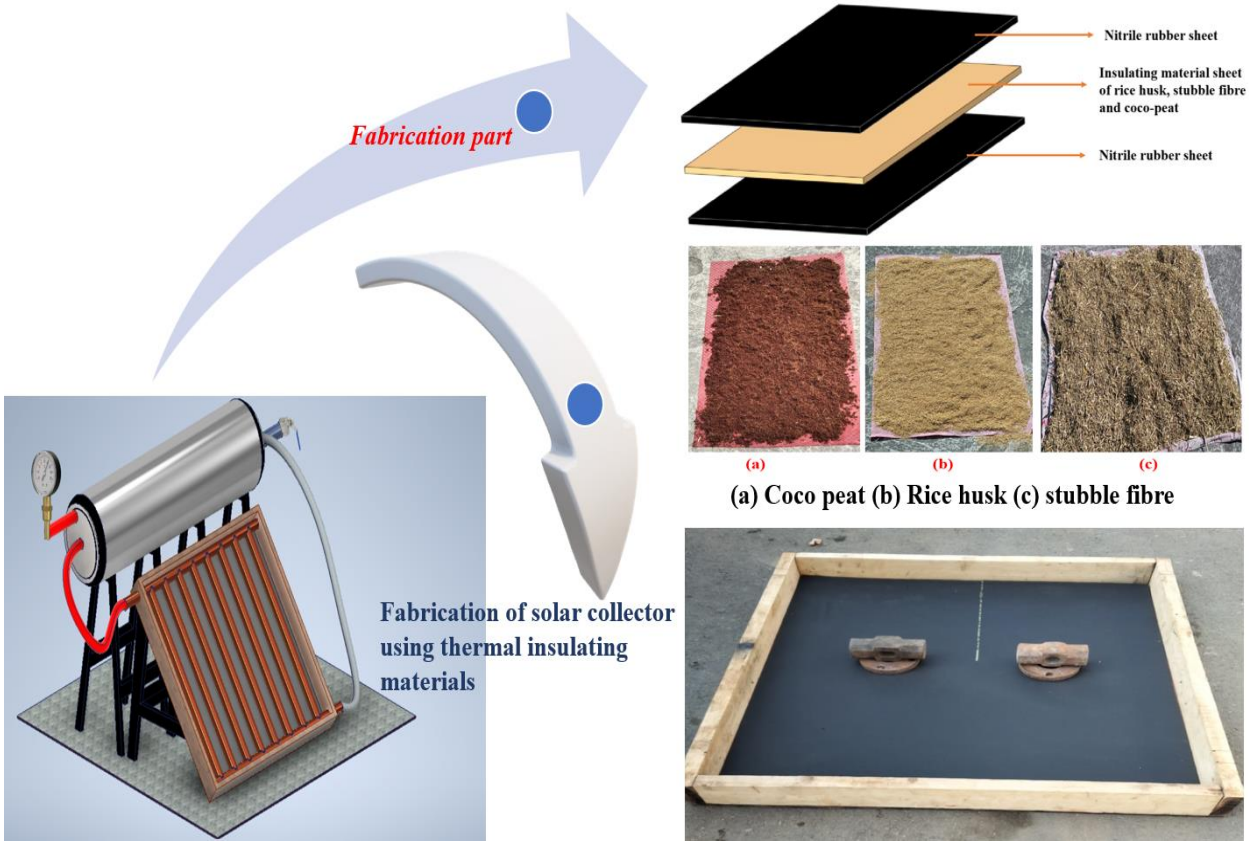

Fig. 4.14. Schematic representation of S-FPC using thermal insulating materials.

The S-FPC (solar flat plate collector) water heating system's effectiveness was assessed in diverse weather conditions by employing specifically designed insulation materials. To gauge the system's performance, various factors were measured, including the water's mass flow rate, the temperatures of the fluid at the inlet/outlet, the collector area, and the I_s. The efficiency of S-FPC (denoted as η) is calculated using the subsequent formula.

$$\eta = \frac{Q_u}{I} = \frac{\dot{m}C_p(T_{fo}-T_{fi})}{A_c I_S} \quad (1)$$

In the equation provided by [105], the solar collector efficiency (η), expressed as a percentage, is determined by several variables. These variables include the useful heat output (Qu) in watts (W), the mass flow rate (ṁ) in kilograms per second (kg/s), the specific heat capacity of water (CP) in joules per kilogram per degree Celsius (J/kg˚C), the gross collector area (A_c) in square meters (m^2), the incident global solar radiation (I_s) in watts per square meter (W/m^2), and the fluid outlet temperature (T_{fo}) and inlet temperature (T_{fi}) in degrees Celsius (˚C).

4.3.1 Results and discussion

4.3.1.1 Influence of the insulting materials on the thermal performance of the S-FPC

The performance of the S-FPC is evaluated by using special type of biodegradable insulating materials such as risk husk, stubble fibre and coco-peat. The thickness of sandwich insulation of nitrile rubber of 50 mm and 70 mm were used to examine the parametric influence of these sandwich sheets on the performance of S-FPC. The various graph is plotted with respect to time of system using sandwich sheet of risk husk, stubble fibre and coco-peat are shown in Figs. 4.15-4.16. Experimentation was carried out during the duration of 11.00-16-00 h. The insulation thicknesses of 50 mm were taken during the first round of experiment of each set of materials of Risk husk, stubble fibre and coco-peat and see their influence on the outlet temperature of water. First, we look at the effect of rice husk on a nitrile rubber sheet with thicknesses of 50 and 70 mm to see how it affects the system's performance. The width of the insulation is a key factor in how well S-FPC works. To keep heat from escaping, the thickness of the shielding materials must fall within the range of the Indian standard (IS 3346). In this study, rice husk, stubble fibre, and coco peat with thicknesses of 50 mm and 70 mm are used instead of rockwool, which is usually used as insulation. Figure 4.15 shows the effect of rice husk with changing outlet-inlet water temperature, outdoor temperature, and I_s over time. The experimentation is carried out from 11:00 a.m. to 16:00 p.m. The T_{fi} of water varies from 30-35˚C due to the variation in I_s. The average temperature of water at the inlet is 34˚C. The I_s at the initial period of experiment is 1000 W/m^2 then it increased up to approx. 1170 W/m^2 at the noon time the it starts decrease due to decreasing period of sunshine hours. The T_{fo} of water is also vary in accordance to variation of solar intensity.

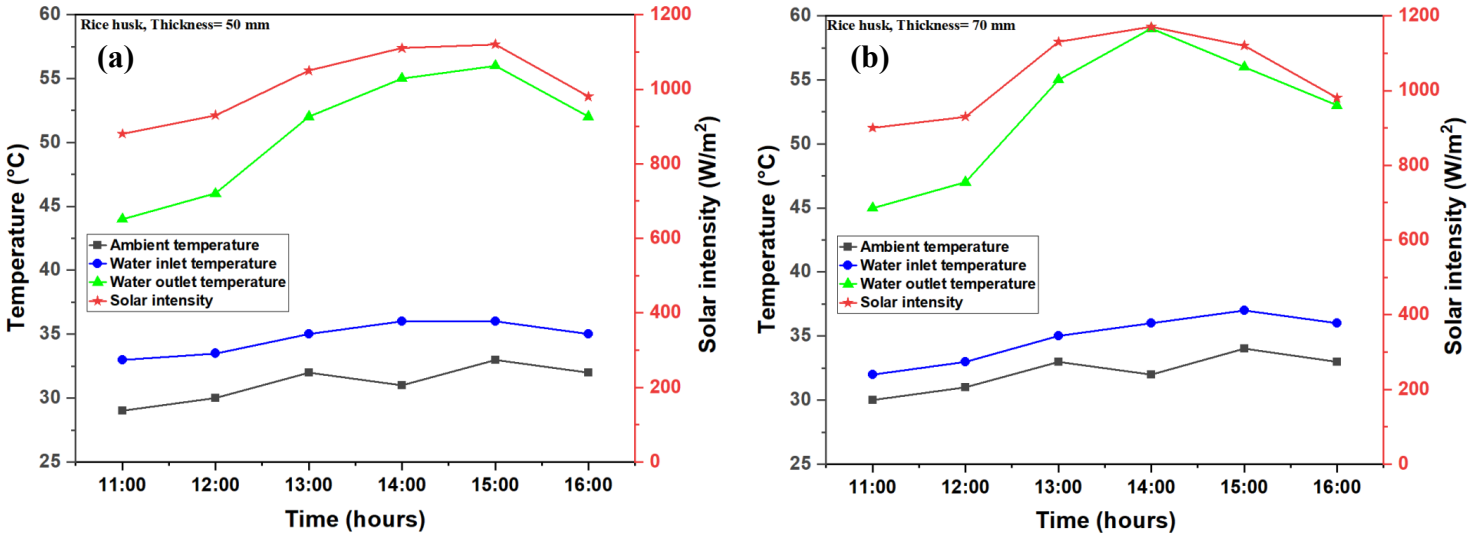

Fig. 4.15 Influence of rice husk on outlet-inlet water temperature, ambient temperature, and I_s over time.

The sandwich sheet of rice husk and nitrile rubber that are used as the thermal insulator in this study, play a very key role for the enhancement of outlet water temperature. Initially the sandwich sheet is gaining heat from the solar radiation and start gaining heat continuously that intern gave the conductive heat to the absorber pipe that are installed inside the collector. The absorber heats continuously gaining heat by two ways, in the first way the absorber pipe absorb heat from the sandwich sheet of rice husk and nitrile rubber and secondly it gets heat by direct falling of solar radiation on the collector. In this way the system start worked and the hot water is obtained. Figure 4.16 depicts the temporal dependence of the outlet-inlet water temperature, ambient temperature, and I_s on the stubble fibre. The sandwich sheet of nitrile rubber and stubble fibre are used for the experimentation. The insulation thickness of 50 mm and 70 mm are used to examine their influence on the output temperature of water. The average T_{fo} varies from 30-36˚C. The I_s are varies with respect to time. From the experimental examination it was examined that the heat absorption capacity of the stubble is low as compared to rice husk. The average optimum temperature obtained after examination is 56˚C by using the stubble fire with 70 mm of insulation.

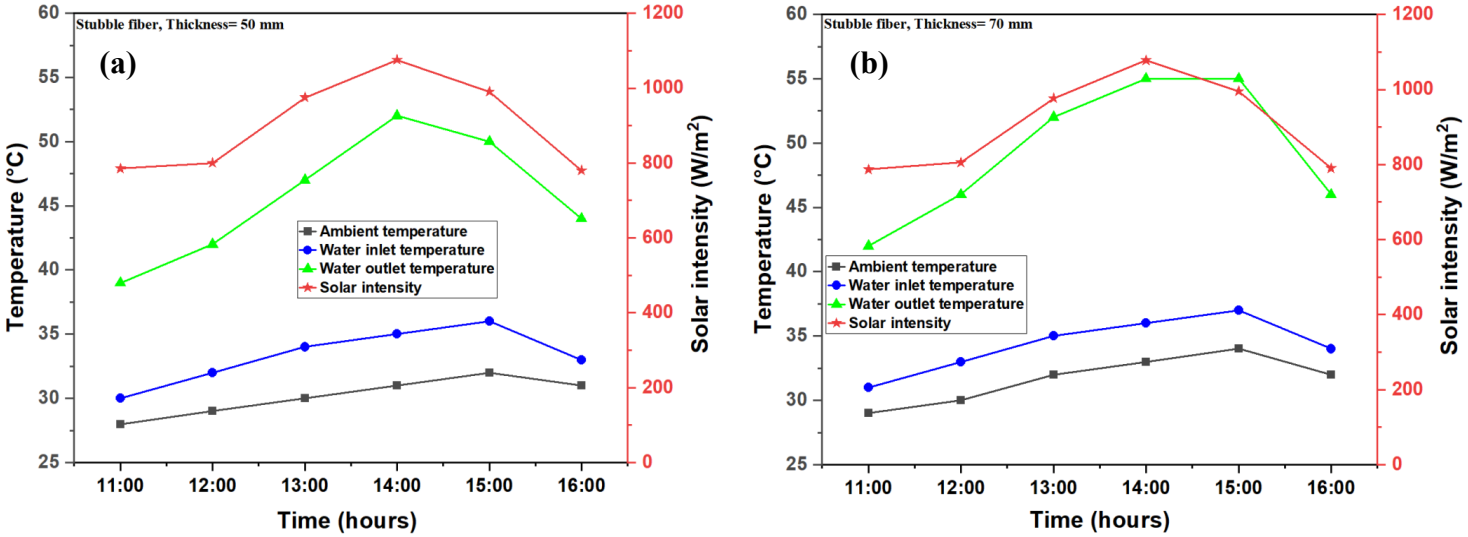

Fig. 4.16 Influence of stubble fiber on outlet-inlet water temperature, ambient temperature, and I_s over time.

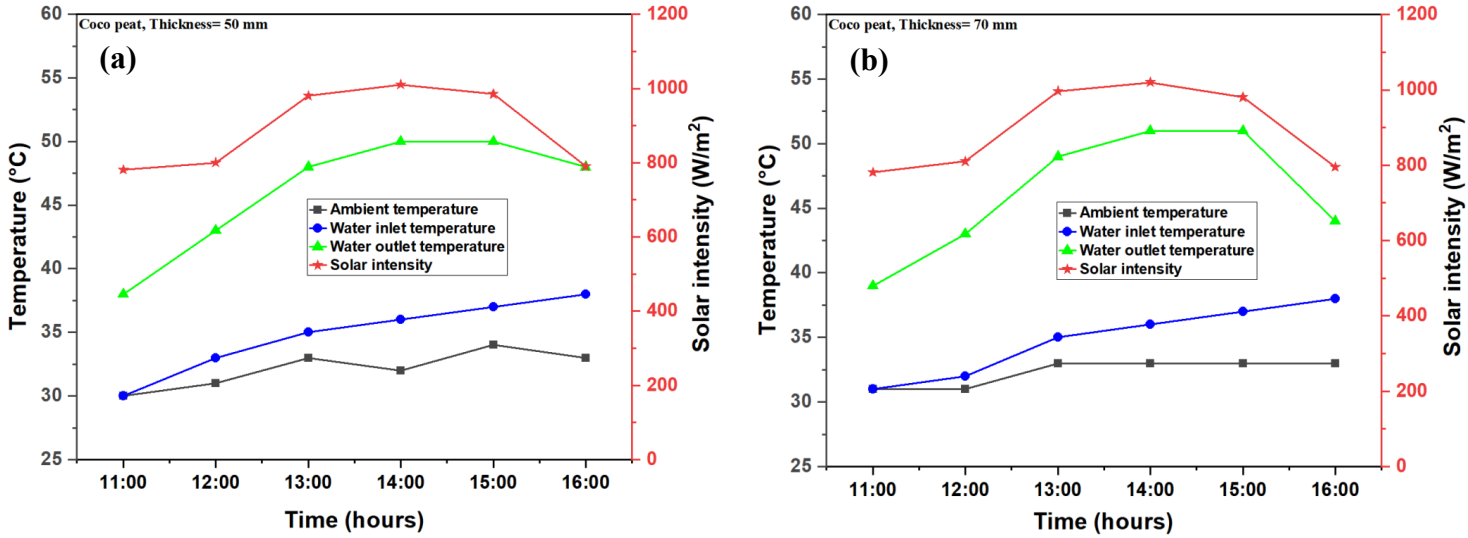

Fig. 4.17 Influence of coco-peat on outlet-inlet water temperature, ambient temperature, and I_s over time.

Figure 4.17 depicts the temporal dependence of the outlet-inlet water temperature, ambient temperature, and I_s on the used coco peat insulation. It is also concluded from the examination that the coco-peat does not show much impact as compared to other two insulation materials. There a comparative thermal efficiency is examined for these three insulation materials to show their influence on the performance of the system. The optimum thermal efficiency if found for

rice husk with thickness of insulation sheet is 70 mm as shown on figure 4.18. The lower thermal efficiency is found for coco-peat with insulation thickness of 50 mm.

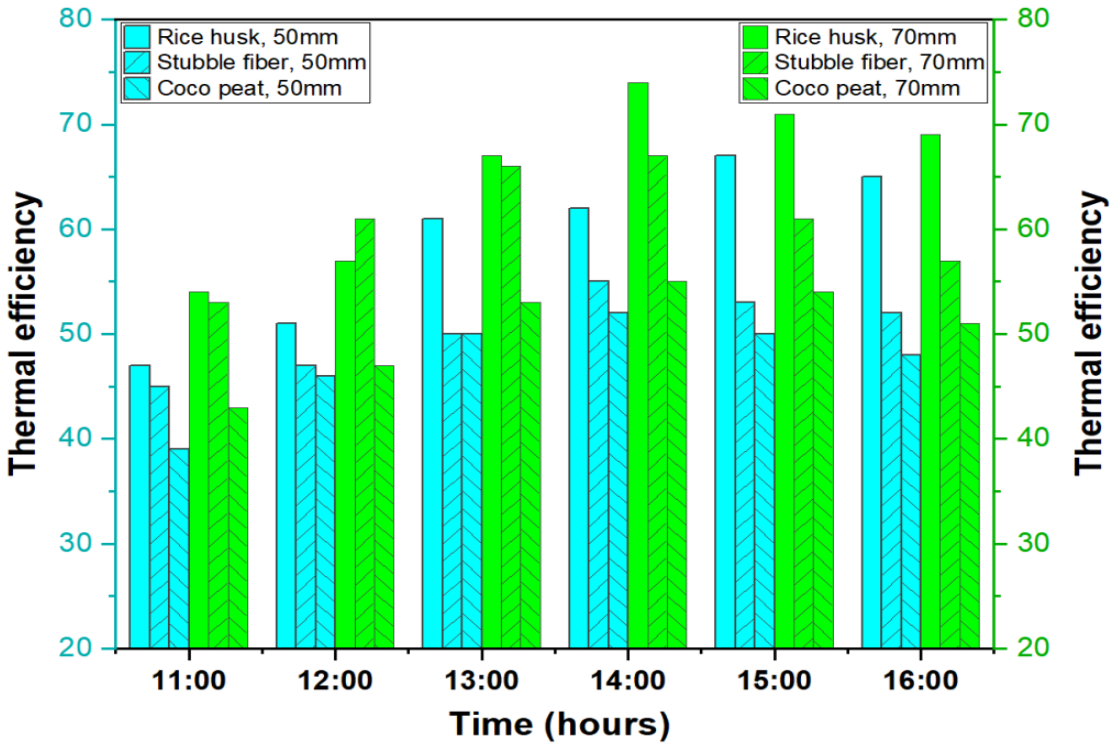

Fig. 4.18 Thermal efficiency calculation of rice husk, stubble fibre and coco-peat with insulation thickness of 50 and 70 mm.

The efficiency of S-FPC with different natural insulating materials and thickness are shown in Table 4.13. In table 4.13 the various parameter is taken into consideration such as insulating materials, thickness, T_{fi}, T_{fo}, I_g and η_{avg}. It is observed from the table for the insulating material of coco-peat with thickness 50 mm and 70 mm the average thermal efficiency is found to be 53-54%. In case of stubble fibre and rice husk the average thermal efficiency is found to be 55-66% which is well in the range of 51-80% of conventionally used insulating materials in SWHS [106, 107]. The reason behind to attain the maximum efficiency of 66% with insulating thickness of 70 mm rice husk is due to lower heat losses form the collector.

Table 4.13: Thermal efficiency of S-FPC with various insulating materials and thickness.

Insulating materials	**Insulation thickness**	T_{fi} **(Avg.) (˚C)**	T_{fo} **(Avg.) (˚C)**	I_g **(avg.) (W/m²)**	η_{avg} **(%)**
Coco peat	50mm	34.5	49.5	1057	53
	70mm	35.5	50.1	1026	54
Stubble fibre	50mm	33.20	50.4	1075	60
	70mm	36.2	50.8	1075	57
Rice husk	50mm	34	52	1070	64
	70mm	34.10	52.9	1070	66

CONCLUSIONS AND RECOMMENDATION FOR FUTURE WORK

This chapter summarized the conclusion remarks from the experimental studies and is discussed below.

5.1 Conclusions from Experiment

The following conclusion has been drawn from the experimental studies in SWHS with MCDM approach in Perforated and non-perforated delta obstacle. Additionally, the author made an attempt to utilize the naturally occurring biodegradable insulating materials with different thickness for fabricating S-FPC. The key points from the experimental results are listed below:

Case I: Key points on MCDM approach in Perforated delta obstacle

- The design alternatives significantly affect the SWHS's evaluated performance criteria. The largest Nusselt number (90.55) was attained by design alternative having *Re* =1200, angle of attack = 45°, and pitch ratio = 1. The friction factor remains lowest (0.38) for the design alternative having *Re* =1200, angle of attack = 15°, and pitch ratio = 0.5. On the other hand, the largest thermo-hydraulic efficiency (2.75) was attained by design alternative having a combination of *Re*= 400, angle of attack = 45°, and pitch ratio = 1.
- The AHP-ARAS results show that the SWHS design alternative has geometric and flow arrangement as *Re* =1200, angle of attack = 45°, and pitch ratio = 1, giving the best-optimized performance among the investigated alternatives. The study shows that when the performance criteria for a set of alternatives are heavily dependent on geometric and flow arrangements and show no discernible pattern in the performance, the hybrid AHP-ARAS technique is an excellent optimization tool for identifying the best SWHS design.
- In the sensitivity analysis, the different weight exchange scenarios did not significantly affect the ranking result. Comparison with the other prominent decision-making tools,

such as VIKOR, TOPSIS, and COPRAS, was performed to validate the stability of the proposed model.

Case II: Key points on MCDM approach in non-perforated delta obstacle

- The highest value of Nusselt number (95.90) has been recorded against the design alternative-25, with Reynolds number = 1800, pitch ratio = 0.5 and blockage ratio = 0.25, whereas lowest friction factor (0.534) recorded for design alternative-5, with Reynolds number = 1800, pitch ratio = 0.5 and blockage ratio = 0.15.
- The highest thermo-hydraulic efficiency (2.91) was recorded for design alternative-6, with a combination of Reynolds number = 200, pitch ratio = 0.5, and blockage ratio = 0.20.
- The CRITIC - COPRAS technique results describe that the design alternative A-10, with Reynolds number = 1800, pitch ratio = 0.5, blockage ratio = 0.20, and angle of attack = 45°, delivers the overall best-optimized performance among the examined alternatives.

Case III: Key points on the utilize the naturally occurring biodegradable insulating materials with different thickness for fabricating S-FPC

- Rice husk and stubble fibre show the promising sustainable insulating materials that has the capability to replace the inorganic materials, since they are widely available in this region, are non-polluting, and can be recycled.
- It was found form the experimentation that the thermal performance of S-FPC is slightly higher by using the insulating sandwich sheet of nitrile rubber and rice husk as compared to stubble fibre insulating sheet.
- By increasing the thickness of insulating sheet to 70 mm the T_{fo} is subsequently rise and the η_{avg} is attain to 66%.

- For regions where these wastes are widely available, it is simple to design and construct the locally built system employing waste materials. In addition, compared to systems sold commercially, the related cost is similarly minimal.

 # Thesis Point:

Thesis point contains three parts and the topic are **"CRITIC-COPRAS MCDM optimization approach applies on non-perforated delta obstacles", "AHP-ARAS MCDM optimization approach applies on perforated delta obstacles Overview of integrated AHP-ARAS method",** and **Experimental examination of eco-friendly insulating materials to analyses their impact on heat transfer characteristics"** respectively. The detailed thesis points are discussed below:

- **1st Thesis point: CRITIC-COPRAS MCDM optimization approach applies on non-perforated delta obstacles.**

This study reports on the performance of delta-shaped obstacles in a solar water heating system (SWHS) through experimental analysis and optimization. The influence of different parameter combinations such as Reynolds number (200, 600, 1000, 1400, 1800), pitch ratio (0.5, 1, 1.5), blockage ratio (0.15, 0.20, 0.25), and angle of attack (45°) on Nusselt number, friction factor and thermo-hydraulic performance of SWHS were analyzed. For the combination of Reynolds number=1800 and pitch ratio = 0.5, the Nusselt number remains highest for 0.25 of blockage ratio, whereas the friction factor remains lowest for a blockage ratio of 0.15. The maximum thermo-hydraulic efficiency was achieved using Reynolds number=200, pitch ratio=0.5, and blockage ratio=0.20. The obtained results were intensely dependent on parameter combinations without any pronounced trend. Therefore, criteria importance through inter-criteria correlation (CRITIC) and complex proportional assessment (COPRAS) approach was implemented to find

optimal design alternative. The results of the hybrid CRITIC-COPRAS approach showed that the combination of Reynolds number=1800, pitch ratio=0.5, blockage ratio=0.20, and angle of attack=45° is the best alternative for maximum thermal enhancement in SWHS. The sensitivity analysis proves the robustness of the results that the first-ranked alternative is the most dominant in all scenarios.

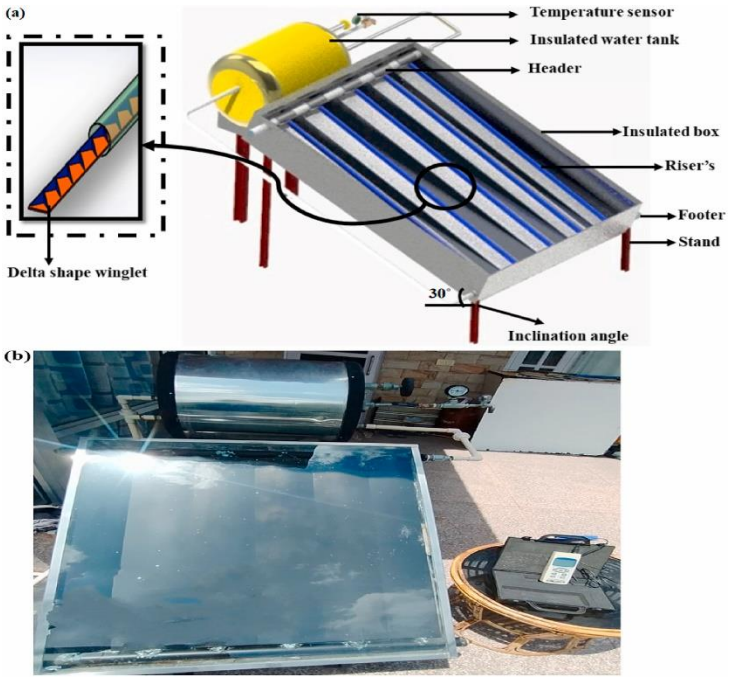

Figure1. represent Schematic and Real view of the SWHS.

Related articles of the 1st thesis point:

Rohit Khargotra, Raj Kumar, Kovács András, Gusztáv Fekete, Tej Singh, (2022). Thermo-hydraulic characterization and design optimization of delta-shaped obstacles in solar water heating system using CRITIC-COPRAS approach. Energy. 2022 Dec 15; 261:125236. **D1 [I. F= 9].**

- **2nd Thesis point: AHP-ARAS MCDM optimization approach applies on perforated delta obstacles Overview of integrated AHP-ARAS method.**

Solar water heating system (SWHS) is a cost-effective technology with high household adoption rates worldwide. The performance of SWHS significantly deteriorates due to several factors, including design parameters as well as radiative and convective heat losses from the system, which considerably impair the system's efficiency. Novel designs and unique heat transfer techniques are increasingly being explored to improve the efficiency of SWHS. In this framework, the following research focuses on designing and optimizing an SWHS integrated with perforated delta obstacles. The influence of Reynolds number (400, 800, 1200), angle of attack (15°, 30°, 45°), and pitch ratio (0.5, 1, 1.5, 2.0) on the friction factor, Nusselt number, and thermo-hydraulic performance was investigated and optimized. The combination of Reynolds number = 1200, angle of attack = 45°, and pitch ratio = 1 yielded the most significant Nusselt number (90.55). In contrast, the combination of Reynolds number = 1200, angle of attack = 15°, and pitch ratio = 0.5 yielded the lowest friction factor (0.38). The largest thermo-hydraulic efficiency (2.75) was obtained using Reynolds number = 400, angle of attack = 45°, and pitch ratio = 1. Since no single SWHS design alternative can meet all desired performance criteria, selecting the best among SWHS design alternatives is not easy. Therefore, a hybrid multi-criteria decision-making approach called AHP (*analytic hierarchy process*)-ARAS (additive ratio assessment) was implemented, suggesting the SWHS design alternative having the angle of attack = 45°, Reynolds number = 1200, and pitch ratio = 1 satisfies the preset performance criteria. Finally, sensitivity analysis and validation with other decision-making approaches were performed to verify the proposed decision-making framework's effectiveness, proving the results' robustness.

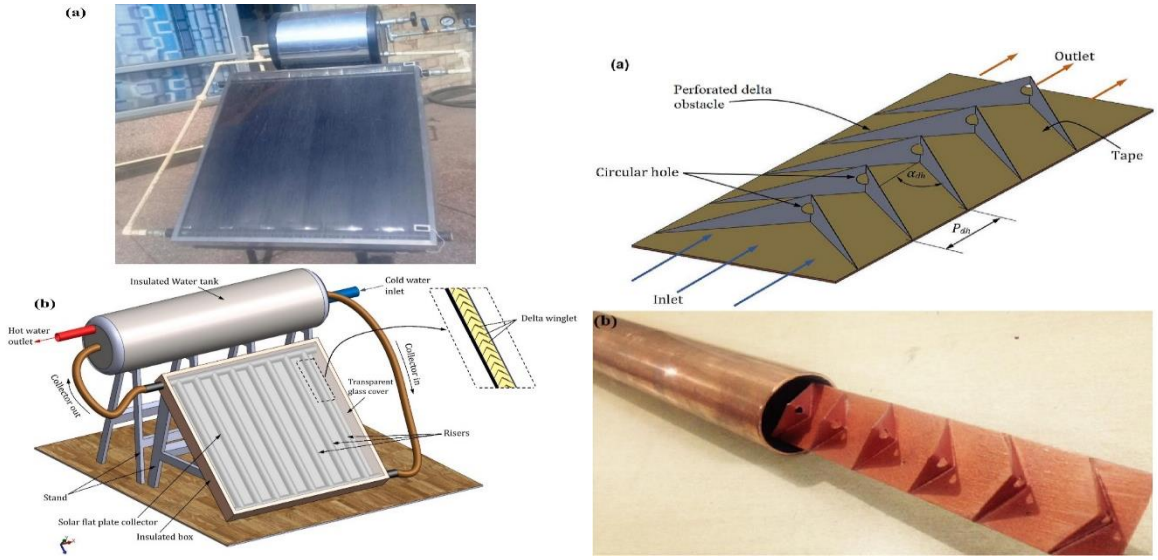

Fig. 2. (a) Real and (b) Schematic view of SWHS. Fig. 3. Perforated obstacle design (a) Schematic, (b) Real.

Related articles of the 2nd thesis point:

Rohit Khargotra, Raj Kumar, Ashutosh Sharma, Tej Singh, **(2023).** Design and performance optimization of solar water heating system with perforated obstacle using hybrid multi-criteria decision-making approach. Journal of Energy Storage. 2023 Jul 1; 63:107099. **D1 [I. F= 9.4]**

- **3rd Thesis point: Experimental examination of eco-friendly insulating materials to analyse their impact on heat transfer characteristics.**

The conventional solar flat plate collector commonly uses rock wool or other insulating materials to lower thermal losses. These inorganic materials are one of the significant concerns to the industry and the environment. Thus, reducing these inorganic materials and utilizing the naturally occurring biodegradable materials available in abundance and without any environmental hazards to the system is imperative. The current research presents agricultural waste as an insulating material for S-FPC fabrication. The novelty of this current research work is the utilization of rice husk, stubble fibre, coco-peat, and nitrile rubber as an insulating material for the fabrication of S-FPC. Experimentation is performed with insulating thicknesses

of 50 mm and 70 mm. The optimum temperature is attaining 50-53˚C with an average thermal efficiency of 64-66% by using rice husk as the insulating material with a thickness of 70 mm.

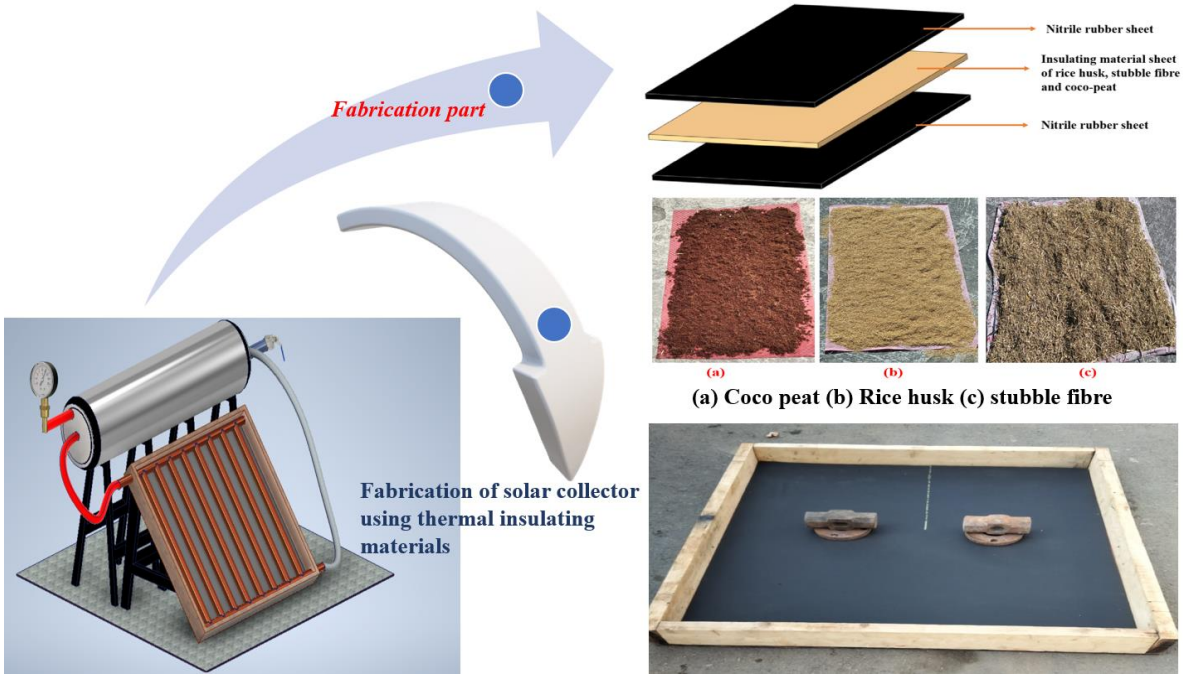

Fig. 4. Schematic representation of S-FPC using thermal insulating materials.

Related articles of the 3rd thesis point:

Rohit Khargotra*, Alam T, Thu K, András K, Siddiqui TU, Singh T. Influence of heat enhancement technique on the thermal performance of solar water heater for sustainable built environment. Start-of-the-art review. Sustainable Energy Technologies and Assessments. 2023 Jun 1; 57:103293. **Q1 [I. F= 8]**

Rohit Khargotra, Kumar, R., Kovács, A. et al. Techno-economic analysis of solar thermal collector for sustainable built environment. J Therm Anal Calorim 149, 1175–1184 (2024). **Q1 [I. F= 4.4]**

Rohit Khargotra* Tabish Alam, Kovács András, Tej Singh. **Indigenous solar thermal collector for hill climates: An experimental study of eco-friendly insulating materials.** Results in Engineering. 2023 Dec 16:101681. **Q2 [I. F= 5]**

CHAPTER 6

REFERENCES

1. Adnan Shariah, M-Ali Al-Akhras, IA & Al-Omari W 2002, 'Optimizing the tilt angle of solar collectors, Renewable Energy', vol. 26, pp. 587-598.
2. Agbo, SN & Okoroigwe, EC 2007, 'Analysis of Thermal Losses in the flat plate collector of a thermosyphon solar water heater', Research Journal of Physics, vol. 1, no. 1, pp. 35-41.
3. Agbo, SN & Unachukwu, GO 2006, 'Performance Evaluation and Optimization of the NCERD Thermo-siphon Solar Water Heater', Proc. World Renewable Energy Congress Florence Italy, Aug. pp. 19-25.
4. Ahmet Koca, Hakan, FO, Tansel Koyun & Yasin Varol 2008, 'Energy and exergy analysis of a latent heat storage system with phase change material for a solar collector', Renewable energy, vol. 33, pp. 567-574.
5. Ajay Kumar, K & Sharma, RP 2012, 'Experimental investigation of solar air heater using porous medium', International Journal of Mechanical Engineering and Technology, vol. 3, no. 2, pp. 387-396.
6. Al-Madani 2006, 'The performance of a cylindrical solar water heater', Renewable Energy, vol. 31, pp. 1751–1763.
7. Ammari, HD & Nimir, YL 2003, 'Experimental and theoretical evaluation of the performance of a tar solar water heater', Energy Conversion and Management, vol. 44, pp. 3037–3055.
8. Arun Kumar Tiwari, Pradyumna Ghosh & Jahar Sarkar 2013, 'Solar water heating using nanofluids -A comprehensive overview and environmental impact analysis', International Journal of Emerging Technology and Advanced Engineering, vol. 3, no. 3, pp. 221-224.

9. Avargani VM, Rahimi A, Divband M. Coupled optical and thermal analyses of a new type of solar water heaters using parabolic trough reflectors. Sustainable Energy Technologies and Assessments. 2020 Aug 1;40:100780.

10. Balaji K, Iniyan S, Goic R. Thermal performance of solar water heater using velocity enhancer. Renewable Energy. 2018 Jan 1;115:887-95.

11. Balaji K, Iniyan S, Swami MV. Exergy, economic and environmental analysis of forced circulation flat plate solar collector using heat transfer enhancer in riser tube. Journal of Cleaner Production. 2018 Jan 10;171:1118-27.

12. Balaram Kundu 2002, 'Performance analysis and optimization of absorber plates of different geometry for a flat plate solar collector: A comparative study', Applied Thermal Engineering, vol. 22, pp. 999-1012. 228

13. Balashanmugam, P, Balasubramanian, G & Balasubramaniyan, K 2013, 'Fabrication and Testing of An Integral Compact Solar Water Heater', International Journal of Advanced Scientific and Technical Research, vol. 5, no.3, pp. 554-572.

14. Behrooz M Ziapour, & Azad Aghamiri 2014, 'Simulation of an enhanced integrated collector-storage solar water heater', Energy Conservation and Management, vol. 78, pp. 193-203.

15. Ben Zalba, Jos M Marin, Luisa F Cabeza & Harald Mehling 2003, 'Review on thermal storage with Phase Change: Materials, heat transfer analysis and applications', Applied Thermal Engineering, International Journal of current Engineering and Technology, vol. 23, pp. 251-283.

16. Bhatt, MK, Gaderia, SN & Channiwala, SA 2011, 'Experimental Investigations on Top Loss Coefficients of Solar Flat Plate Collector at Different Tilt Angle', World Academy of Science, Engineering and Technology, vol. 79, pp. 432-436.

17. Bhattacharyya S, Chattopadhyay H, Haldar A. Design of twisted tape turbulator at different entrance angle for heat transfer enhancement in a solar heater. Beni-Suef University Journal of Basic and Applied Sciences. 2018; 17(1):118-26.

18. Bhattacharyya S, Chattopadhyay H, Haldar A. Design of twisted tape turbulator at different entrance angle for heat transfer enhancement in a solar heater. Beni-Suef University Journal of Basic and Applied Sciences. 2018; 17(1):118-26.

19. Bhupendra Gupta, Gopal Prasad Manikpuri, Jitendra Kumar Waiker & Mohit Pandya 2013, 'Experimental invstigation of double pass solar air heater using different type of porous media', International Journal of current Engineering and Technology, vol. 3, no. 5, pp. 2006-2009.

20. Bliss Jr RW. The derivations of several "plate-efficiency factors" useful in the design of flat-plate solar heat collectors. Solar energy. 1959 Dec 1;3(4):55-64.

21. Bukola, O, Bolaji 2006, 'Flow design collector performance of a natural circulation solar water heater', Journal of Engineering and Applied sciences, vol. 1, pp. 7-13.

22. Charles Smith 1995, 'History of Solar Energy, Revisiting, Past Solar Power Technology Review. Available from: < http://solarenergy. com/infohistory>.

23. Chuawittayawuth K, Kumar S. Experimental investigation of temperature and flow distribution in a thermosyphon solar water heating system. Renewable Energy. 2002 Jul 1;26(3):431-48.

24. Da Silva FA, Dezan DJ, Pantaleão AV, Salviano LO. Longitudinal vortex generator applied to heat transfer enhancement of a flat plate solar water heater. Applied Thermal Engineering. 2019; 158:113790.

25. Dara, JE, Ikebudu, KO, Ubani, NO, Chinwuko, CE & Ubachukwu, OA 2013, 'Evaluation of a Passive Flat-Plate Solar Collector', International Journal of Advancements in Research & Technology, vol. 2, no. 1, pp. 1-6.

26. Das, SK, Choi, SUS, Yu, W & Pradeep, T 2007,. Nanofluid Science and Technology, John Wiley & Sons, Inc., Publication.

27. David Faiman, Haim Hazan, & Ido Laufer 2001, 'Reducing the heat loss at night from solar waters of the integrated collector-storage variety', Solar Energy, vol. 7, no. 2, pp. 87-93. 229

28. De Beijer, HA 1998, 'Product Development in Solar Water Heating', Renewable Energy, vol. 15, pp. 201-204.

29. Dhrupad Sarma, Parimal Bakul Barua, & Diganta Hatibaruah 2014, 'Optimization of Glazing Cover Parameters of a Solar Flat Plate Collector', International Journal of Engineering Trends and Technology (IJETT), vol. 14, no. 2, pp. 2231-5381.

30. Didier Hillot, Xavier Py, Vincent Goetz, & Mohamed Benabdelkarim 2008, 'Storage composites for the optimization of solar water heating systems', Chemical Engineering Research and Design, vol. 86, pp. 612-617.

31. Domenico Borello, Alessandro Corsini, Giovanni Delibra, Sara Evangelisti & Andrea Micangeli 2012, 'Experimental and computational investigation of a new solar integrated collector storage system', Applied energy vol. 97, pp. 982-989.

32. Duffie, JA & Beckman, WA 1991, 'Solar Engineering of Thermal Processes', John Wiley and Sons, New York.

33. Durmuş A, Durmuş A, Esen M. Investigation of heat transfer and pressure drop in a concentric heat exchanger with snail entrance. Applied Thermal Engineering. 2002 Mar 1;22(3):321-32.

34. Eames, PC & Griffiths, PW 2006, 'Thermal behaviour of integrated solar collector/storage unit with 65oC phase change material', Energy conservation and Management, vol. 47, pp. 3611-3618.

35. Ecevit, A, Al-Shariah, AM &Apaydin, ED 1989, 'Triangular built-instorage solar water heater', Solar Energy, vol. 42, pp. 253-265.

36. Ecevit, A, Chaik Vais, MAM & Adnan Shariah 1990, 'A comparative evaluation of the performances of three built-in-storage-type Solar Water Heaters', Solar Energy, vol. 40, no. 1, pp. 23-36.

37. Ella Talmatsky & Abraham Kribus 2008, 'PCM storage for solar DHW: An unfulfilled promise?', Solar Energy, vol. 82, pp. 861-869.

38. Eman-Bellah S Mettawee & Ghazy MR Assassa 2006, 'Experimental study of compact PCM solar collector', Energy, vol. 31, pp. 2958- 2968.

39. Enibe, SO 2003, 'Thermal analysis of a natural circulation solar air heater with phase change material energy storage', Renewable Energy, vol. 28, pp. 2269-2299. 230

40. Faizal M, Saidur, R &Mekhilef, S 2013, 'Potential of size reduction of flat-plate solar collectors when applying MWCNT nanofluid', 4 th International Conference on Energy and Environment (ICEE 2013), Conf. Series: Earth and Environmental Science, pp. 1-4.

41. Fatigun, AT, Adesakin, GE &Gwami, M 2012, 'Experimental determination of the effect of tube spacing on the performance of a flat plate solar collector', International Journal of Environmental Sciences, vol. 3, no. 1, pp. 363-370.

42. Fawaz HE, Badawy MT, Rabbo MA, Elfeky A. Numerical investigation of fully developed periodic turbulent flow in a square channel fitted with 45 in-line V-baffle turbulators pointing upstream. Alexandria Engineering Journal. 2018; 157(2):633-42.

43. Feizabadi A, Khoshvaght-Aliabadi M, Rahimi AB. Experimental evaluation of thermal performance and entropy generation inside a twisted U-tube equipped with twisted-tape inserts. International Journal of Thermal Sciences. 2019; 1145:106051.

44. Florez, WF, Power, H &Chejne, F 2002, 'Numerical solution of thermal convection problems using the multi-domain boundary element method', Numerical Methods for Partial Differential Equations, vol. 18, no. 4, pp. 469-489.

45. Fotukian, SM & Nasr Esfahany, M 2010, 'Experimental study of turbulent convective heat transfer and pressure drop of dilute CuO/ water nanofluid inside a circular tube', International Communication of Heat Mass Transfer, vol. 36, pp. 214–219.

46. Furbo, S &Jivan Shah, L 2003, 'Thermal advantages for solar heating systems with a glass cover with antireflection surfaces', Solar Energy, vol. 74, no. 6, pp. 513-523.

47. Garg, H & Rani, U 1982, Theoretical and experimental studies on collector/storage type solar water heater', Solar Energy, vol. 29, no. 6, pp. 467–478.

48. Garg, HP, Hrishikesan, DS & Ranjana Jha 1998, 'System Performance of built-in-storage type solar water heater with transparent insulation', Solar & Wind Technology, vol. 5, no. 5, pp. 533-538.

49. Garnier, C, Currie, J & Muneer, T 2009, 'Integrated collector storage solar water heater: Temperature stratification', Applied Energy, vol. 86, pp. 1465-1469.

50. George Simons & Joe McCabe 2005, Integrated Energy Policy Report, California Solar Resources, California Research and Development, Energy Research and Development Division. Available from: 231.

51. Gerardo Diaz 2013, 'Experimental characterization of an aluminumbased mini-channel solar water heater', Proceedings of the ASME 2013 Summer Heat Transfer Conference, Minneapolis, USA, pp. 1-6.

52. Gertzos, KP &Caouris, YG 2008a, 'Optimal arrangement of structural and functional parts in a flat plate integrated collector storage solar water heater', Experimental Thermal and Fluid Science, vol. 32, pp. 1105-1117.

53. Gertzos, KP, Caouris, YG &PanidisThi 2010, 'Optimal design and placement of serpentine heat exchangers for indirect heat withdrawal, inside flat plate integrated collector storage solar water heater', Renewable energy, vol. 35, pp. 1741- 1750.

54. Gertzos, KP, Pnevmatikakis, SE &Caouris, YG 2008b, 'Experimental and numerical study of heat transfer phenomena, inside a flat-plate integrated collector storage solar water heater (ICSSWH), with indirect heat withdrawal', Energy Conservation and Management, vol. 49, pp. 3104-4115.

55. Gomes, DG & Fico, NJR 2004, 'Experimental study of energy loss in solar energy collectors', Journal of Energy Engineering, vol. 126, pp. 1101-1105.

56. Govind Singh Chauhan & Ram Kumar Agarwal 2013, 'Experimental analysis of a batch type solar water heater with integrated collector water storage system', International Journal of Emerging technology and advanced engineering, vol. 3, no. 5, pp. 269-274.

57. Greentech Knowledge Solution (P) Ltd, 2010, Global Solar Water Heating Project, Ministry of New and Renewable Energy. Available from.

58. Singh DB, Tiwari GN. Energy, exergy and cost analyses of N identical evacuated tubular collectors integrated basin type solar stills: a comparative study. Solar Energy. 2017 Oct 1; 155:829-46.

59. Hahne, E & Chen, Y 1998, 'Numerical study of flow and heat transfer characteristics in hot water stores', Solar Energy, vol. 64, no. 98, pp. 9-18.

60. Hai, A &Qurat-ul-Ain 2013, 'To investigate the surface properties for increasing efficiency of solar water heater', 6th Vacuum and Surface Sciences Conference of Asia and Australia, pp. 1-6.

61. Hamid El Qarnia 2009, 'Numerical analysis of a coupled solar collector latent heat storage unit using various phase change materials for heating the water', Energy conservation and Management, vol. 50, pp. 247-254.

62. Hassan, E &Fath, S 1995, 'Thermal performance of a simple design solar air heater with built-in thermal energy storage system', Renewable energy, vol. 6, pp. 1033-1039.

63. Hassanzadeh R, Tokgoz N. Analysis of heat and fluid flow between parallel plates by inserting triangular cross-section rods in the cross-stream plane. Applied Thermal Engineering. 2019; 1160:113981.

64. Ho CD, Chen TC. The recycle effect on the collector efficiency improvement of double-pass sheet-and-tube solar water heaters with external recycle. Renewable Energy. 2006 Jun 1;31(7):953-70.

65. Hobbi A, Siddiqui K. Experimental study on the effect of heat transfer enhancement devices in flat-plate solar collectors. International Journal of Heat and Mass Transfer. 2009 Sep 1;52(19-20):4650-8.

66. Hobbi A, Siddiqui K. Experimental study on the effect of heat transfer enhancement devices in flat-plate solar collectors. International Journal of Heat and Mass Transfer. 2009 Sep 1;52(19-20):4650-8.

67. Hobbi A, Siddiqui K. Optimal design of a forced circulation solar water heating system for a residential unit in cold climate using TRNSYS. Solar energy. 2009 May 1;83(5):700-14.

68. Hosni I Abu-Mulaweh 2012, 'Design and development of solar water heating system experimental apparatus', Global Journal of Engineering Education, vol. 14, no. 1, pp. 99-105.

69. Hossein Chaji, Yahya Ajabshirchi, EsmaeilEsmaeilzadeh, SaeidZeinaliHeris, Mahdi Hedayatizadeh& Mostafa Kahani 2013, 'Experimental study on Thermal Efficiency of

Flat Plate Solar Collector using TiO2 / Water Nanofluid', Modern Applied Science, vol. 7, no. 10, pp. 60-69.

70. Huang WC, Chen CA, Shen C, San JY. Effects of characteristic parameters on heat transfer enhancement of repeated ring-type ribs in circular tubes. Experimental Thermal and Fluid Science. 2015 Nov 1;68:371-80.

71. Pathak SK, Tyagi VV, Chopra K, Rejikumar R, Pandey AK. Integration of emerging PCMs and nano-enhanced PCMs with different solar water heating systems for sustainable energy future: A systematic review. Solar Energy Materials and Solar Cells. 2023 Jun 1; 254:112237.

72. Li T, Wang Z, Yu J, Mao Q. Experimental and simulation on night heat dissipation characteristics and freezing process of evacuated tube solar water heaters. International Journal of Thermal Sciences. 2023 Oct 1; 192:108455.

73. Chopra K, Tyagi VV, Pathak SK, Tripathi PA, Sharma RK, Singh G, Pandey AK. Thermal and chemical reliability of paraffin wax and its impact on thermal performance and economic analysis of solar water heater. Energy for Sustainable Development. 2023 Apr 1; 73:39-53.

74. Wang Y, Nasajpour-Esfahani N, Alizadeh AA, Smaisim GF, Abed AM, Hadrawi SK, Hashemi A, Hekmatifar M. Numerical simulation of the melting of solid paraffin in a solar water heater and the effect of the number of fins and the height of the fins. Case Studies in Thermal Engineering. 2023 Jan 1; 41:102653.

75. Yari S, Safarzadeh H, Bahiraei M. Experimental study of storage system of a solar water heater equipped with an innovative absorber spherical double-walled tank immersed in a phase change material. Journal of Energy Storage. 2023 May 1; 61:106782.

76. Pambudi NA, Nanda IR, Saputro AD. The energy efficiency of a modified v-corrugated zinc collector on the performance of solar water heater (SWH). Results in Engineering. 2023 Jun 1; 18:101174.

77. Esmaeili Z, Akbarzadeh S, Rashidi S, Valipour MS. Effects of hybrid nanofluids and turbulator on efficiency improvement of parabolic trough solar collectors. Engineering Analysis with Boundary Elements. 2023 Mar 1; 148:114-25.

78. Ravanbakhsh M, Gholizadeh M, Rezapour M. 3E thermodynamic modeling and optimization a novel of ARS-CPVT with the effect of inserting a turbulator in the solar collector. Renewable Energy. 2023 Jun 1; 209:591-607.

79. Khargotra R, Kumar R, Sharma A, Singh T. Design and performance optimization of solar water heating system with perforated obstacle using hybrid multi-criteria decision-making approach. Journal of Energy Storage. 2023 Jul 1; 63:107099.

80. Negeed ES, Alhazmy M, Bokhary AY, Abulkhair H, Almas MA, Hedia HS. Numerical simulation of flat plate solar collector equipped with a turbulator containing water/copper-graphene hybrid nanofluid utilizing a two-phase model. Engineering Analysis with Boundary Elements. 2023 Nov 1; 156:90-113.

81. Poongavanam GK, Prabakaran R, Salman M, Velraj R, Kim SC. Exploring the performance of a novel solar water heater by combining three augmentation approaches (nanofluids, absorber roughness, and surface coating). Case Studies in Thermal Engineering. 2023 Sep 1; 49:103177.

82. Variyenli Hİ, Amini A, Tuncer AD, Khanlari A, Kolay Ş. Experimental and numerical analysis of a helically-coiled solar water collector at various angular placements. International Journal of Thermal Sciences. 2023 Jun 1; 188:108177.

83. Ghanbari G, Marzban A, Yousefzadeh S. Improving the thermal efficiency of parabolic trough collector equipped with combined turbulator containing two-phase magnetic

hybrid nanofluid. Engineering Analysis with Boundary Elements. 2023 Oct 1; 155:565-83.

84. Abdalla AN, Shahsavar A. Numerical investigation of the effect of rotary propeller type turbulator on the energy and exergy efficiencies of a concentrating photovoltaic/thermal hybrid collector. Journal of Cleaner Production. 2023 Mar 20; 393:136225.

85. Dittus FW. Heat transfer in automobile radiators of the tubler type. Univ. Calif. Pubs. Eng. 1930; 2: 443.

86. Blasius H. The boundary layers in fluids with little friction. Zeitschrift für mathematik und physik. 1950 Feb 1;56(NACA-TM-1256).

87. Kline SJ. Describing uncertainty in single sample experiments. Mech. Engineering. 1953; 75: 3-8.

88. Wang Y, Zhang S, Wang D, Liu Y. Experimental study on the influence of temperature and humidity on the thermal conductivity of building insulation materials. Energy and Built Environment. 2023 Aug 1;4(4):386-98.

89. Kamel E, Memari AM. Residential building envelope energy retrofit methods, simulation tools, and example projects: a review of the literature. Buildings. 2022 Jul 5;12(7):954.

90. Chen Z, Liu T. Development and application status of glass wool, rock wool, and ceramic wool. In Thermal Insulation and Radiation Control Technologies for Buildings 2022 Jun 7 (pp. 129-161). Cham: Springer International Publishing.

91. Diakoulaki D, Mavrotas G, Papayannakis L. Determining objective weights in multiple criteria problems: The critic method. Computers & Operations Research 1995; 22:763-70.

92. Zavadskas EK, Kaklauskas A, Peldschus F, Turskis Z. Multi-attribute assessment of road design solutions by using the COPRAS method. The Baltic Journal of Road and Bridge Engineering 2007; 27:195-203.

93. M.C. Mukeshimana, Z.-Y. Zhao, M. Ahmad, M. Irfan. Analysis on barriers to biogas dissemination in Rwanda: AHP approach. Renewable Energy 163, 2021, 1127-1137.

94. S. Duleba, Z. Szádoczki. Comparing aggregation methods in large-scale group AHP: Time for the shift to distance-based aggregation. Expert Systems with Applications 196, 2022, 116667.

95. S.R. Chaurasia, R.M. Sarviya. Comparative thermal performance analysis on helical screw inserts in tube with number of strips with nanofluid at laminar flow regime. Journal of Thermal Science and Engineering Applications 13, 2021, 011017.

96. T. Dagdevir, O. Keklikcioglu, V. Ozceyhan. Heat transfer performance and flow characteristic in enhanced tube with the trapezoidal dimples. International Communications in Heat and Mass Transfer 108, 2019, 104299.

97. A. Kumar, R.P. Saini, J.S. Saini. Effect of roughness width ratio in discrete Multi v-shaped rib roughness on thermo-hydraulic performance of solar air heater. Heat and Mass Transfer 51, 2015, 209-220.

98. M. Singla, V.S. Hans, S. Singh. CFD analysis of rib roughened solar evacuated tube collector for air heating. Renewable Energy 183, 2022, 78-89.

99. M. Behzad, S.H. Zolfani, D. Pamucar, M. Behzad. A comparative assessment of solid waste management performance in the Nordic countries based on BWM-EDAS. Journal of Cleaner Production 266, 2020, 122008.

100. G. Poongavanam, V. Sivalingam, R. Prabakaran, M. Salman, S.C. Kim. Selection of the best refrigerant for replacing R134a in automobile air conditioning system using

different MCDM methods: A comparative study. Case Studies in Thermal Engineering 27, 2021, 101344.

101. P.K. Mishra, R. Nadda, R. Kumar, A. Rana, M. Sethi, A. Ekileski. Optimization of multiple arcs protrusion obstacle parameters using AHP-TOPSIS approach in an impingement jet solar air passage. Heat and Mass Transfer 52, 2018, 3797-3808.

102. A. Sharma, R. Chauhan, T. Singh, A. Kumar, R. Kumar, M. Sethi. Optimizing discrete V obstacle parameters using a novel Entropy-VIKOR approach in a solar air flow channel. Renewable Energy 106, 2017, 310-320.

103. R. Khargotra, R. Kumar, K. András, G. Fekete, T. Singh. Thermo-hydraulic characterization and design optimization of delta-shaped obstacles in solar water heating system using CRITIC-COPRAS approach. Energy, 2022; 261, 125236.

104. Chen Z, Liu T. Development and application status of glass wool, rock wool, and ceramic wool. In Thermal Insulation and Radiation Control Technologies for Buildings 2022 Jun 7 (pp. 129-161). Cham: Springer International Publishing.

105. Kaur S, Konwar RJ, Negi P, Dhar S, Singh K, Chandel SS. Utilization of biodegradable novel insulating materials for developing indigenous solar water heater for hill climates. Energy for Sustainable Development. 2022 Apr 1; 67:21-8.

106. Ikpakwu, F., Okoronkwo, A., Okwu, M., & Anyanwu, E. (2017). Experimental study on a line-axis concentrating solar energy collector for water heating. International Journal of Fluid Mechanics & Thermal Science, 3(6), 62–69.

107. Nshimyumuremyi, E., & Junqi, W. (2019). Thermal efficiency and cost analysis of solar water heater made in Rwanda. Energy Exploration & Exploitation, 37(3), 1147-1161.